ADAPTIVE STRATEGIES FOR CONTROLS OF FLEXIBLE ARMS

192P.

Bau-San Yuan

ADAPTIVE STRATEGIES FOR CONTROLS OF

FLEXIBLE ARMS

A Thesis

Presented to

The Academic Faculty

By

Bau-San Yuan

In Partial Fulfillment

of the Requirements for the Degree

Doctor of Philosophy

in the George W. Woodruff School of Mechanical Engineering

Georgia Institute of Technology

April, 1989

To my mother, brother and sisters and their families in Taiwan.

To the memory of my father, Chin-Chung Yuan, 1921-1981.

ACKNOWLEDGEMENTS

TABLE OF CONTENTS

Page

CHAPTER V. CONTROL IMPLEMENTATION AND EXPERIMENTAL INVESTIGATION

CHAPTER VI. CONCLUSIONS AND RECOMMENDATIONS

LIST OF TABLES

LIST OF ILLUSTRATIONS

Figure   Page

Figure

Figure

Figure

Figure

SUMMARY

This research seeks to provide a modern manipulator control strategy for tracking a desired trajectory over a wide range of flexible manipulator motion and payload variations. Due to the presence of nonlinearities, uncertainty, and link flexibility in the dynamic model, "Adaptive Control" is proposed to meet these goals. The signal-synthesis adaptation implemented here results in a robust stability design which reduces the burden of on-line computation and satisfies the characteristics of flexibility.

A recursive dynamic model has been derived by the Lagrange-Euler formula with the assumed mode method and the measurements form the output matrix. The finite element method is used here to predict system vibrations and assumed mode shapes. The adaptive controller design is based on asymptotical stability via the Lyapunov criterion, while the output error between the system and the reference model is used as the actuating control signal. Computer simulations were carried out to test the design. The combination of the adaptive controller and estimator show that the flexible arm should move along a pre-defined trajectory with high-speed motion and fast vibration setting time.

A computer-controlled prototype two link manipulator, RALF (Robotic Arm, Large Flexible), with a parallel mechanism driven by hydraulic actuators exists in the Flexible Automation Laboratory at Georgia Tech. Experiments on RALF were performed to verify the mathematical analysis. The experimental results illustrate that assumed modes found from finite element techniques can be used to derive

the equations of motion with acceptable accuracy. The robust adaptive (modal) control is implemented to compensate for unmodelled modes and nonlinearities and is compared with the joint feedback control in additional experiments. Preliminary results show promise for the experimental control algorithm.

CHAPTER I

INTRODUCTION

The need to improve industrial productivity has over the years greatly motivated the implementation of a variety of forms of automation. Programmable multifunctional manipulators, or industrial robots, have become increasingly important in this respect. Robot control is one factor which can improve robot performance by improving robot motion.

One of the major drawbacks of today's robots is that they offer slow response since the robot motion speed is severely limited by the weight of the manipulator arm. The excessive arm weight not only hampers the rapid motion and workspace range of the manipulator arm, but also increases the robot's consumption of energy and the size of the required actuators.

1.1 Motivation

The reduction of component structural weight has been proposed as one way to reduce the cost of industrial manipulators while improving high speed performance. In exchange for a light-weight arm, one must accept an increase in system flexibility along with the associated difficulty in accurately controlling a flexible structure. Increased manipulator performance requires a controller which allows for both non-linear link dynamics and link flexibility. It is to establish methods of controlling such light-weight arms that this research has been initiated.

1.2 Why Advanced Control?

The primary existing schemes of control do not satisfactorily treat both non-

linear dynamics and flexibility, although many suggested schemes satisfy one or the other of these needs. In some research, linear quadratic control design is used to stabilize the flexibility in a large scale structure and nonlinear feedback is used to decouple coupling terms in the nonlinear system. A new adaptive control strategy is introduced here to solve the problems addressed above and to improve the system performance. Adaptive control is a simple type of nonlinear feedback control, when there is not a scheme to control the whole nonlinear system globally.

The reasons for implementing an adaptive strategy here for position control of flexible arms is that it can:

1. eliminate the steady-state error in responses,

2. compensate for the unmodelled modes when the dynamic model adopted is close to the real one,

3. decouple the nonlinear terms in some respects,

4. be insensitive to the variation of the payload,

5. eliminate the effect of structure disturbances and uncertainties of system parameters along the working paths,

6. reduce on-line computation and be implemented simply.

1.3 Background

1.3.1 History and Concept of Adaptive Control

The term and the concept of adaptive control were introduced in the 1950's when the complexity of aircraft led to the need for a more effective control system for plants whose parameters may vary over a wide range.

A system is adaptive if it makes use of the information on either external actions, dynamic characteristics of the plant, or its control system, obtained in the course of operation, to change the structure or the gains of the controller as

necessary to achieve the required properties of the closed-loop system.

The schemes of adaptive control are classified into three classes: gain scheduling, model reference control, and the self-tuning regulator [Astrom,1983,1989].

1. Gain Scheduling - The controller is automatically tuned at a number of operating points. The resulting control laws are then stored away for subsequent use whenever the corresponding operating condition is indicated by auxiliary measurement (Fig. 1.1) [Goodwin and Sin 1984]. The transition between different operating conditions will happen when the scheduling variables change along with the variation of auxiliary measurements. Many applications have been found [Kallstrom, Astrom, Thorell, Erisksson and Stein 1979].

However, there exist two major drawbacks of this scheme. One is that gain scheduling is an open-loop compensation, or can be viewed as a feedback control system where the feedback gains are adjusted by feedforward compensation. The other is that the design is time-consuming.

2. Self-tuning - This is one approach to the automatic tuning problem. It can be viewed either as a tuning aid for control laws that are more complex than PID but which have fixed parameters, or as a means by which a time-varying process can be controlled in a consistent way (Fig. 1.2) [Clarke, Gawthrop 1981].

The adaptive regulator can be thought of as composed of two loops. The inner loop consists of the process and an ordinary linear feedback regulator. The parameters of the regulator are adjusted by the outer loop, which is composed of a recursive parameter estimator and a design calculation [Astrom and Wittenmark 1987].

Self-tuning was originally proposed by Kalman [1955], who built a special-purpose computer to implement the regulator. Later, the theory was revived and extended to cover stochastic aspects by Peteka [1970], but it was not until the

key paper of Astrom and Wittenmark [1973] that the current great interest in the subject was initiated. One disadvantage is the difficulty of application to the MIMO (multi-input, multi-output) case.

3. MRAC (Model Reference Adaptive Control) - This was one of the methods originally suggested for the servo problem by Whitskew, Yamron and Kezer [1958]. Further work was performed by Parks [1966] on methods using a Lyapunov function. Hang and Parks [1973], Monopoli [1973], and Landau [1974] also continuously worked in this area.

The reference model is introduced as a part of the MRAC system shown in Fig. 1.3. The whole system is described in two loops. The inner loop is an ordinary feedback loop composed of the process and the regulator. The parameters of the regulator are adjusted by the outer loop in such a way that the error e between the process output y and the model output y_m become small. The key problem is to determine the adjustment mechanism so that a stable system which brings the error to zero is obtained.

1.3.2 Adaptive Control of Robot Motion

The MRAC approach was originally implemented by Dubowsky and Desforges [1979] on robot control. A linear, uncoupled, constant parameter reference model was selected for each degree of freedom of the robot arm. For the development of the control algorithm, the coupling of the system was neglected and nonlinear manipulator dynamics were simplified such that the system dynamics were described in a linear second order differential equation for each individual degree of freedom. The position and velocity feedback with adjustable gains were assumed to control the robot motion. This was based on an adaptive scheme of steepest descent (Gradient Search Technique) [Donalsun and Leondes 1963] which minimized the quadratic

error between the outputs of the plant and the model by commanding a time rate of change of the feedback gains. However, global stability of this simplified adaptive controller is not always guaranteed. The experimental results [Dubowsky and Kornbluh 1985] were presented with PD and PID feedforward compensation. PID control is applied as if joints were decoupled to reduce the steady-state error.

Another simple MRAC developed by Takegaki and Arimoto [1981] was applied in the task-oriented coordinate control of a manipulator when the target trajectory was planned and expressed in the task-oriented coordinate space. It was assumed that the effect of gravity could be compensated and the second and higher-order terms were neglected in the dynamic system. The perturbed variables method was introduced to get the linear equation around the nominal points. The control system needed to complete two jobs. First, the adjustable laws were designed by stability analysis with a Lyapunov function without an explicit reference model. Second, the feedforward controller drives the system to the set point and compensated any unknown disturbance.

Horowitz and Tomizuka [1980] proposed an application of an MRAC scheme to adaptively compensate the nonlinearities and decouple the joint motions. The adaptively model parameters can be estimated by applying hyperstability theory [Landau 1979] so that the computed torque input can cancel the nonlinear terms and accomplish the decoupling by the feedforward method. Due to the constant gains chosen which ensure adaptive system stability, the reference model can simply be a double integrator. As a result, the simple fixed PID type controller closes the loop.

The robot dynamic equation may be viewed as a class of nonlinear and time varying systems. When applying hyperstability theory, Balestrino et.al. proposed a MRAC based on Adaptive Model-following Control [1982] which is a signal syn-

thesis adaptation. In comparison with the control law in the Lyapunov design, the gain matrices are divided into an adjustable and a fixed part. The adaptation mechanism in the adjustable part makes the system asymptotically stable in the large if the perfect model following conditions are met [Erzberger 1968] and the linear compensator [Anderson 1967] and the adaptation matrices are properly chosen.

Although the Lyapunov design presented above guarantees asymptotical stability, the transient time of the error is not specified. Therefore, large state error and oscillations may occur in the transient time. To deal with this difficulty and to improve the speed of convergence, an auxiliary input can be introduced [Lim and Eslami 1986].

It has been proven that the robotic system with PD feedback is stable [Asada and Slotine 1986]. The computed-torque method is a common approach in robotic control research. Therefore, this allows us to construct a MRAC scheme that makes full use of known parameters and only adjusts the estimates of the unknown parameters [Craig 1987] [Slotine 1987].

If the dynamic equation of a manipulator is represented by a discrete-time model, system identification techniques can be applied to sample input-output data. This results in a self-tuning design of robot control using the discrete-time dynamic equation found in most modern controllers [Hsia 1986].

Two major alternatives exist: 1. If the corresponding model of the plant is known, the controller is designed to achieve the control goal. 2. If the parameters of the system can be estimated on-line, then the controller is adjusted along with the estimated parameters. When applying self-tuning methods for simplicity of design, the model of the robot is usually chosen as a linear and slowly time-varying plant such that the parameter estimation problem can be solved by the popular recursive algorithms [Astrom and Wittenmark 1989] [Goodwin and Sin 1984] [Ljung 1977].

Koivo and Guo [1983] have considered a performance criterion which gives a simple control law to minimize the error between the outputs of the system and reference model. Moreover, if the nominal control input can be computed from the given desired state trajectory, the robot states along this nominal point can be represented in a linear perturbation form. A self-tuning design based on this linear perturbation discrete model has been investigated by Lee and Chung [1982, 1984]. However, this design heavily depends on the computational speed in real-time control.

1.3.3 Control of Flexible Systems

In recent years, many algorithms have proposed to control distributed parameter systems [Takahashi 1972] which would include flexible structures also undergoing rigid body motion. However, applications of those works mostly appear in the field of the large scale structures of aerospace. A primary example [Andeen 1964] which was the stabilization of flexible vehicles by considering the rigid-body and elastic-mode responses independently.

For modal control of distributed systems with distributed feedback, Gould and Murray-Lasso [1966] presented a linear operator acting on functions of time and distance separately. To implement the control system, it was assumed that the distance dependent part of the output and forcing functions had a finite number of eigenfunctions. Classical techniques are applied to synthesize the feedback control system. Therefore, a solution to the problem of controlling a class of linear, time invariant, distributed parameter system was established.

Vaughan [1968], who applied wave propagation concepts to the control of bending vibrations, was interested in determining impedance matrices for passive end-point attachment. This resulted in the method of transfer matrices for analyzing

the distributed parameter system. Book [1974] used this method to approach the flexible manipulator arm problem.

Distributed and lumped parameter models of various arm components were combined via transfer matrices to represent the complete arm model and numerical techniques were used to derive frequency domain information by Book [1974]. These results were interpreted to indicate the limitations which the flexibility of a given arm design imposed on the feedback gains of the joint control assumed. Maizza-Neto [1974] used assumed modes and the Langrangian formulation of the dynamic system to perform time domain analysis of flexible arms. To control a linearized model in state space form, one could propose linear feedback of the flexible system state variables, if all state variables were measurable. Furthermore, three types of linear feedback schemes, joint angle and velocity feedback with and without cross joint feedback, and feedback of flexible state variables, were proposed to show some results for the models [Book 1975].

Balas [1978] developed a feedback controller for a finite number of modes of a flexible system. The controllability and observability conditions of the system necessary for successful operation were displayed. The control and observation spillover due to the residual (uncontrolled) modes were examined and the combined effect of control and observation spillover was shown to lead to potential instabilities in the closed-loop system. Those results were useful in designing the adaptive control of large scale systems.

Book, Majette and Ma [1979,1981] continued to develop transfer matrix techniques for the frequency domain analysis of the flexible arms. However, the controller design was via combined state space and frequency domain techniques [Book and Majette 1983].

Canon and Schmitz [1984] discussed charactistics of a very flexible manipulator

with an open truss construction. The end-point position was measured by an optical sensor external to the manipulator system. An LQG approach was used to design the feedback controller.

A truncated modal series was used for modelling and control of flexible manipulator arms by Truckenbrodt [1981]. Linear equations were derived from a linearization with respect to a prescribed reference motion or reference position. Unfortunately, the control algorithm is incompletely described. Usoro, Nadira and Mahil [1984] proposed the concept of linear quadratic control with a prescribed degree of stability to linearized versions of a flexible manipulator nonlinear model.

Sangveraphunsiri [1984] applied optimal control methods to obtain controller design for a single link arm. Stochastic and deterministic steady-state regulators were simulated with a linear model and the Bang-Bang controller was implemented to solve minimum time position control problems. Hastings [1986] verified the regular results through experiments.

An approach based on singular perturbation control theory [Saksena] [Kokotovic 1984] was investigated on flexible manipulator control [Siciliano and Book]. The rigid body motion constitutes the slow subsystem, for which ordinary tracking control can be synthesized, while the flexible motion plays the role of the fast subsystem, which must be stabilized around the rigid body path. For a flexible beam treated with a constrained viscoelastic layer damping treatment, the dynamics was derived as a modified beam equation [Alberts]. Adding damping moves the poles to the left in the complex plane and thus improves the stability of the system. Control of gross and fine motions of flexible manipulators was studied by Centinkunt [1987].

1.4 Problem Statements

A flexible manipulator arm moves in the operating space. The joint actuactors,

which are the only control actuation, are used to track the predefined path. The link rotates around the joint which is the location of the actuator so that oscillations occur along with the link. The measurements of joint position and velocity and link strain form the output matrix.

Due to its mass and flexibility, the distributed parameter nature of the link has to be taken into consideration. Upon applying the control law, the end effector position and vibration modes of the system need to be adequately controlled. A main goal of this work is to control the flexible arm to move along a predefined joint trajectory with high-speed and fast vibration-setting time.

The accuracy of the distributed parameter model is essential to success in achieving accurate control. However, unpredicted disturbances, e.g. Coulomb and viscous friction of the joint, measurement noise and saturation of the actuators, are considered as uncertainties in the dynamics such that the feedback system can be demonstrated to be robust. Experiments with a computer-controlled prototype of a two-link, non-serial, hydraulically driven manipulator, RALF (Robotic Arm, Large and Flexible), in the Flexible Automation Laboratory at Georgia Tech are performed to verify the applicability of the mathematical analysis.

1.5 Approach

To establish a successful feedback control for a mechanical system, dynamic modelling is an important prerequisite. An approach based* on Lagrange-Euler is used in developing the governing dynamic equations for the large and flexible manipulator. The position of every point along each link is described by a vector combination of flexible deflections. The deflection is treated as a finite series of separable modes which are products of admissible functions and time-dependent generalized coordinates. The finite element method is used to find the admissi-

ble functions since the link is not homogeneous and the boundary conditions are complicated. Due to the recursive description of link position and velocity, the manipulator dynamics is derived efficiently.

Before applying the control algorithm, some basic control properties need to be verified for flexible manipulator dynamics. In this case, the number of degrees of freedom of the system is much higher than the number of the input variables, whereas for rigid manipulators every degree of freedom has a corresponding input variable. Measurements are also limited, representing only some state variables, not all.

The next step is to provide a modern control strategy for tracking a desired path with fast vibration-setting time over a wide range of flexible manipulator motions and payload variations. In order to reduce the burden of on-line computation and satisfy the characteristics of the flexibility, signal-synthesis adaptation is implemented here to produce a robustly stable design via the Lyapunov criterion. Each link can be considered as a subsystem of the overall system so that a decentralization technique can be utilized to simplify the control structure. The system is, therefore, stabilized by local state feedback, while the interconnection terms between subsystems are considered as one of the uncertainties in the system and are bounded.

Computer simulations are carried out to test the design. The experimental results illustrate that assumed modes found from finite element methods can be used to find improved mode shapes. Adaptive strategies for control of flexible manipulators are used to compensate unmodeled modes and nonlinearities. They are compared with the conventional joint feedback control in experiments.
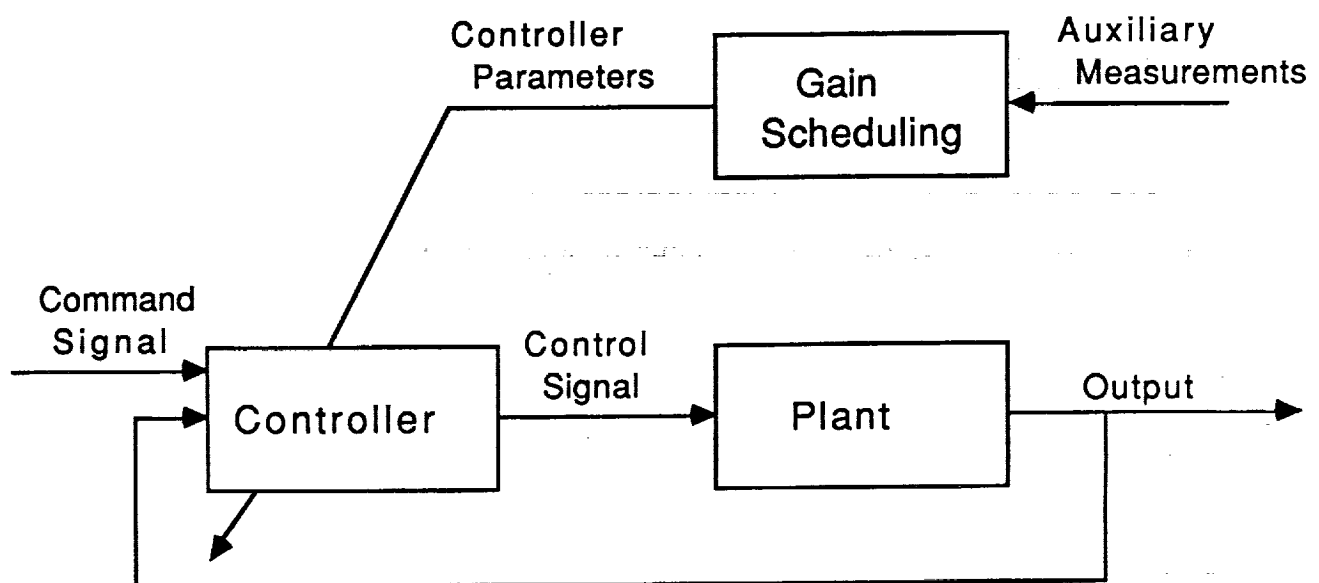
Figure 1.1 Block diagram of gain scheduling adaptive control.
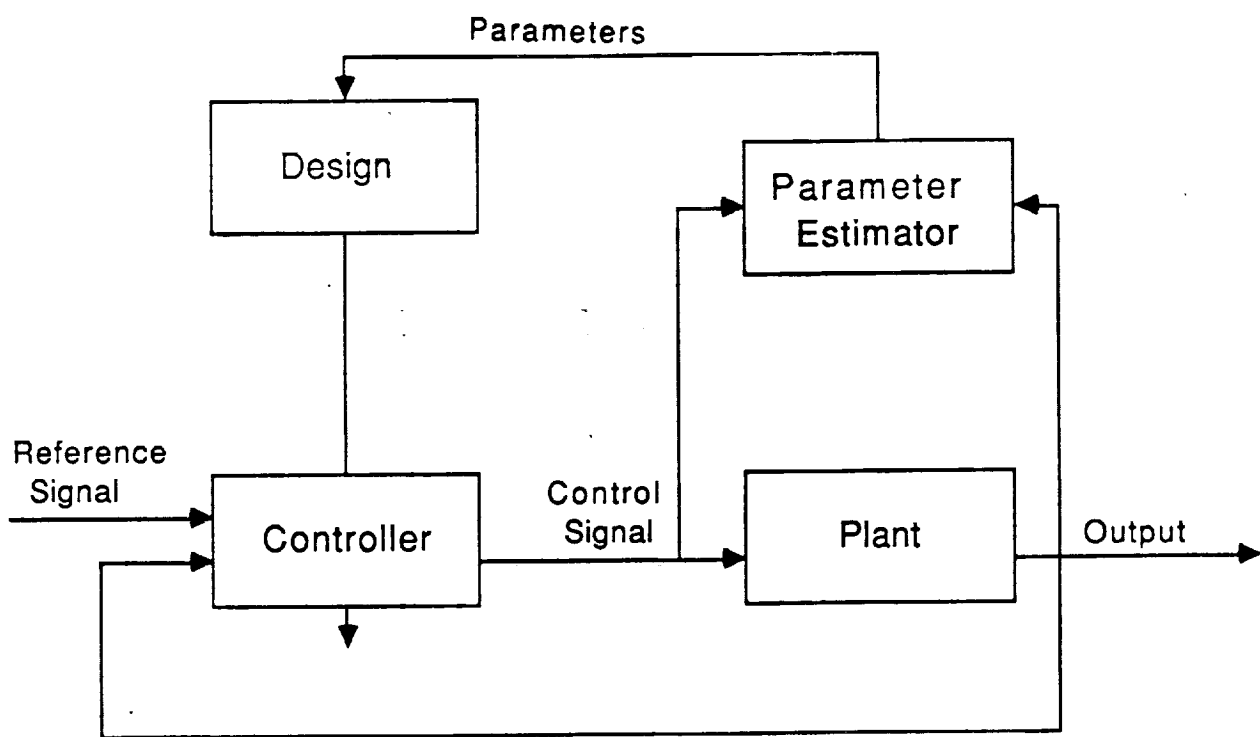
Figure 1.2 Block diagram of self-tuning control.
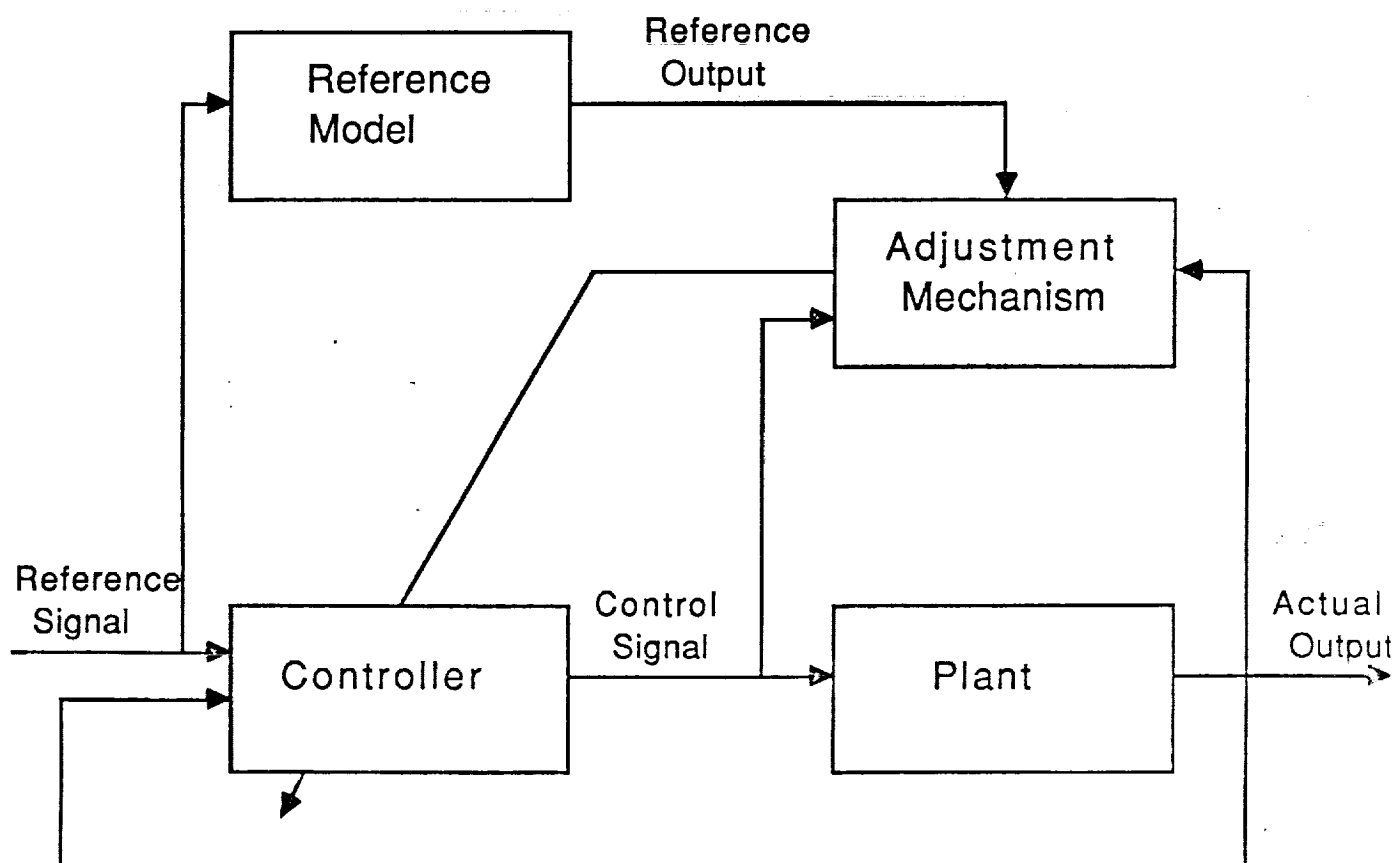
Figure 1.3 Block diagram of model reference adaptive control.

CHAPTER II

DYNAMIC MODELING

Much work has been done in the formulation of the dynamic equations of motion for mechanical manipulators with flexible links. This section describes the velocity of a point on a link as a linear combination of rigid body motion and vibratory modes for flexible motion in order to form the kinetic energy. Due to the distributed character of the flexible links, the total potential energy includes the gravity as well as strain energy. The total potential and kinetic energy is taken into account by integrating over the entire system. Therefore, the differential equations of motion can be formed through Lagrange's equation.

2.1 Flexible Arm Kinematics

A robot positioning task is naturally specified in Cartesian coordinates by a position vector P and a matrix of direction cosines R. Thus, the position of an arbitrary point attached to the rigid body can be represented as a 4×4 matrix A in the fixed coordinate system as shown in Figure 2.1.

$$A = \begin{bmatrix} R & P \\ 0 & 1 \end{bmatrix} .$$

(2.1)

In other words, the matrix A is a transformation between two coordinate systems.

In the case of flexible arms, a point along the beam can be described in a fixed reference coordinate system by two transformations (A_i and E_i) between the coordinate systems (Figure 2.2) [Book, 1984]. The transformation (A_i) relates system i', the point before deflection, to system $i-1$. The transformation E_i relates system i to system i'. The combined relation is

$$x_{i-1} = A_i E_i x_i ,$$

(2.2)

where

$$x_{i-1} = [\,P_{i-1}^T, 1\,]^T = \text{the position of the point in system } i-1,$$

$$A_i = \text{transformation for joint } i-1,$$

$$E_i = \text{transformation due to link deflection,}$$

and

$$x_i = \text{the position of the point in system } i.$$

Considering the ith consecutive coordinate transformation along a serial linkage, we can derive the location (r_i) of a point along the ith coordinate viewed from the base frame.

$$r_i = T_i \,{}^i r_i, \tag{2.3a}$$

where

$$T_i = A_1 E_1 A_2 E_2 \cdots A_{i-1} E_{i-1} A_i, \tag{2.3b}$$

and ${}^i r_i$ is the position vector related to the ith coordinate before the transformation due to link deflection E_i.

It is useful to distinguish between undeformed joint and deflection transformations as follows

$$T_j = T_{j-1} E_{j-1} A_j = \hat{T}_{j-1} A_j. \tag{2.3c}$$

With the revolute joint, for example, let z_i of the ith coordinate be on the ith link, A_i can be specified from the Euler transformation (Figure 2.3).

$$A_i = \begin{bmatrix} \cos\phi_i \cos\theta_i \cos\psi_i - \sin\phi_i \sin\psi_i & -\cos\phi_i \cos\theta_i \sin\psi_i - \sin\phi_i \cos\psi_i \\ \sin\phi_i \cos\theta_i \cos\psi_i + \cos\phi_i \sin\psi_i & -\sin\phi_i \cos\theta_i \sin\psi_i + \cos\phi_i \cos\psi_i \\ -\sin\theta_i \cos\psi_i & \sin\theta_i \sin\psi_i \\ 0 & 0 \end{bmatrix}$$

$$\begin{bmatrix} \cos\phi_i \sin\theta_i & 0 \\ \sin\phi_i \sin\theta_i & 0 \\ \cos\theta_i & 0 \\ 0 & 1 \end{bmatrix}.$$

$$\tag{2.4}$$

The flexible deflection is assumed to be a finite series of separable modes which are the product of admissible shape functions and time-dependent generalized coordinates. Higher modes are comparatively small in amplitude. With small deflections, the matrix E_i can then be expressed as

$$E_i = \sum_{j=1}^{m_i} \delta_{ij} \begin{bmatrix} 0 & -\theta_{zij} & \theta_{yij} & u_{ij} \\ \theta_{zij} & 0 & -\theta_{xij} & v_{ij} \\ -\theta_{yij} & \theta_{xij} & 0 & w_{ij} \\ 0 & 0 & 0 & 0 \end{bmatrix} + \begin{bmatrix} 1 & 0 & 0 & 0 \\ 0 & 1 & 0 & 0 \\ 0 & 0 & 1 & l_i \\ 0 & 0 & 0 & 1 \end{bmatrix}, \qquad (2.5)$$

where δ_{ij} is the time-dependent amplitude of mode j of link i; $\theta_{x_{ij}}$, $\theta_{y_{ij}}$ and $\theta_{z_{ij}}$ are the angles of rotation about the x_i, y_i and z_i; u_i, v_i and w_i are the x_i, y_i and z_i deflection components of mode j of link i; and m_i is the number of modes used to describe the deflection of link i. l_i is the length of link i.

A_i is a function of the joint displacement (q_i) and E_i is a function of link deflections (δ_{ij}). Transformation equation (2.3a), therefore, illustrates the functional relationship between the position of a point along the ith link and the displacements of all the joints and link deflections involved in the kinematic chain.

Taking a simple instance used later where the orientation is only specified by rotation about one joint axis and no rotation exists due to the deflection, matrices A_i and E_i can be simplified (Figure 2.4) as

$$A_i = \begin{bmatrix} \cos\beta_i & \sin\beta_i & 0 & 0 \\ -\sin\beta_i & \cos\beta_i & 0 & 0 \\ 0 & 0 & 1 & 0 \\ 0 & 0 & 0 & 1 \end{bmatrix}, \qquad (2.6)$$

$$E_i = \sum_{j=1}^{m_j} \delta_{ij} \begin{bmatrix} 0 & 0 & 0 & u_{ij} \\ 0 & 0 & 0 & 0 \\ 0 & 0 & 0 & 0 \\ 0 & 0 & 0 & 0 \end{bmatrix} + \begin{bmatrix} 1 & 0 & 0 & 0 \\ 0 & 1 & 0 & 0 \\ 0 & 0 & 1 & l_i \\ 0 & 0 & 0 & 1 \end{bmatrix}.$$

The position vector $^i r_i$ then becomes

$$^i r_i^T = \sum_{j=1}^{m_i} \delta_{ij} \left[u_{ij}, 0, 0, 0 \right] + \left[0, 0, l_i, 1 \right].$$

(2.7)

2.2 Dynamics

2.2.1 Lagrangian Formulation

The equation of manipulator motion can be derived from several techniques [Greenwood] [Meirovitch], but the Lagrangian Formulation is known for its simplicity and systematical approach. To compare with the Newton-Euler method [Craig], the Lagrangian is described in terms of work and energy with generalized coordinate to develop the system dynamics so that all the workless forces and constraint forces are not necessarily considered. Therefore, the resultant equations are generally compact and provide a closed form expression by joint torques and displacements.

In the case of flexible arms, the general coordinate (x) contains all the joint displacements and link deflections. The kinetic energy (KE) for a differential element is written then integrated over the link. The potential energy (PE) includes the stored energy due to joint and link deflections and the gravitational effect. Since the kinetic and potential energies are functions of x and $\dot{x}$, we can write Lagrange's formula as

$$\frac{d}{dt}\left(\frac{\partial KE}{\partial \dot{x}_i}\right) - \frac{\partial KE}{\partial x_i} + \frac{\partial PE}{\partial x_i} = Q_i,$$

(2.8)

since the potential energy (PE) is usually not a function of $\dot{x}$. Q_i is the generalized force corresponding to x_i, such that $Q_i \dot{x}_i$ is the power input to the system when x_i changes.

2.2.2 Kinetic Energy

In this section, the expression for the system kinetic energy is developed for use in Lagrange's equations. First of all, consider the kinetic energy of a point on

the ith link:

$$KE_i = \int_{\text{link}i} dKE_i = \frac{1}{2} \int_{\text{link}i} Trace \left(\frac{dr_i}{dt} \frac{dr_i^T}{dt} \right) dm, \qquad (2.9)$$

where dr/dt is called the velocity vector.

Taking the derivative of the transformation (2.3a) with respect to time,

$$\frac{dr_i}{dt} = \dot{T}_i \, {}^i r_i + T_i \, {}^i \dot{r}_i. \qquad (2.10)$$

Because of the recursive nature of the transformation chain, it is efficient to relate the position and velocity of a point transformation in the product. The velocity $\dot{T}_i$ and accelerations $\ddot{T}_i$ are easily derived by straight forward differentiation

$$\begin{aligned} \dot{T}_j &= \dot{\hat{T}}_{j-1} A_j + \hat{T}_{j-1} \dot{A}_j \\ &= \dot{\hat{T}}_{j-1} A_j + \hat{T}_{j-1} \frac{\partial A_j}{\partial q_j} \dot{q}_j, \end{aligned} \qquad (2.11a)$$

$$\begin{aligned} \ddot{T}_j &= \ddot{\hat{T}}_{j-1} A_j + 2\dot{\hat{T}}_{j-1} \dot{A}_j + \hat{T}_{j-1} \ddot{A}_j \\ &= \ddot{\hat{T}}_{j-1} + 2\dot{\hat{T}}_{j-1} \frac{\partial A_j}{\partial q_j} \dot{q}_j + \dot{\hat{T}}_{i-1} \frac{\partial^2 A_j}{\partial q_j^2} \ddot{q}_j. \end{aligned} \qquad (2.11b)$$

Since A_j is a function of the joint displacement (q_j), $\dot{T}_j$ and $\ddot{T}_j$ can be computed recursively from $\dot{\hat{T}}_{j-1}$ and $\ddot{\hat{T}}_{j-1}$. A similar approach is applied to find $\dot{\hat{T}}_{j-1}$ and its derivative with the transformation E_j which is a function of link deflection (δ_j).

$$\hat{T}_j = T_j E_j, \qquad (2.12a)$$

$$\begin{aligned} \dot{\hat{T}}_j &= \dot{T}_j E_j + T_j \dot{E}_j \\ &= \dot{T}_j E_j + T_j \sum_{k=1}^{m_i} \dot{\delta}_{jk} N_{jk}, \end{aligned} \qquad (2.12b)$$

$$\begin{aligned} \ddot{\hat{T}}_j &= \ddot{T}_j E_j + 2\dot{T}_j \dot{E}_j + T_j \ddot{E}_j \\ &= \ddot{T}_j E_j + 2\dot{T}_j \sum_{k=1}^{m_j} \dot{\delta}_{jk} N_{jk} + T_j \sum_{k=1}^{m_j} \ddot{\delta}_{jk} N_{jk}, \end{aligned} \qquad (2.12c)$$

where

$$N_{jk} = \begin{bmatrix} 0 & -\theta_{zjk} & \theta_{yjk} & u_{jk} \\ \theta_{zjk} & 0 & -\theta_{xjk} & v_{jk} \\ -\theta_{yjk} & \theta_{xjk} & 0 & w_{jk} \\ 0 & 0 & 0 & 0 \end{bmatrix} .$$

Differentiating the position vector related to the ith coordinate $^i r_i$ with respect to time becomes

$$^i \dot{r}_i = \sum_{j=1}^{m_i} \dot{\delta}_{ij} [u_{ij}, v_{ij}, w_{ij}, 0]^T . \tag{2.13}$$

Therefore, the kinetic energy for link i can be derived from (2.9) by integrating over the link.

$$KE_i = \frac{1}{2} \int_{\text{link}_i} (\dot{T}_i\, ^i r_i\, ^i r_i^T \dot{T}_i^T + 2\dot{T}_i\, ^i r_i\, ^i \dot{r}_i^T T_i + T_i\, ^i \dot{r}_i\, ^i \dot{r}_i^T T_i^T)\, dm . \tag{2.14}$$

Summing over all n links, one finds the system kinetic energy to be

$$KE = \sum_{i=1}^{n} \int_{\text{link}_i} dKE_i , \tag{2.15a}$$

$$KE = \sum_{i=1}^{n} Trace\, (\dot{T}_i B_{3i} \dot{T}_i^T + 2\dot{T}_i B_{2i} T_i^T + T_i B_{1i} T_i^T) , \tag{2.15b}$$

where

$$B_{1i} = \sum_{j=1}^{m_i} \sum_{k=1}^{m_i} \dot{\delta}_{ij} \dot{\delta}_{ik} C_{ikj} , \tag{2.15c}$$

and

$$C_{ikj} = \frac{1}{2} \int_{\text{link}_i} [u_{ik}, v_{ik}, w_{ik}, 0]^T [u_{ij}, v_{ij}, w_{ij}, 0]\, dm ; \tag{2.15d}$$

$$B_{2i} = \sum_{j=1}^{m_i} \dot{\delta}_{ij} C_{ij} + \sum_{k=1}^{m_i} \sum_{j=1}^{m_i} \delta_{jk} \dot{\delta}_{ij} C_{ikj} , \tag{2.15e}$$

and

$$C_{ij} = \frac{1}{2} \int_{\text{link}_i} [0, 0, z_i, 1]^T [u_{ij}, v_{ij}, w_{ij}, 0]\, dm ; \tag{2.15f}$$

$$B_{3i} = C_i + \sum_{j=1}^{m_i} \delta_{ij} [C_{ij} + C_{ij}^T] + \sum_{k=1}^{m_i} \sum_{j=1}^{m_i} \delta_{jk} \delta_{ij} C_{ikj} , \tag{2.15g}$$

and

$$C_i = \frac{1}{2} \int_{\text{link}i} [\,0, 0, z_i, 1\,]^T [\,0, 0, z_i, 1\,] \, dm \,. \qquad (2.15h)$$

It should be mentioned that the kinetic energy for rigid robotic arms can be obtained with the same procedure without considering link deflection [Hollerbach], and the steps leading to these terms are found in the reference [Book,1983]. With assumption of separation of variables, the link deflection is described by a product of generalized coordinates and normal modes. Normal modes can be found by finite element techniques for irregular link cross sections for given boundary conditions as will be discussed in the next chapter.

Alternatively, the kinetic energy can be expressed by

$$KE = \sum_{i=1}^{n} KE_i = \frac{1}{2} \sum_{i=1}^{n} \dot{x}_i^T M \dot{x}_i = \frac{1}{2} \sum_{j=1}^{n} \sum_{k=1}^{n} M_{jk} \dot{x}_j \dot{x}_k \,, \qquad (2.16)$$

where the M_{ij} are the elements of the inertial matrix M and $\dot{x}_j$ is the velocity vector including all generalized velocities, for example, $\dot{q}_j$ and $\dot{\delta}_{jk}$.

To equate (2.15b) and (2.16), first let the derivative of T_i with respect to time be

$$\dot{T}_i = \sum_{h=1}^{i} \hat{T}_{h-1} U_h \tilde{T}_i \dot{q}_h + \sum_{h=1}^{i-1} \sum_{k=1}^{m_h} T_h N_{hk} {}^h\hat{T}_i \dot{\delta}_{hk} \,, \qquad (2.17a)$$

where

$$U_h = \frac{\partial A_h}{\partial q_h} \,,$$

and

$$
\begin{aligned}
T_i &= A_1 E_1 A_2 E_2 \cdots A_h E_h \cdots E_{i-1} A_i \\
&= \hat{T}_{h-1} A_h E_h {}^h\hat{T}_i \\
&= \hat{T}_{h-1} A_h {}^h\tilde{T}_i \\
&= T_h E_h {}^h\hat{T}_i \,,
\end{aligned}
\qquad (2.17b)
$$

where

$$\hat{T}_{h-1} = A_1 E_1 \cdots A_{h-1} E_{h-1}$$

$$^h\tilde{T}_i = E_h A_{h+1} \cdots E_{i-1} A_i \qquad (2.17c)$$

$$^h\hat{T}_i = A_{h+1} E_{h+1} \cdots E_{i-1} A_i$$

In order to derive the inertia matrix in (2.16), it is convenient to define the following:

$$D_{ik} = C_{ik} + \sum_{l=1}^{m_i} \delta_{il} C_{ilk} \,, \qquad (2.18a)$$

$$F_i = C_i + \sum_{k=1}^{m_i} \delta_{ik} \left[(C_{ik} + C_{ik}^T) + \sum_{j=1}^{m_i} \delta_{ij} C_{ijk} \right]. \qquad (2.18b)$$

Then, through exchanging the trace and sum operation and collecting the terms along with arranging them for efficient computation, the inertia coefficients in (2.16) are divided into three groups: the joint angles $\dot{q}_i \dot{q}_j$, the joint angle and link deflection $\dot{q}_i \dot{\delta}_{jk}$, and the link deflections $\dot{\delta}_{ik} \dot{\delta}_{jl}$.

All occurances of $\dot{q}_i \dot{q}_j$ are in the first term of the right-hand side of equation (2.15b).

$$\frac{1}{2} \sum_{i=1}^{n} \sum_{\alpha=1}^{i} \sum_{h=1}^{i} Trace \left[(\tilde{T}_{\alpha-1} U_\alpha \,^\alpha\tilde{T}_i) F_i (\hat{T}_{h-1} U_h \,^h\tilde{T}_i)^T \right] \dot{q}_\alpha \dot{q}_h \,. \qquad (2.19a)$$

However, the inertia coefficients of $\dot{q}_i \dot{\delta}_{jk}$ come from the first and second terms of equation (2.15b) and are shown as

$$\frac{1}{2} \sum_{i=1}^{n} \sum_{h=1}^{i} \left\{ \sum_{\alpha=1}^{i-1} \sum_{\beta=1}^{m_\alpha} Trace \left[(\hat{T}_{h-1} U_h \,^h\tilde{T}_i) F_i (T_\alpha N_{\alpha\beta} \,^\alpha\hat{T}_i)^T \right] \dot{q}_h \dot{\delta}_{\alpha\beta} \right.$$

$$\left. + \sum_{j=1}^{m_i} 2 Trace \left[(\hat{T}_{h-1} U_h \,^h\tilde{T}_{h-1} U_h \,^h\tilde{T}_i) D_{ij} T_i^T \right] \dot{q}_h \dot{\delta}_{ij} \right\} . \qquad (2.19b)$$

The three terms of the right-hand side of equation (2.15b) which include $\dot{\delta}_{ik} \dot{\delta}_{jl}$

are expressed as follows:

$$\frac{1}{2} \sum_{i=1}^{n} \left\{ \sum_{h=1}^{i-1} \sum_{k=1}^{m_h} \left(\sum_{\alpha=1}^{i-1} \sum_{\beta=1}^{m_\alpha} Trace \left[(T_h N_{hk} \, {}^h\hat{T}_i) F_i (T_\alpha N_{\alpha\beta} \, {}^\alpha\hat{T}_i)^T \right] \dot{\delta}_{hk} \dot{\delta}_{\alpha\beta} \right. \right.$$

$$\left. + 2 Trace \left[(T_h N_{hk} \, {}^h\hat{T}_i) D_{ik} T_i^T \right] \dot{\delta}_{hk} \dot{\delta}_{ij} \right) + \sum_{j=1}^{m_i} \sum_{k=1}^{m_i} Trace \left[T_i C_{ikj} T_i^T \right] \dot{\delta}_{ij} \dot{\delta}_{ik} \left. \right\} .$$

$$(2.19c)$$

2.2.3 Potential Energy

In addition to the computation of the kinetic energy, we need to find the potential energy in order to derive Lagrange's equations of motion for the dynamic system. The potential energy of the system arises from three sources as considered here: joint elasticity, gravity and link deformation. The first term is associated with joint coordinate q_i, the second term is a function of position, and the last term, called the strain energy, results from the energy stored in the link due to deformation. Therefore, the potential energy related to the gravity and link deflection can be derived from integrating over the length of the individual link, and then summing over all links.

2.2.3.1 Elastic Joint Potential Energy

We consider an n-link manipulator with revolute joints, and model the elasticity of the ith joint as an equivalent torsional spring with stiffness K_{ei} since each kinematic joint is actuated directly with some sort of actuator. However for a linear actuator used to rotate a revolute joint through the use of a four-bar linkage, the equivalent stiffness can be found by the corresponding transformation between joint and measurement spaces [Craig,1986].

The coordinate $\bar{q}_i$ in the joint transformation A_i along with the equivalent stiffness K_{ei} constitute the elastic joint potential energy which does not involve the

coordinates associated with link deflections. The formula for this potential energy is described as

$$PE_e = \sum_{i=1}^{n} PE_{ei} = \sum_{i=1}^{n} \frac{1}{2} K_{ei} \bar{q}_i^2 \,. \tag{2.20}$$

Note that the coordinate $\bar{q}_i$ is measured from the unstretched position q_{0i} to q_i. In other words, the elastic joint potential energy has the positive value relative to the "basic energy" which is a function of q_{0i}.

2.2.3.2 Gravity Potential Energy

In robotic arms with elasticity, the gravity potential energy for a differential element on the ith link is

$$dPE_{gi} = -g^T T_i \, {}^i r_i \, dm \,, \tag{2.21a}$$

where the gravity vector g has the form

$$g^T = [\, g_x, g_y, g_z, 0 \,] \,. \tag{2.21b}$$

Integrating over the link and summing over all links, the gravity potential energy becomes

$$PE_g = -g^T \sum_{i=1}^{n} T_i h_i \,, \tag{2.22a}$$

where

$$h_i = m_i h_{mi} + \sum_{k=1}^{m_i} \delta_{ik} \epsilon_{ik} \,, \tag{2.22b}$$

m_i = the total mass of link i, $h_{mi} = [\, 0, 0, h_{zi}, 1 \,]^T$ = a vector to the center of gravity from joint i (undeformed), and

$$\epsilon_{ik} = \int_0^{l_i} [\, u_{ik}, v_{ik}, w_{ik}, 0 \,]^T \, dm \,. \tag{2.22c}$$

From the above we know that if the link is homogeneous, the total distance of the center of gravity is the addition of those of the deformed and undeformed parts.

However, the gravity potential energy is a function of generalized coordinates, q_i and δ_{ij}.

2.2.3.3 Link Strain Potential Energy

The link deflection for a slender beam is assumed to be a linear combination of the general coordinates $\delta_{ik}(t)$ and mode shapes u_{ik}, v_{ik} and w_{ik} in x, y and z axes respectively, while the rotational components θ_{zik} of the link deflection are taken into account in the z axis. Compression is not initially included as it is generally much smaller. With a truncated modal approximation for the ith link deformation, the equation in the x-direction is shown as

$$u_{xi} = \sum_{k=1}^{m_i} \delta_{ik} u_{ik} \, . \qquad (2.23a)$$

v_{yi} is then represented in y-direction and

$$\theta_{iz} = \sum_{k=1}^{m_i} \delta_{ik} \theta_{zik} \, . \qquad (2.23b)$$

The strain potential energy related to the link deformation which is integrated along the z_i-axis coincident with the link is described as

$$PE_{di} = \frac{1}{2} \int_0^{l_i} \left[EI_x (\frac{\partial^2 u_{xi}}{\partial z_i^2})^2 + EI_y (\frac{\partial^2 v_{yi}}{\partial z_i^2})^2 + E_G J_z (\frac{\partial \theta_{zi}}{\partial z_i})^2 \right] dz_i \, , \qquad (2.24)$$

where E is Young's modulus of elasticity and I_x and I_y are the area moments of inertia of the link about an axis parallel to the x and y axes, respectively, and through the centroid of the cross section. E_G is the shear modulus and J_z is the polar area moment of inertia of the link.

By taking the modal summations (2.23) and its corresponding y-component, the link strain potential energy of the ith link PE_i can also be represented by summation of the potential energies in x, y and z directions. Those are PE_{xi}, PE_{yi}

and PE_{zi}.

$$PE_{xi} = \frac{1}{2} \int_0^{l_i} EI_x \left(\sum_{j=1}^{n} \delta_{ij} \frac{d^2 u_{ij}}{dz_i^2} \right) \left(\sum_{k=1}^{n} \delta_{ik} \frac{d^2 u_{ik}}{dz_i^2} \right) dz_i$$

$$= \frac{1}{2} \sum_{j=1}^{m_i} \sum_{k=1}^{m_i} \delta_{ij} \delta_{ik} \left(\int_0^{l_i} EI_x \frac{d^2 u_{ij}}{dz_i^2} \frac{d^2 u_{ik}}{dz_i^2} dz_i \right) ,$$

(2.25a)

$$PE_{yi} = \frac{1}{2} \sum_{j=1}^{m_i} \sum_{k=1}^{m_i} \delta_{ij} \delta_{ik} \left(\int_0^{l_i} EI_y \frac{d^2 v_{ij}}{dz_i^2} \frac{d^2 v_{ik}}{dz_i^2} dz_i \right) , \qquad (2.25b)$$

$$PE_{zi} = \frac{1}{2} \sum_{j=1}^{m_i} \sum_{k=1}^{m_i} \delta_{ij} \delta_{ik} \left(\int_0^{l_i} E_G J_z \frac{d\theta_{zij}}{dz_i} \frac{d\theta_{zik}}{dz_i} dz_i \right) . \qquad (2.25c)$$

Summing the above equations, PE_{di} in (2.24) then becomes

$$PE_{di} = \frac{1}{2} \sum_{j=1}^{m_i} \sum_{k=1}^{m_i} \delta_{ij} \delta_{ik} \left(K_{xijk} + K_{yijk} + K_{zijk} \right), \qquad (2.26)$$

where K_{xijk}, K_{yijk} and K_{zijk} are stiffness coefficients.

$$K_{xijk} = \int_0^{l_i} EI_x \frac{d^2 u_{ij}}{dz_i^2} \frac{d^2 u_{ik}}{dz_i^2} dz_i ,$$

$$K_{yijk}, K_{zijk} = etc.$$

Note that the stiffness coefficient must be symmetric, for example, $K_{xijk} = K_{xikj}$. The link strain potential energy for the total system PE_d can therefore be written as

$$PE_d = \frac{1}{2} \sum_{i=1}^{n} \sum_{j=1}^{m_i} \sum_{k=1}^{m_i} \delta_{ij} \delta_{ik} K_{dijk} , \qquad (2.27)$$

where $K_{dijk} = K_{xijk} + K_{yijk} + K_{zijk}$.

It is mentioned that PE_d is independent of q_i, the joint coordinate. In fact, equation (2.27) can be made much more general than the initial assumptions regarding the link strain energy. Compression strain energy and link forms other than

beams, for example, can also be represented in this form. The values of coefficients K_{dijk} can be determined analytically or numerically, e.g. by finite element methods.

2.2.4 Equations of Motion

The Lagrangian formulation (2.8) leads to a compact system of equations which is appealing from both the dynamic modeling and control engineering points of view. To continue the development, it is convenient to define all generalized coordinates as x_{ij} and let

$$x_{ij} = \begin{cases} q_i & j = 0 \\ \delta_{ij} & j = 1, 2, \cdots, m_i \end{cases} \tag{2.28}$$

By collecting (2.19a), (2.19b) and (2.19c), the kinetic energy thus becomes summation of coordinates $\dot{x}_{ij}\dot{x}_{\alpha\beta}$ multiplying the inertia coefficient $m_{ij\alpha\beta}$, which is analogous to (2.16).

$$KE = \frac{1}{2} \sum_{i=1}^{n} \sum_{j=0}^{m_i} \sum_{\alpha=1}^{n} \sum_{\beta=0}^{m_\alpha} m_{ij\alpha\beta}\dot{x}_{ij}\dot{x}_{\alpha\beta} . \tag{2.29}$$

The potential energy for the elastic joint (2.20) is then

$$PE_e = \frac{1}{2} \sum_{i=1}^{n} K_{ei}\bar{x}_{i0}^2 . \tag{2.30}$$

Note that j equals to 0 since the link deflection is not involved in this case. The gravity energy is a function of position so that it can be represented as

$$PE_g = PE_g(x_{ij}) \begin{cases} i = 1, \cdots, n \\ j = 0, \cdots, m_i \end{cases} . \tag{2.31}$$

Furthermore, the link strain potential energy (2.27) which does not involve the joint coordinate is shown as

$$PE_d = \frac{1}{2} \sum_{i=1}^{n} \sum_{j=1}^{m_i} \sum_{k=1}^{m_i} K_{dijk}x_{ij}x_{ik} . \tag{2.32}$$

Now we are going to derive the Lagrangian equation of motion. Since $m_{ij\alpha\beta}$ is a function of x_{ij} or $x_{\alpha\beta}$ in (2.29), the first term in (2.8) is computed as

$$
\begin{aligned}
\frac{d}{dt}\left(\frac{\partial KE}{\partial \dot{x}_{pq}}\right) &= \frac{d}{dt}\left(\sum_{i=1}^{n}\sum_{j=0}^{m_i} m_{ijpq}\dot{x}_{ij}\right) \\
&= \sum_{i=1}^{n}\sum_{j=0}^{m_i} m_{ijpq}\ddot{x}_{ij} + \sum_{i=1}^{n}\sum_{j=0}^{m_i} \frac{dm_{ijpq}}{dt}\dot{x}_{ij} \\
&= \sum_{i=1}^{n}\sum_{j=0}^{m_i} m_{ijpq}\ddot{x}_{ij} + \sum_{i=1}^{n}\sum_{j=0}^{m_i}\sum_{\alpha=1}^{n}\sum_{\beta=0}^{m_\alpha} \frac{\partial m_{ijpq}}{\partial x_{\alpha\beta}}\dot{x}_{ij}\dot{x}_{\alpha\beta} .
\end{aligned}
\tag{2.33}
$$

The second term in (2.8) includes the partial derivative of the kinetic energy given by

$$
\begin{aligned}
\frac{\partial KE}{\partial x_{pq}} &= \frac{\partial}{\partial x_{pq}}\left(\frac{1}{2}\sum_{i=1}^{n}\sum_{j=0}^{m_i}\sum_{\alpha=1}^{n}\sum_{\beta=0}^{m_\alpha} m_{ij\alpha\beta}\dot{x}_{ij}\dot{x}_{\alpha\beta}\right) \\
&= \frac{1}{2}\sum_{i=1}^{n}\sum_{j=0}^{m_i}\sum_{\alpha=1}^{n}\sum_{\beta=0}^{m_\alpha} \frac{\partial m_{ij\alpha\beta}}{\partial x_{pq}}\dot{x}_{ij}\dot{x}_{\alpha\beta} .
\end{aligned}
\tag{2.34}
$$

Taking the partial derivative of the potential energies of the elastic joint and the link deflection leads to

$$
\frac{\partial(PE_e + PE_d)}{\partial x_{pq}} = \sum_{l=0}^{m_i} K_{plq}x_{pl} ,
\tag{2.35}
$$

where

$$
K_{plq} = \begin{cases} K_e \text{ in } (2.20) & \text{when } l = 0 \\ K_{dijk} \text{ in } (2.27) & \text{when } l \neq 0 \end{cases} .
\tag{2.36}
$$

And the gravity term comes from (2.22) or (2.31).

$$
\frac{\partial PE_g}{\partial x_{pq}} = \begin{cases} -g^T \sum_{i=p}^{n} \frac{\partial T_i}{\partial x_{pq}} h_i - g^T T_p \epsilon_{pq} & \text{when } q \neq 0 \\ -g^T \sum_{i=p}^{n} \frac{\partial T_i}{\partial x_{pq}} h_i & \text{when } q = 0 \end{cases} .
\tag{2.37}
$$

Note that $\sum_{i=p}^{n} \frac{\partial T_i}{\partial x_{pq}} = \frac{\partial A_n}{\partial q_n} = 0$ when $p = n$ and $q \neq 0$. Henceforth, the gravity term is a function of x_{pq} and we define $G(x) = [G_{pq}]$ with elements (2.37).

Finally, combining (2.33), (2.34), (2.35) and (2.37), we can obtain the equations of motion for x_{pq}.

$$\sum_{i=1}^{n}\sum_{j=0}^{m_i} m_{ijpq}\ddot{x}_{ij}$$

$$+ \sum_{i=1}^{n}\sum_{j=0}^{m_i}\sum_{\alpha=1}^{n}\sum_{\beta=0}^{m_\alpha} H_{ij\alpha\beta pq}\dot{x}_{ij}\dot{x}_{\alpha\beta} \qquad (2.38a)$$

$$+ \sum_{l=0}^{m_l} K_{plq}x_{pl} + G_{pq} = Q_{pq} ,$$

where

$$H_{ij\alpha\beta pq} = \frac{\partial m_{ijpq}}{\partial x_{\alpha\beta}} - \frac{1}{2}\frac{\partial m_{ij\alpha\beta}}{\partial x_{pq}} . \qquad (2.38b)$$

Note that Q_{pq} is the generalized forces which are assumed to act on the individual joint. Therefore,

$$Q_{pq} = 0 \text{ when } q \neq 0 . \qquad (2.39)$$

The dynamic equation (2.38) can also be written in Matrix-Vector form as

$$M(x)\ddot{x} + H(x,\dot{x})\dot{x} + Kx + G(x) = Q . \qquad (2.40)$$

In the above equation (2.40), we ignore friction, backlash and other disturbances that are called uncertainties, $R(x,\dot{x})$. Those will be included when the feedback control applied. K is known as the stiffness matrix.

2.2.4.1 Some Properties of Coefficient Matrices

To compare (2.40) with (2.38a), the inertia matrix $M(x)$ and coupling matrix $H(x,\dot{x})$ can defined as $[m_{ijpq}]$ and $[H_{ijpq}]$ respectively, while the element of the vector x corresponds to x_{ij} in (2.38a). In the following, it is illustrated that the inertia matrix is positive definite as well as symmetric and $(\dot{M} - 2H)$ is skew-symmetric.

From equation (2.10), $\dot{r}_i$ can also be represented as

$$\dot{r}_i = J_i \dot{x} , \qquad (2.41)$$

where J_i is the $4 \times [n \times (m_i + 1)]$ matrix. Then, the kinetic energy on the ith link (2.9) becomes

$$KE_i = \frac{1}{2} \int_{\text{link } i} Tr(\dot{x} J_i^T J_i \dot{x}) \, dm , \qquad (2.42)$$

where $J_i^T J_i$ is symmetric. Summing over all n links, one finds the corresponding equation (2.29) in a scalar form. Therefore, it is again shown that $[m_{ij\alpha\beta}]$ in (2.29) or $[m_{ijpq}]$ in (2.38) is symmetric.

The kinetic energy in (2.29) can be expressed as a quadratic form in the generalized velocities and is a positive value by physical reasoning. The necessary and sufficient conditions for this are that the inertia matrix satisfies positive definiteness, unless the system is at rest.

The coupling element which represents the coefficient in the second term in (2.38a) has the following relation:

$$\sum_{i=1}^{n} \sum_{j=0}^{m_i} \sum_{\alpha=1}^{n} \sum_{\beta=0}^{m_\alpha} \left(\frac{\partial m_{ijpq}}{\partial x_{\alpha\beta}} - \frac{\partial m_{ij\alpha\beta}}{\partial x_{pq}} \right) \dot{x}_{ij} \dot{x}_{\alpha\beta}$$

$$= \frac{1}{2} \sum_{i=1}^{n} \sum_{j=0}^{m_i} \left[\sum_{\alpha=1}^{n} \sum_{\beta=0}^{m_\alpha} \frac{\partial m_{ijpq}}{\partial x_{\alpha\beta}} \dot{x}_{\alpha\beta} \right] \dot{x}_{ij}$$

$$+ \frac{1}{2} \sum_{i=1}^{n} \sum_{j=0}^{m_i} \left[\sum_{\alpha=1}^{n} \sum_{\beta=0}^{m_\alpha} \left(\frac{\partial m_{\alpha\beta pq}}{\partial x_{ij}} - \frac{\partial m_{\alpha\beta ij}}{\partial x_{pq}} \right) \dot{x}_{\alpha\beta} \right] \dot{x}_{ij} \qquad (2.43)$$

By comparing it with (2.40) and defining the element of the coupling matrix H as $[H_{ijpq}]$, we can derive

$$[H_{ijpq}] = \frac{1}{2} \sum_{\alpha=1}^{n} \sum_{\beta=0}^{m_\alpha} \frac{\partial m_{ijpq}}{\partial x_{\alpha\beta}} \dot{x}_{\alpha\beta} + \frac{1}{2} \sum_{\alpha=1}^{n} \sum_{\beta=0}^{m_\alpha} \left(\frac{\partial m_{\alpha\beta pq}}{\partial x_{ij}} - \frac{\partial m_{\alpha\beta ij}}{\partial x_{pq}} \right) \dot{x}_{\alpha\beta}$$

$$= \frac{1}{2} [\dot{m}_{ijpq}] + \frac{1}{2} \sum_{\alpha=1}^{n} \sum_{\beta=0}^{m_\alpha} \left(\frac{\partial m_{\alpha\beta pq}}{\partial x_{ij}} - \frac{\partial m_{\alpha\beta ij}}{\partial x_{pq}} \right) \dot{x}_{\alpha\beta} \qquad (2.44)$$

Defining $W = \dot{M} - 2H$, the above (2.44) gives

$$W_{ijpq} = \sum_{\alpha=1}^{n} \sum_{\beta=0}^{m_\alpha} \left(\frac{\partial m_{\alpha\beta pq}}{\partial x_{ij}} - \frac{\partial m_{\alpha\beta pq}}{x_{pq}} \right) \dot{x}_{\alpha\beta} , \qquad (2.45a)$$

and

$$W_{pqij} = \sum_{\alpha=1}^{n} \sum_{\beta=0}^{m_\alpha} \left(\frac{\partial m_{\alpha\beta ij}}{\partial x_{pq}} - \frac{\partial m_{\alpha\beta pq}}{\partial x_{ij}} \right) \dot{x}_{\alpha\beta} . \qquad (2.45b)$$

$$= -W_{ijpq}$$

This shows that $(\dot{M} - 2H)$ is skew-symmetric; i.e., $W + W^T = 0$. By setting $m_\alpha = 0$ in (2.43), it becomes the case of rigid robotic arms, which was found in reference [Asada, 1986].

2.3 Summary

A transformation between two coordinates which includes rigid body motion and deformation has been established in the form of a 4 × 4 matrix. Therefore, any point on the robotic arm can be described from the base coordinate in terms of those transformations. The kinetic and potential energies have been obtained by integrating the velocity and position of a point over the total system. These energies were used in Lagrangian equations. It is noted that the structures of the equations of motion for rigid [Asada,1986] and flexible robotic arms are very similar as given in equation (2.40); while the generalized coordinate variables are different for those two cases. Additional variables, namely the deflection coordinates δ_{ij}, are used to describe the link deformation so that the stiffness coefficient in (2.40) originates from the strain energy. Furthermore, the inertia matrix is shown to be symmetric as well as positive definite and the matrix $W = M - 2H$ is skew-symmetric.

So far, some uncertainties, such as friction, backlash and actuator dynamics have not been modeled and a revolute joint must connect two links. The flexible deformation which is valid for small deflection of the link is represented by a product

of mode shapes and time-dependent coordinates, while the structural damping is not involved. Nevertheless, the proper mode shape is the determining factor for dynamics, especially the system natural frequency, and will be discussed next.
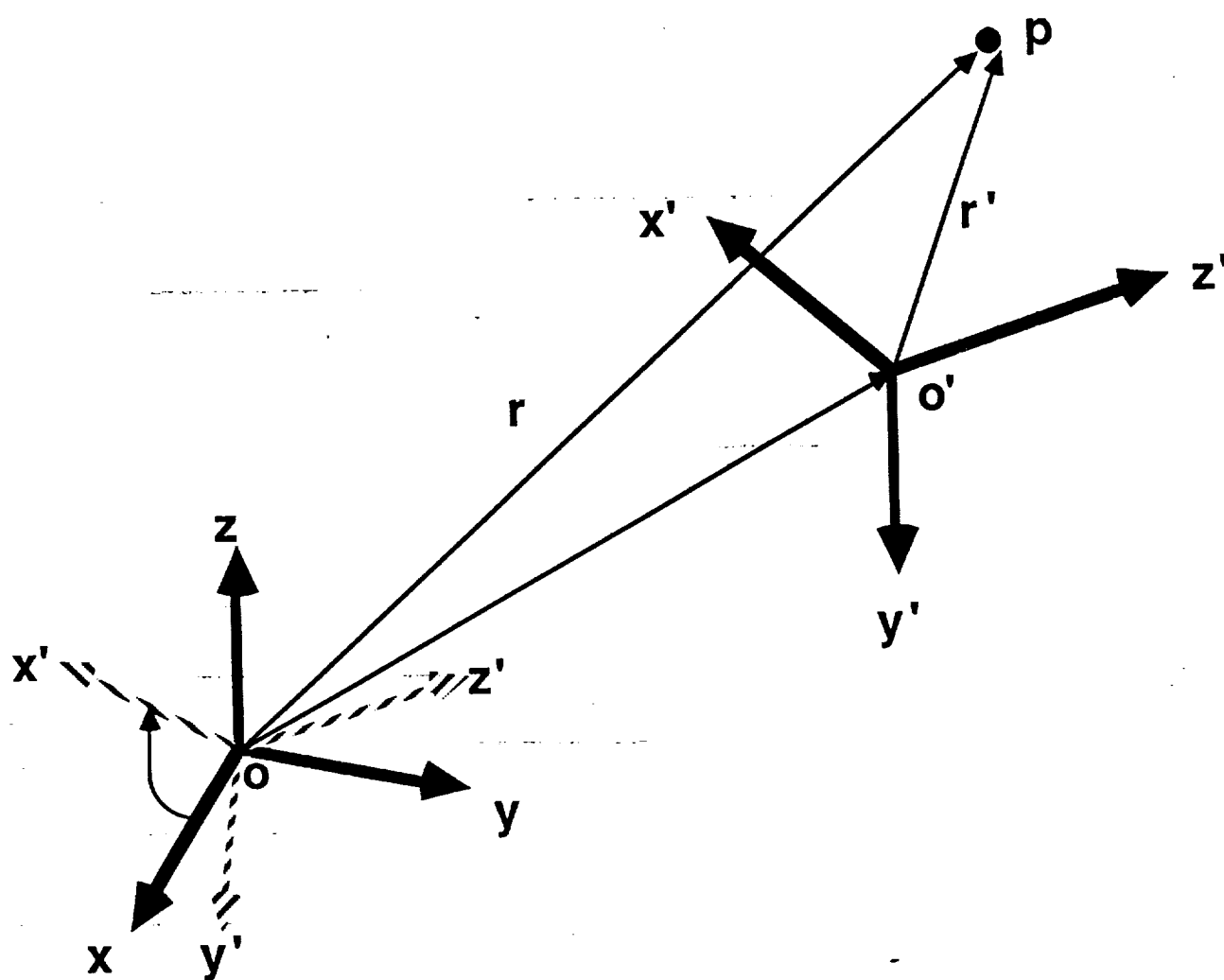
Figure 2.1 Coordinate transformation.
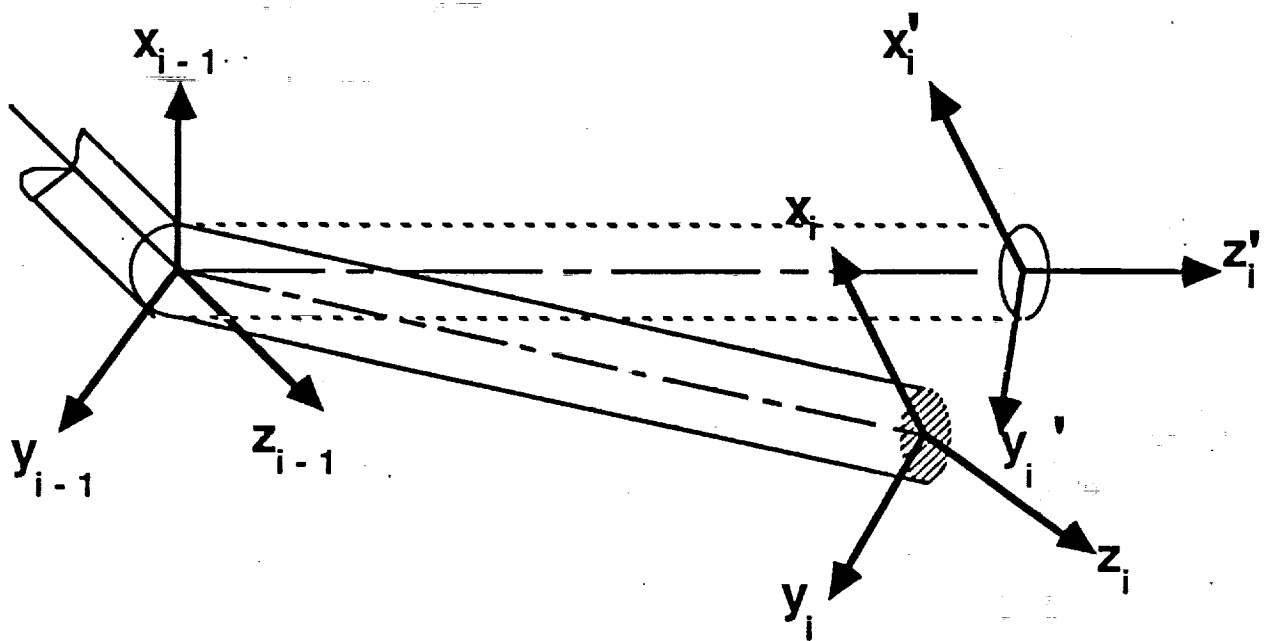
Figure 2.2 Transformation due to rigid rotation and link deflection.
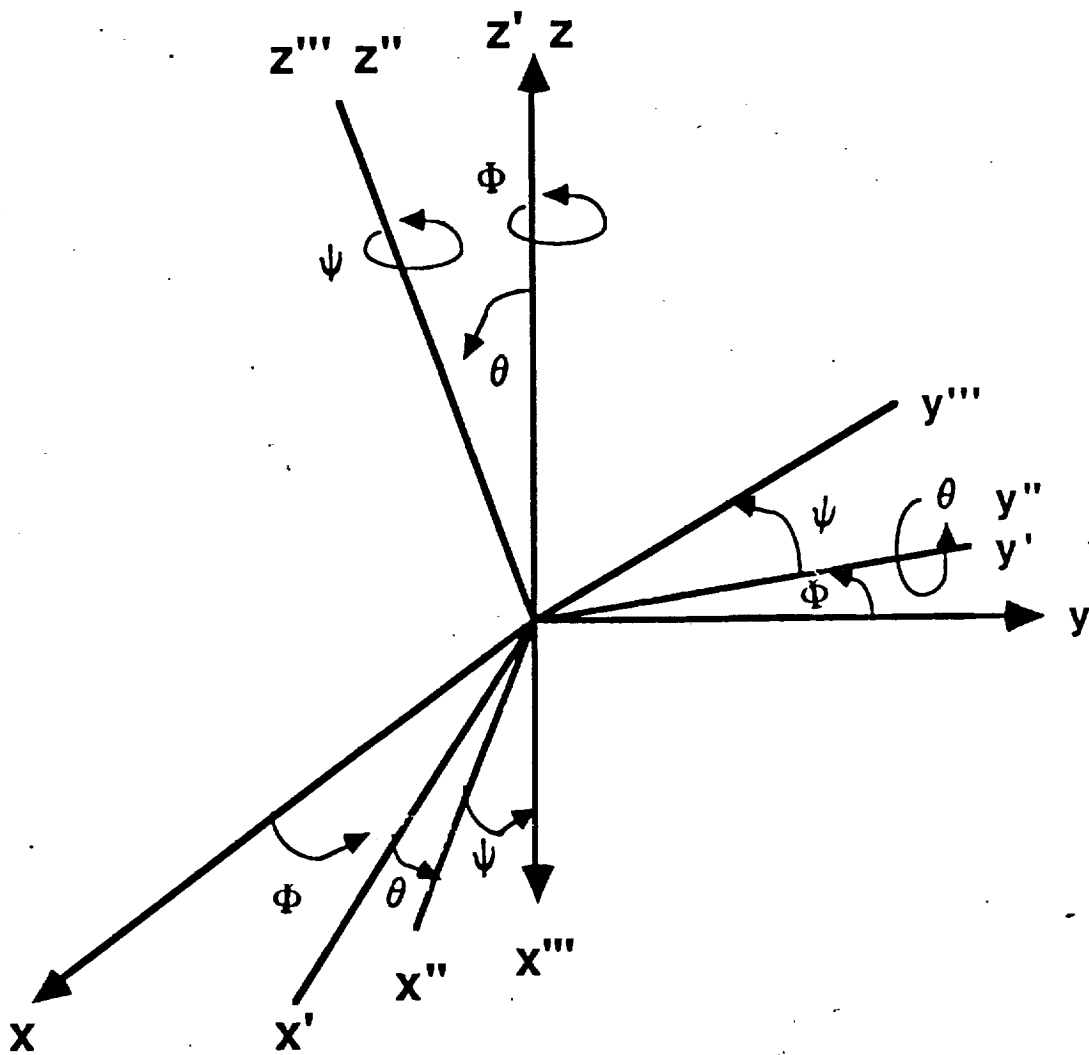
Figure 2.3 Euler transformation.
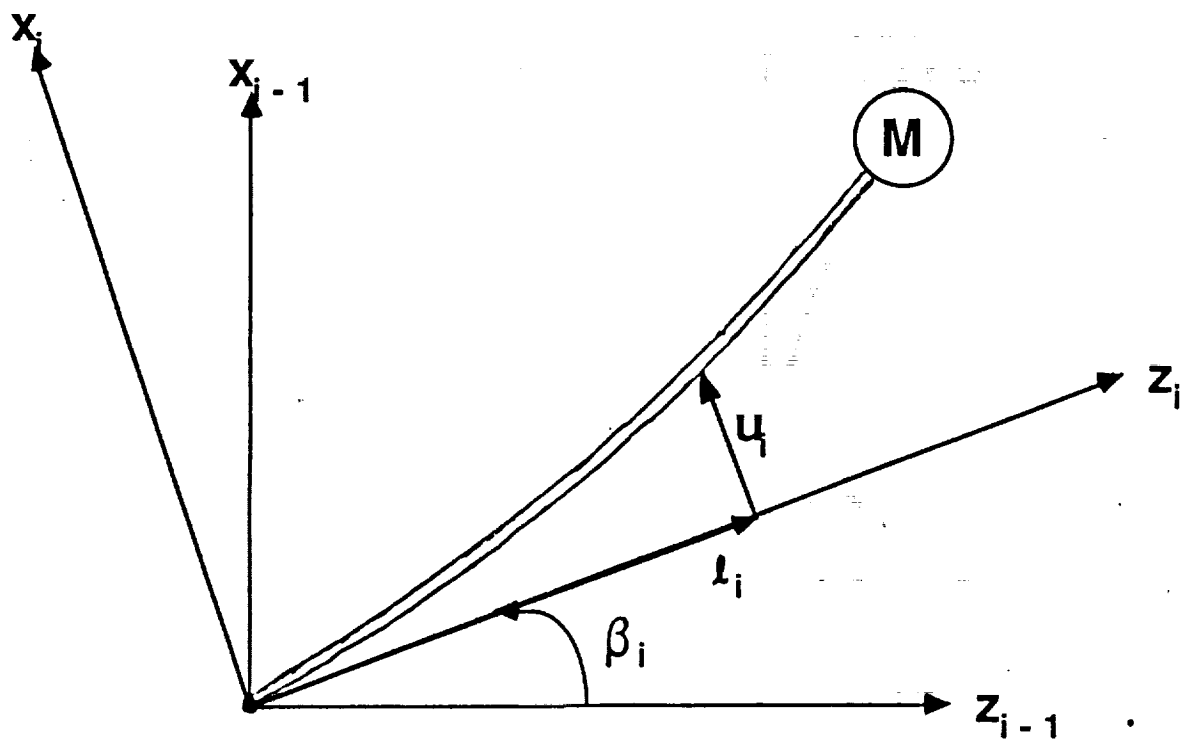
Figure 2.4 Point position coordinate.

CHAPTER III

VERIFICATION OF SYSTEM DYNAMICS

In this chapter, two prototype models of flexible robotic arms are used to verify the dynamic equations obtained from the previous chapter. The frequency and time responses are two approaches one can use to demonstrate agreement between analytical and experimental results. The actuator dynamics will be considered in this chapter because it is essential from the experimental point of view. However, a linear case has been adapted for comparing analytical and experimental results, using sufficiently slow and small motion of the links.

3.1 Two Cases of Experimental Setup

There have been two different experiments established at the Flexible Automation Laboratory at Georgia Tech. The first experimental apparatus (Figure 3.1) is a one-link flexible manipulator driven by an electric torque motor. The arm, which is a four foot aluminum beam with the section oriented so that there is increased flexibility in the horizontal plane. Two strain gauges mounted at the base and at mid-length of the beam measure the link deflection. Table 3.1 lists the physical properties [Hastings, 1986].

The other apparatus is a two link manipulator, RALF (Robotic Arm, Large and Flexible), with a parallel mechanism (Figure 3.2). Each link is a cylindrical hollow beam, ten feet long. The parallel mechanism's function is force transmission for the upper link which is made of rectangular shape. The weight of the robotic structure is about seventy pounds. More details are given in Table 3.2. The analytical work involved is more complicated than the first case.

3.2 The Case of a One-Link Flexible Manipulator

The process of forming the dynamic model for flexible manipulators has been discussed in the last chapter. One difference from the rigid manipulator is the existence of the stiffness term in (2.40) which determines the system vibration due to the flexible link deflection. Since the one-link beam moves only in the horizontal plane, the flexible deflection is simply described by an infinite series of separable modes without regard to the structural damping effect. In other words, the deflections in x- and z-directions of E_1 in (2.6) has been ignored and the deflection in y-direction is given by

$$v(z,t) = \sum_{i=1}^{n} v_i(z)\delta_i(t).$$

(3.1)

However, the first few modes will be accurate enough to describe the flexible deflection because the amplitudes of higher modes of the flexible link are small compared to the amplitudes of the lower modes. Here, n is selected to be 2. The transformation of a rigid-body motion has been expressed as A_1 in (2.6). Thus, the equation of motion can be derived as presented in Appendix 1.

3.2.1 Comparison of System Frequencies

The beam, directly driven by the torque motor (which is here considered as a high bandwidth torque source), is controlled by feedback signals from the joint in the case of a one-link manipulator. Therefore, the clamped-mass boundary conditions are imposed such that the mode shapes $v_i(z)$ in (3.1) can be derived from the Bernoulli-Euler beam formulation. Because it is a simple structure, the solution can be obtained analytically [Sangveraphusiri]. It should be noted that the numerical result by finite element methods shows agreement of mode shapes in Figures 3.3-3.4. Table 3.3 compares the measured modal frequencies (see Figure 3.5) to those computed from the linear dynamical equations with the mode shapes using the

analytical and finite element methods.

When a small amount of proportional damping is employed, the simulations of the dynamic motion with two modes result in the plots shown in Figure 3.6a for a step change in the desired joint angle. Note that joint feedback has been implemented in this case. The strain measurement at the base is shown in Figure 3.6b. It can be seen that the model implemented with only the first few modes produces results that agree with the experimental data [Hastings, 1986]. Therefore, one concludes that the best mode shape as determined by the boundary conditions is one of the main characteristics of the system. Obviously, the clamped-mass shape is acceptable in representing the link deflection in this case.

3.3 The Case of RALF

The total system of RALF should include the actuator dynamics in addition to the two-link manipulator with a parallel mechanism. Hydraulic actuators are here employed to drive the structure. Since the actuator has an equivalent stiffness for its dynamical characteristic, natural frequencies of the total system may differ from the original static system. Therefore, the hydraulic motors will be discussed first.

3.3.1 Dynamic Representation of Hydraulic Motors

The nonlinear model of the hydraulic system is based on the following [Merritt] [Lai, Nair]

(1) negligible line dynamics and line losses

(2) constant replenishing pressure

(3) negligible external leakage

(4) constant fluid properties

(5) simplified servovalve dynamics

The linearized servovalve flow equation is

$$Q_L = K_q x_v - K_c P_L \, , \qquad (3.2)$$

where

Q_L : load flow,

K_q : valve flow gain,

x_v : valve (stroke) position,

K_c : valve flow-pressure coefficient,

P_L : load pressure difference.

Application of the continuity equation to the motor chamber yields the following formulation for the displacement of piston (x_p).

$$Q_L = A_p \dot{x}_p + C_p P_L + \frac{V_t}{\beta_e} \dot{P}_L \, , \qquad (3.3)$$

where

A_p : area of piston,

C_p : total leakage coefficient,

V_t : total volume of fluid in chambers,

β_e : effective bulk modulus of system.

Applying Newton's Second Law to the forces on the piston, the resulting force equation is

$$F_g = A_p P_L = M_t \ddot{x}_p + F_L \, , \qquad (3.4)$$

where

F_g : force generated or developed by piston,

M_t : mass of piston,

F_L : arbitrary load force on piston.

Finally, equations (3.2), (3.3) and (3.4) are the three basic equations for the hydraulic system and may be solved simultaneously by Laplace Transformation:

$$x_p = \frac{\frac{K_q}{A_p} x_v - \frac{K_{ce}}{A_p^2} \left(1 + \frac{V_t}{\beta_e K_{ce}} s \right) F_L}{s \left(\frac{s^2}{\omega_h^2} + \frac{2\xi_h}{\omega_h} s + 1 \right)} , \qquad (3.5)$$

where K_{ce} = total flow-pressure coefficient,

$$\omega_h = \left[\frac{\beta_e A_p^2}{V_t M_t} \right]^{1/2} = \text{hydraulic natural frequency} , \qquad (3.5a)$$

$$\xi_h = \frac{K_{ce}}{A_p} \left[\frac{\beta_e M_t}{4 V_t} \right]^{1/2} = \text{damping ratio} . \qquad (3.5b)$$

Note that the details for the hydraulic system used here are listed in Appendix 2 [Huggins]. The parameter ω_h is the natural frequency due to interaction of the inertia with the trapped oil springs and is very important because it establishes the overall speed of response of the valve-motor combination. Therefore, we can obtain the hydraulic spring rate k_h from ω_h, while k_h is simply a useful concept in computing hydraulic natural frequencies and interpreting dynamic response,

$$k_h = \frac{\beta_e A_p^2}{V_t} . \qquad (3.6)$$

In general, the bandwidth of the servovalve and amplifier used as parts of the hydraulic circuit are much higher than that of the motor. The servovalve dynamics can then be simplified as a proportional gain (K_v) in the feedback control system. Figure 3.7 shows the block diagram which is applied to an open-loop control.

The actuator is a third order system from the input voltage of the servovalve torque motor to the piston displacement of the hydraulic motor. In order to find the hydraulic spring rate k_h, one can measure the response of the piston position to a swept sine input. Figure 3.8 and 3.9 illustrate Bode plots of the experimental

tests for the joint 1 and 2 actuators respectively without additional load. Note that an LVDT (linear variable-differential-transformer) attached the piston rod is used to measure the displacement data.

Curve fitting the measured frequency response data which is the dashed line in the figure gives a third order transfer function for the motor dynamics block of Figure 3.7 of each joint.

$$\text{For Joint 1:} \quad \frac{x_p}{x_s} = \frac{5.217E3}{s\left(s^2 + 3.836E2\,s + 7.509E4\right)}, \qquad (3.7a)$$

$$\text{For Joint 2:} \quad \frac{x_p}{x_s} = \frac{3.374E3}{s\left(s^2 + 4.838E2\,s + 9.869E4\right)}. \qquad (3.7b)$$

The hydraulic natural frequencies for the actuators at joints 1 and 2 computed by (3.5a) are approximately 43.6 Hz and 50.0 Hz, respectively. Thus, the hydraulic spring rates are calculated to be 1.54E3 lb/in for joint 1 and 6.03E3 for joint 2.

With assumptions made earlier, the above analysis for the actuator dynamics is considered acceptable for generating the input force to the robotic structure from the feedback control viewpoint. The next sections will therefore concentrate on the structure itself without the actuators.

3.3.2 Finite element Method for Modeling RALF

The equation of motion for two serial flexible links has been derived with clamped-free mode shapes by several researchers [Maizza-Neto] [Centikunt]. However, this analytical method may not be suitable for complicated structures such as the RALF mentioned in the previous section. It is easily observed that the major difference between the RALF and two serial-link arms is a parallel link used to drive the upper link in the RALF and forming a closed kinematic chain system. So, finite element methods are used to analyze the system and comparisons are made between the numerical and experimental results. First, the RALF can be divided

into small beam elements and the mode shape of each element is described as a cubic function of displacement that satisfies the boundary conditions [Meirovitch]. By combining discrete elements into the complete structure, one can simultaneously obtain the natural frequency and its corresponding mode shape for the entire system. The essence of the finite element method is to regard the continuous structure as an assemblage of discrete elements. For this assemblage of discrete elements to represent the structure adequately, the boundary impedance must be matched. If the actuators are not attached to the RALF, the boundary in the driving joint in Figure 3.2 is considered to be clamped.

Table 3.4 shows comparison of the results from experiments and finite element methods, while the joint angle between the upper and lower links is 90°. Excitation consisted of sweep sine wave. Measurements were taken by accelerometers alternately placed along the links at 10 points along the link.

When the linear hydraulic actuators are attached to the structure, the clamped boundary condition used previously must be modified. However, the hydraulic spring rate k_h can be thought of as a "dynamic" spring in some sense so that the boundary condition for the driving joint can be modeled as a concentrated spring with an equivalent stiffness. The results for natural frequencies are shown in Table 3.5a; and the first two mode shapes for the upper and lower links are shown in Figures 3.10-3.13. Figures 3.14 and 3.15 illustrate the frequency responses from the upper and the lower links respectively.

Obviously, natural frequencies of the first few modes are approximately identical whereas the mode shapes are closely matched. The only deviation occurs in the mode shapes of the lower link due to measurement errors of complex structures. Note that the cubic spline of curve fitting is used to connect the values of the discrete displacement obtained from experiments and finite element methods. A third

order polynomial is the lowest order that can satisfy the Bernoulli-Euler equation and continuity of bending moments.

With the hydraulic actuators modeled as concentrated springs with equivalent stiffnesses, the analytical results will compare reasonably well with the experiments. Furthermore, the parallel link in the RALF has been simplified as a spring so that the equations of motion as given in (2.45) can be obtained. Thus, the geometrical constraint imposed by the parallel and upper links can be ignored in the dynamics so that the application of real-time control is practical.

According to Hooke's law, the compressional stiffness for a beam is

$$k_m = \frac{EA}{L} , \tag{3.8}$$

where

E : modulus of elasticity,

A : cross sectional area of the beam,

L : beam length.

By combining the hydraulic spring of the second joint and the link elasticity in series, the total stiffness becomes 5.8E3 lb/in. Now, we can mathematically analyze two serial links with elasticity supported by the equivalent springs instead of a parallel mechanism and the hydraulic motors. Finite element techniques are once again applied to obtain natural frequencies and mode shapes of the system as shown in Table 3.5b and Figures 3.10-3.13.

3.3.3 Dynamical Modeling with the Assumed Mode Method

The finite element analyses are quasi-static analyses, i.e., the system to be analyzed must be linear (small motion). An assumed modes model does not have this restriction. To determine the appropriate choice of component mode shapes, experiments were performed on RALF. On examining the mode shape in Figure

3.13, the first mode (5.69Hz) appears in the upper link only as a straight-line due to joint rotation with minimal deflection. In other words, the coordinate transformation of the upper link deflection associated with the first mode described in (2.2) is related to the transformation for the joint. Further assumptions are made below to treat the system as two independent links with proper boundary conditions. As in the previous chapter, equations of motion can be derived from the Lagrangian formulation with assumed modes and then verifed by experiments.

The lower link is treated as a pinned-mass beam with a concentrated mass at the end where the upper link is attached and a concentrated spring at the point of attachment to the hydraulic actuator. The upper link is treated as a pinned-free beam with a concentrated spring at the point of the parallel link attachment. With these boundary conditions, one can obtain the mode shapes for each link to describe the flexible deflection. With the rigid rotation for the joint and the first few modes for the link deformation, equations of motion are therefore derived as (2.45). Ignoring the nonlinear coupling and the gravitational terms results in the linear case of the dynamics due to small motion. The system natural frequencies using two assumed modes on each link are 6.0 Hz and 8.8 Hz, respectively.

The first two frequencies of the experiment are within approximately 7% of those in the analytical system. The frequency of 30Hz is not present in this dynamics model since the parallel link is considered as a massless spring.

In addition to the natural frequencies, the modal vectors constitute what is known in a broad sense as the response of the system. Modal vectors are not dependent on forcing. They are properties of the unforced system. Physical measurements of the time responses of the forced system can be applied to verify the analytical results. The following formulation is required to specify the relation

between measured strains and the modal amplitudes.

$$
\begin{pmatrix} \epsilon(l_1,t) \\ \epsilon(l_2,t) \\ \vdots \\ \epsilon(l_m,t) \end{pmatrix} = \begin{pmatrix} C\phi_1''(l_1) & C\phi_2''(l_1) & \dots & C\phi_n''(l_1) \\ C\phi_1''(l_2) & C\phi_2''(l_2) & \dots & C\phi_n''(l_2) \\ \vdots & \vdots & \ddots & \vdots \\ C\phi_1''(l_m) & C\phi_2''(l_m) & \dots & C\phi_n''(l_m) \end{pmatrix} \begin{pmatrix} \delta_1(t) \\ \delta_2(t) \\ \vdots \\ \delta_m(t) \end{pmatrix} , \qquad (3.9)
$$

where

ϵ : strain,

C : distance from the neutral surface to the measured point,

ϕ : mode shapes,

δ : generalized coordinate for the deflection.

Here, m strain gauges are placed on distance l_1, $l_2 \dots l_m$ along the link, while n is the number of modes selected to represent the deflection.

Figures 3.16-3.17 show the strain responses at the mid-point of each link arising from an impulsive force when the actuators are controlled. It is obvious that the structural damping should be included in the dynamics. From Figures 3.14-3.15, the proportional damping ratio of about 0.2 is selected for use in the simulations. The results are shown in Figures 3.18-3.19.

The responses from experiments and simulations show similar characteristics. A frequency of about 5.7Hz for experiment and 6.1Hz for simulation is most apparent in the lower link and a frequency of about 9.12Hz for experiment and 9.18Hz for simulation is most apparent in the upper link. Furthermore, the sine wave response can also be used to illustrate a property of the dynamics system. Figures 3.21 and 3.23 show the strain responses of simulations for the lower and upper links, while Figures 3.20 and 3.22 show the experimental results. Further tuning of the model might improve the damping ratios of higher frequency modes.

3.4 Summary

In this chapter, two experimental manipulators existing in the Flexible Automation Laboratory have been employed to verify the equations of motion developed in the previous chapter. If one omits the link deformation, the prediction of the dynamical motion will be the same as that of the rigid robotic arms which is widely known. Therefore, the emphasis here is on the link deflection which causes the structural oscillations since it gives the system its characteristic natural frequencies and modal vectors.

The robotic system cannot be operated without the actuators. Thus, the total system model should include the links and the actuator systems. The property of the total system may be different from the component systems, especially in natural frequencies. From the experimental data, the actuator characteristics can be determined and then implemented in the mathematical model. Finite element techniques are applied to find out the link deflection which consists of the mode shape and the generalized coordinate. Equations of motion can then be derived in the standard form of equation (2.45).

In order to compare the experimental results of natural frequencies and time responses measured at the strain gauge with the analytical results, the equation of motion for the above described analytical modal must be linearized. The excellent agreement between the analytical prediction and the experimental data is clearly a result of correct modeling of the system; in particular, the appropriate choice of boundary conditions.

Table 3.1 Physical properties of one-link flexible manipulator.

SYSTEM PARAMETERS

Flexible Beam:

Material	–	Aluminum 6061-T6
Form	–	Rectangular 3/4 X 3/16 in
Length	–	48 in
Area Moment of Inertia	–	4.12E-4 in^4
EI Product	–	4120 $lbf-in^2$

Table 3.2 Dimensions of RALF.

--data of lightweight bracing manipulator

stiffness of lower link EI_1= 241957N-m^2
(Aluminum tube,outside dia. 141.3mm,inside dia.134.49mm)
stiffness of upper link EI_4= 113720N-m^2
(Aluminum tube,outside dia. 114.3mm,inside dia. 108.2mm)
stiffness of actuating link EI_3= 20992 N-m^2
(aluminum column,outside width 101.6mm,inside width 92.25mm,
outside height 44.45mm,inner height 38.1mm)
the length of lower link l_1= 3.048m (10 ft)
the length of connecting link l_2= 0.4662m
the length of actuating link l_3= 3.048m (actual 2.2m)
the length of upper link l_4= 3.958m
the length of rigid part of
upper link l_e= 0.502m
the position length of
small manipulator l_s= 3.048m
mass per unit length of
lower link ρ_1= 3.9817kg/m
connecting link ρ_2= 2.5kg/m
actuating link ρ_3= 2.6545kg/m
rigid section of upper
link ρ_e= 6.58kg/m
flexible section of
upper link ρ_f= 2.893kg/m
the lumped mass at the end
of lower link m_j= 2kg
mass of small manipulator m_s= 25kg
total mass of
lower link m_1= 12.136kg
connecting link m_2= 1.1655kg
actuating link m_3= 8.0909kg
upper link $m4$= 13.284kg
the position length of
center of gravity of
lower link r_1= 1.524m
connecting link r_2= 0.2332m
actuating link r_2= 1.524m
upper link r_4= 1.7903m

Table 3.3 Comparison of modal frequencies (Hz) of One-link case.

Mode	Measured	Analytical	Finite Element
1	2.08	2.096	2.088
2	13.92	13.989	13.955
3	41.38	41.524	41.452
4	81.18	81.225	81.203
5		136.352	136.345

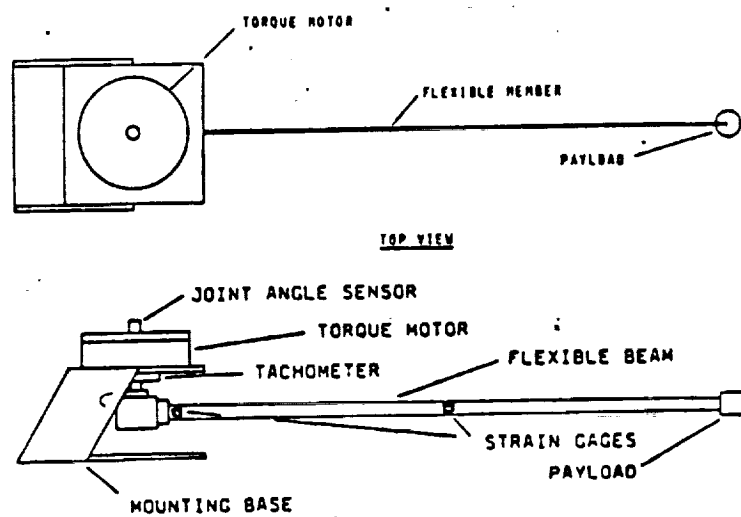**Table 3.4** Comparison of modal frequencies (Hz) of RALF without actuators attached.

Mode	Experiment	Finite Element
1	6.37	5.95
2	12.00	12.78
3	37.87	30.19
4	57.37	60.60
5	94.02	95.05

Table 3.5a Comparison of structural frequencies (Hz, with actuators attached).

Mode	Experiment	Finite Element
1	5.70	6.08
2	9.12	9.12
3	30.00	29.70
4		49.50

Table 3.5b Comparison of structural frequencies (Hz, with actuators attached).

Mode	Experiment	Finite Element
1	5.70	5.82
2	9.12	9.18
3	30.00	
4		55.70

TORQUE MOTOR

FLEXIBLE MEMBER

PAYLOAD

TOP VIEW

JOINT ANGLE SENSOR

TORQUE MOTOR

TACHOMETER

FLEXIBLE BEAM

STRAIN GAGES

PAYLOAD

MOUNTING BASE

Manipulator with Sensors.

Figure 3.1 One-link flexible manipulator.
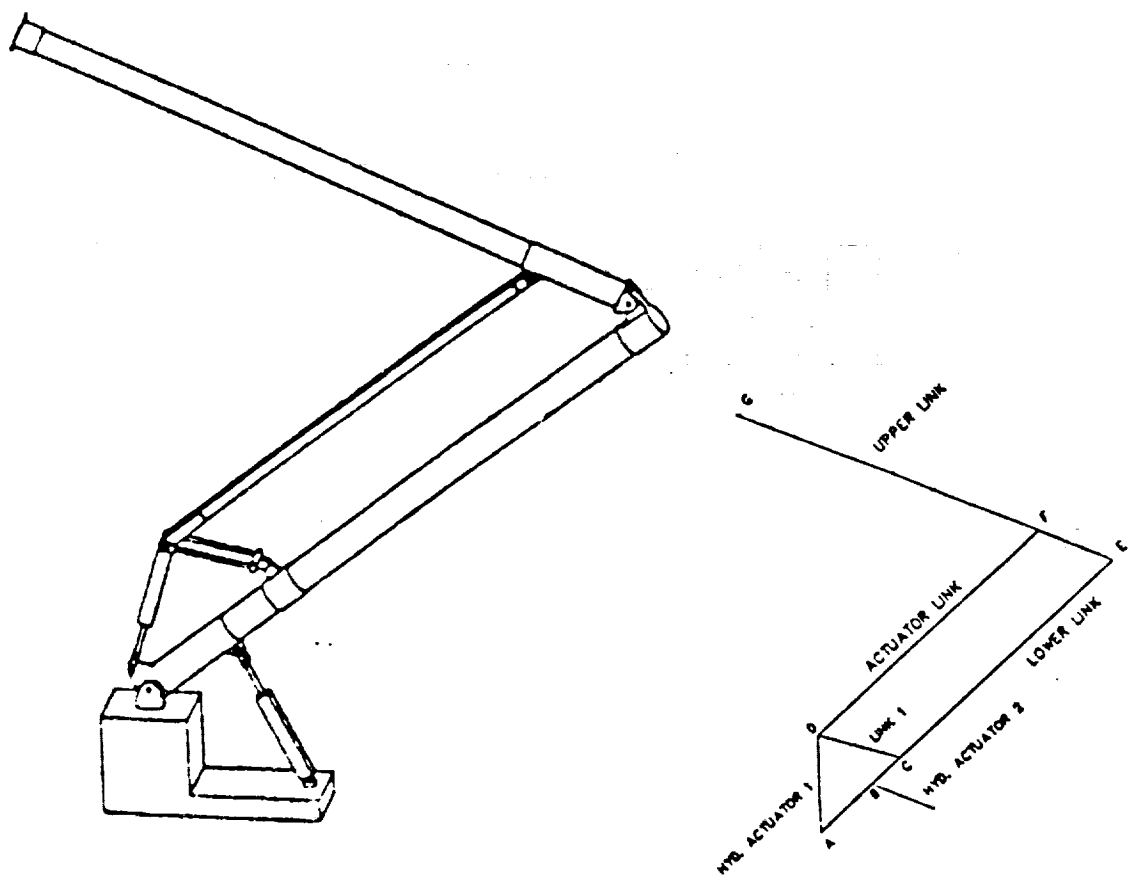
Flexible Manipulator at Georgia Tech

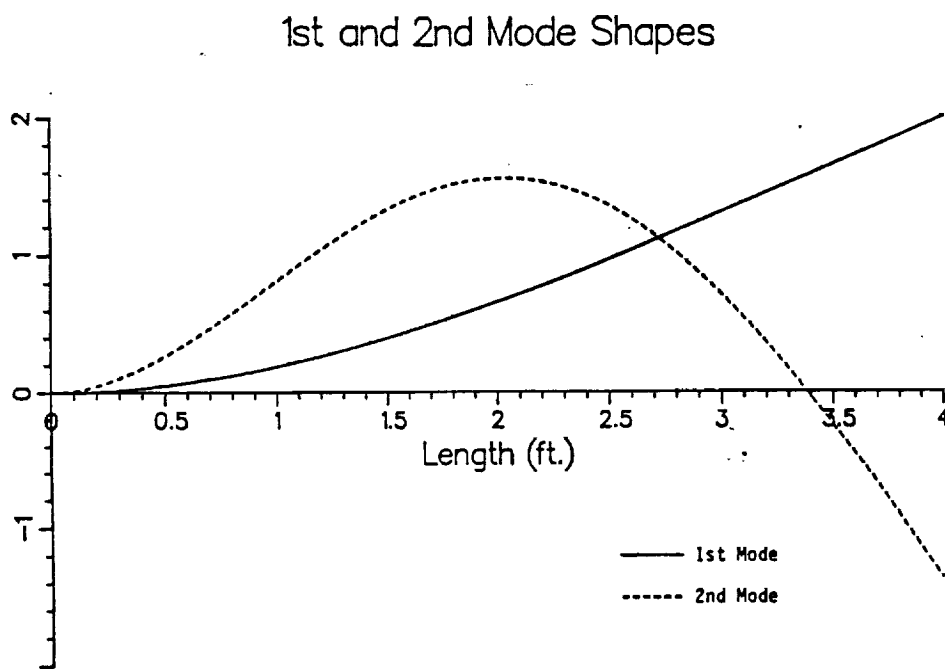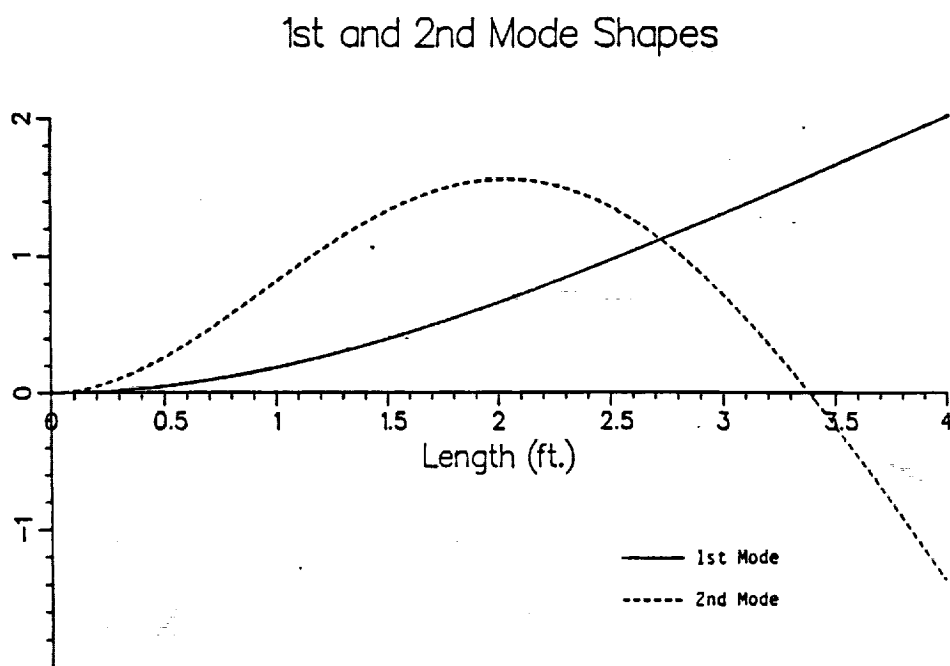**Figure 3.2** RALF (Robotic Arm, Large and Flexible).

1st and 2nd Mode Shapes

Figure 3.3 Mode shapes of analytical method.

1st and 2nd Mode Shapes

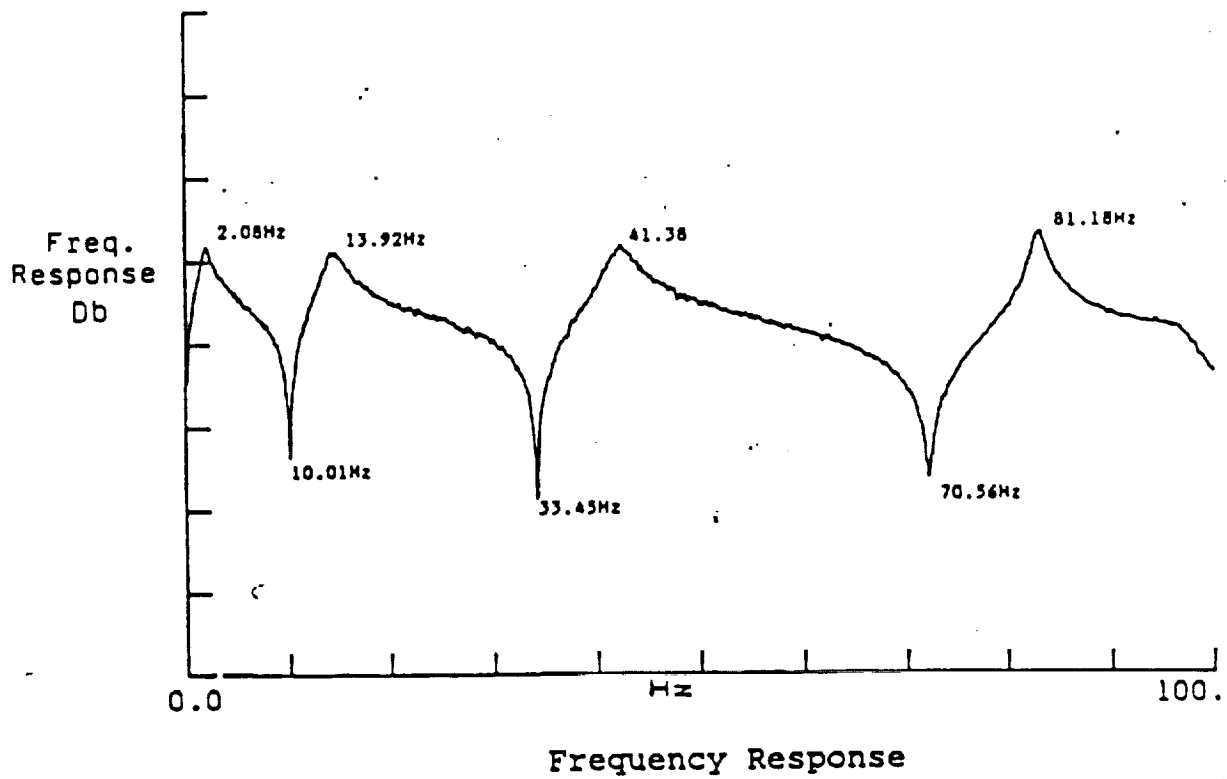**Figure 3.4** Mode shapes of finite element method.
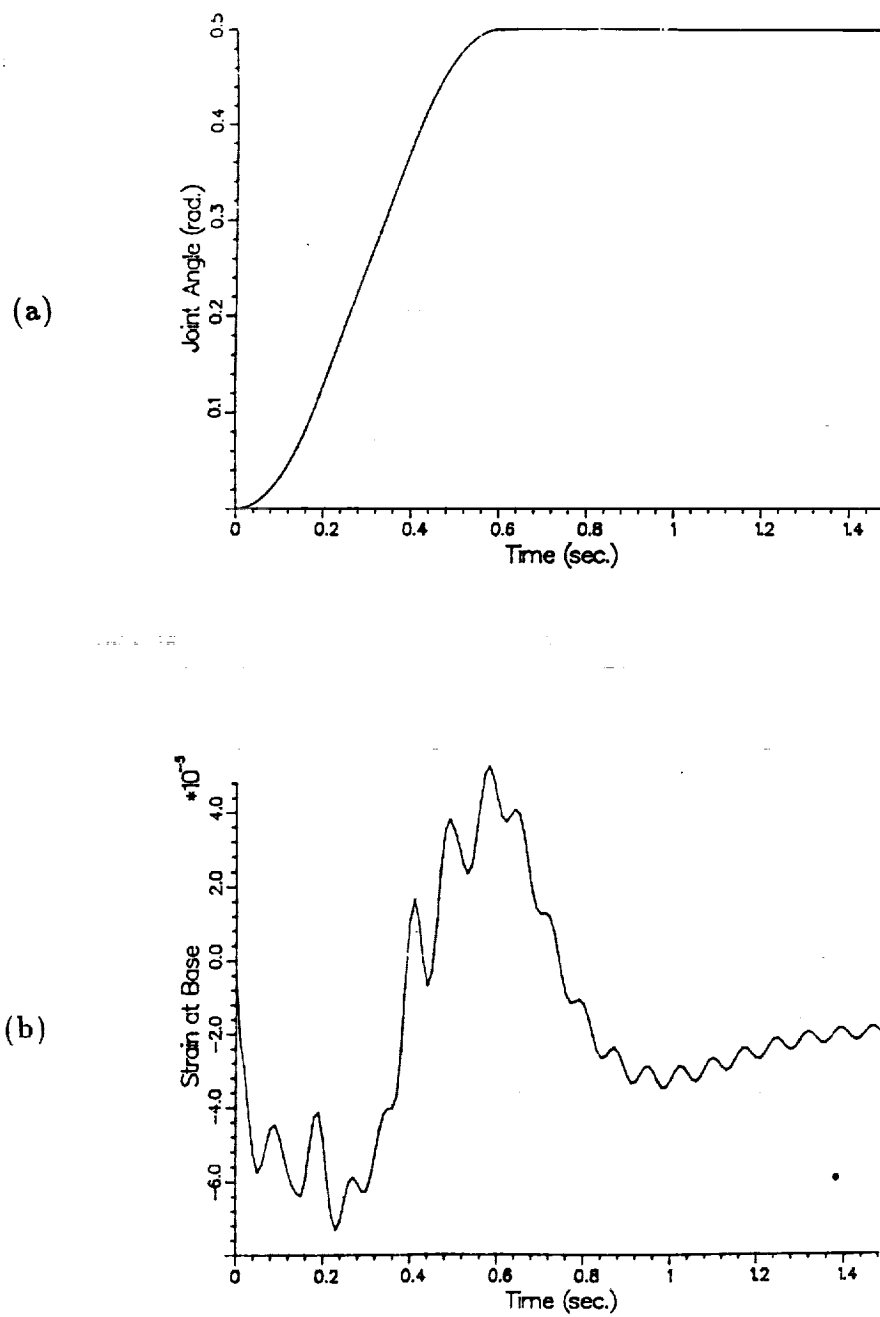
Figure 3.5 Measured modal frequencies.

(a)

(b)

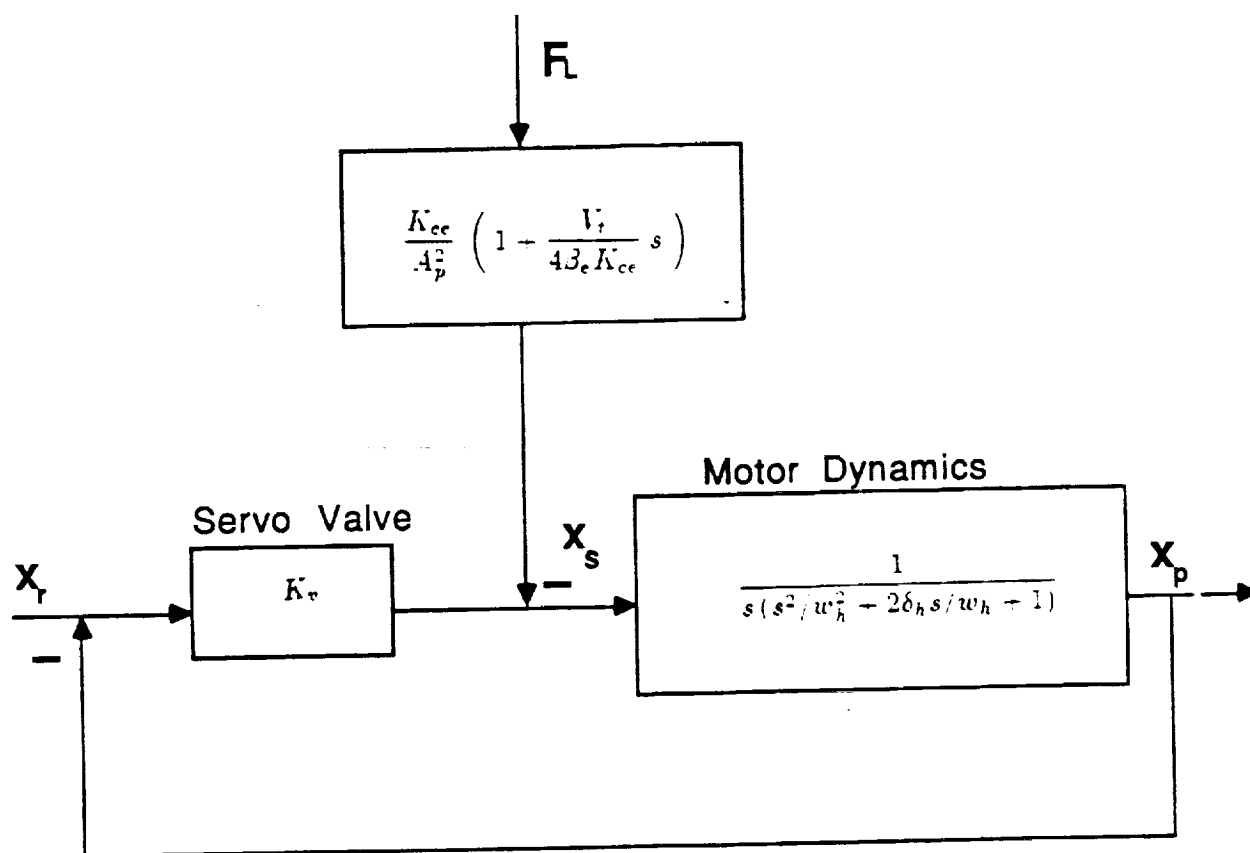**Figure 3.6** (a) Simulated joint angular response. (b) Simulated strain response at base.

Figure 3.7 Block diagram of hydraulic servo system.

X=800.01mHz ΔX=119.9 Hz
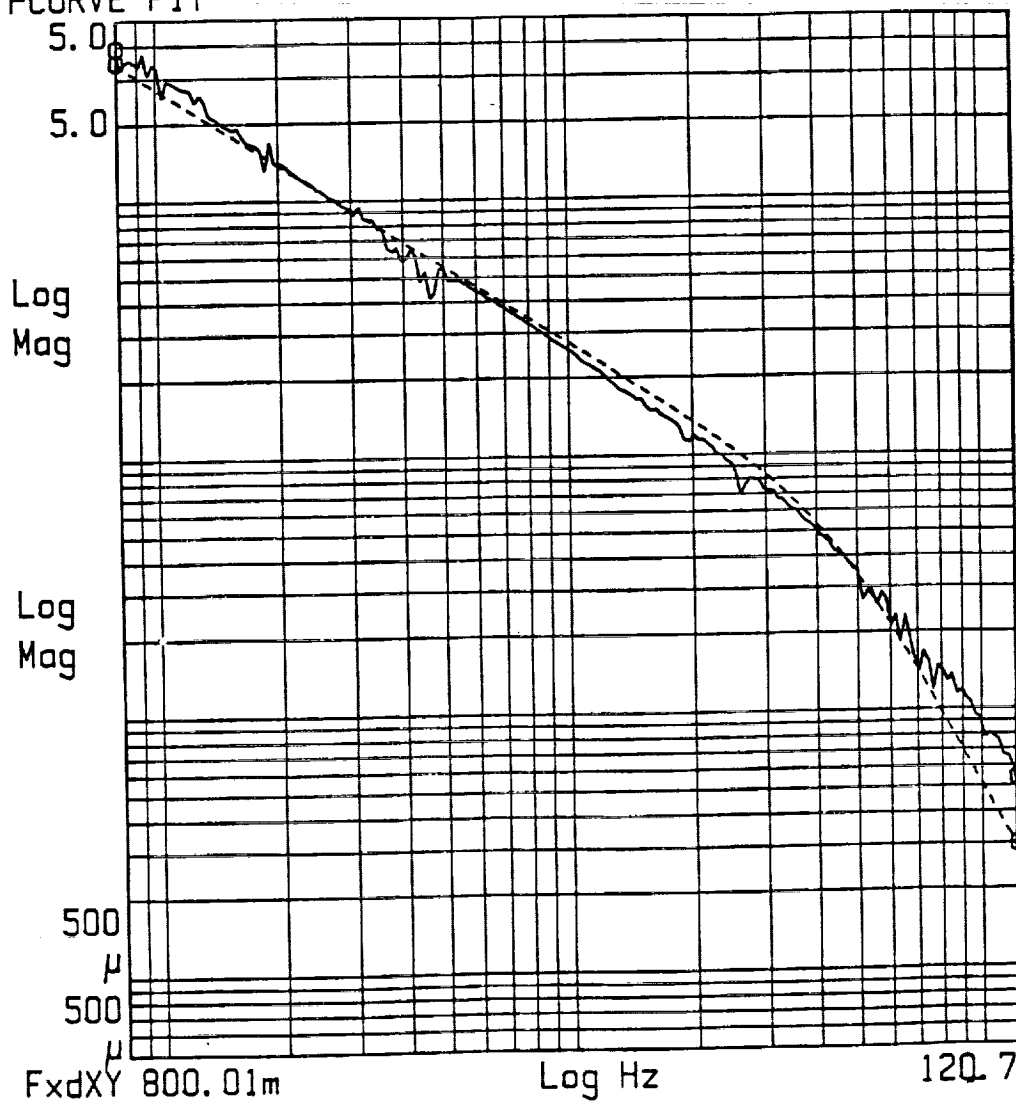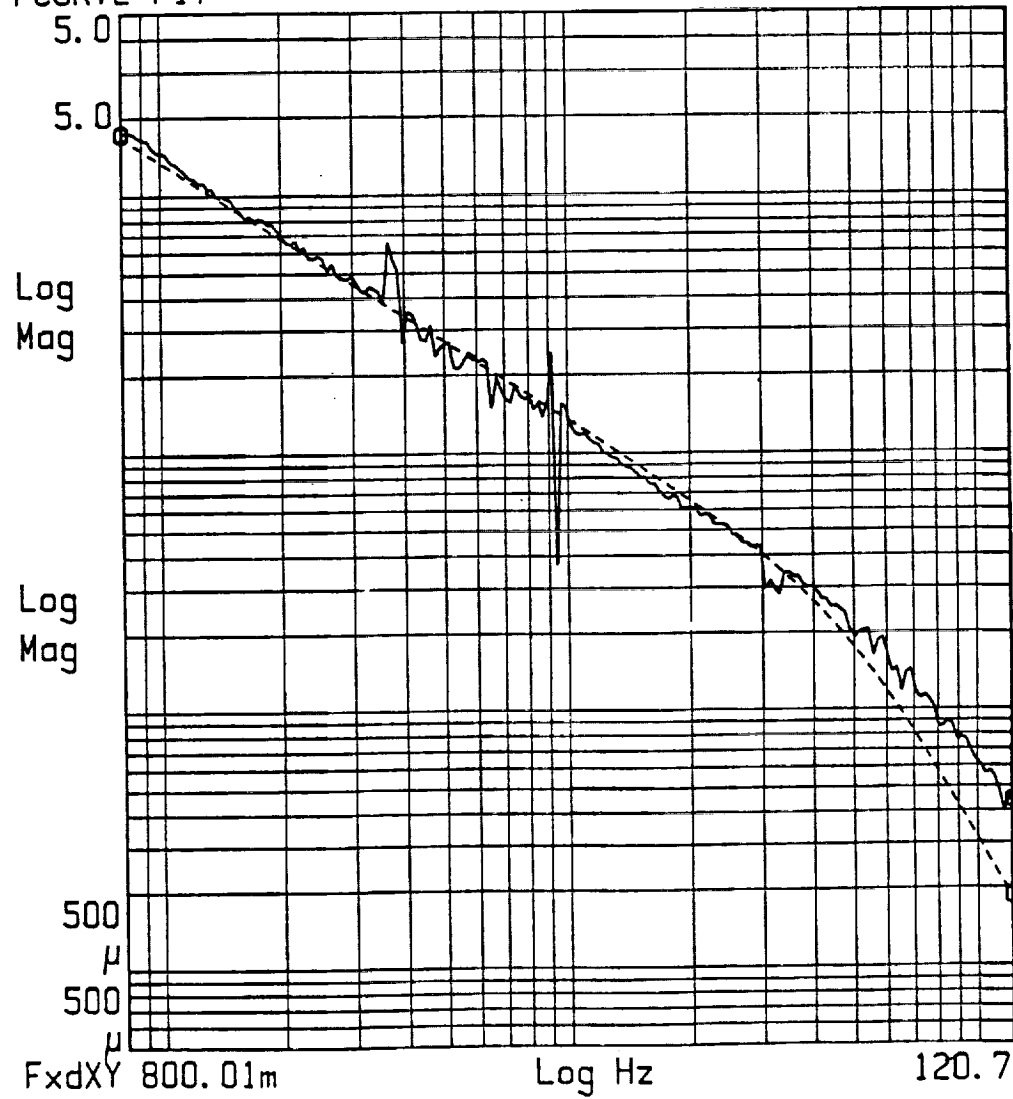Yₐ=3.87881 ΔYₐ=3.873

⊢FREQ RESP

Yb=3.41041 ΔYb=3.407

⊢CURVE FIT

Figure 3.8 Bode plot of the first hydraulic actuator.

X=800.01mHz ΔX=119.9 Hz
Ya=1.71306 ΔYa=1.709

⊢FREQ RESP
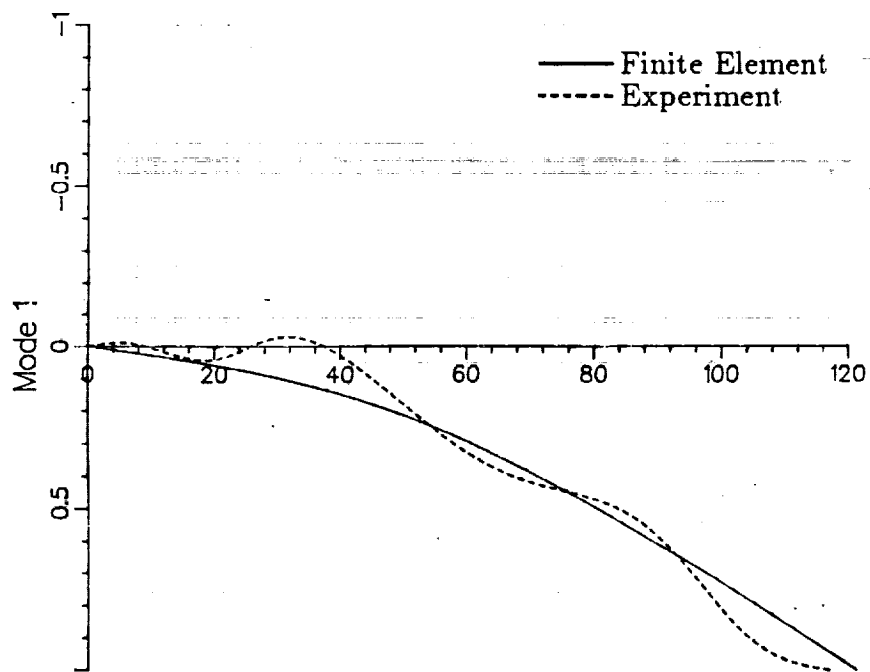
Yb=1.68468 ΔYb=1.683

⊢CURVE FIT

Figure 3.9 Bode plot of the second hydraulic actuator.

Figure 3.10 First mode shape of lower link.
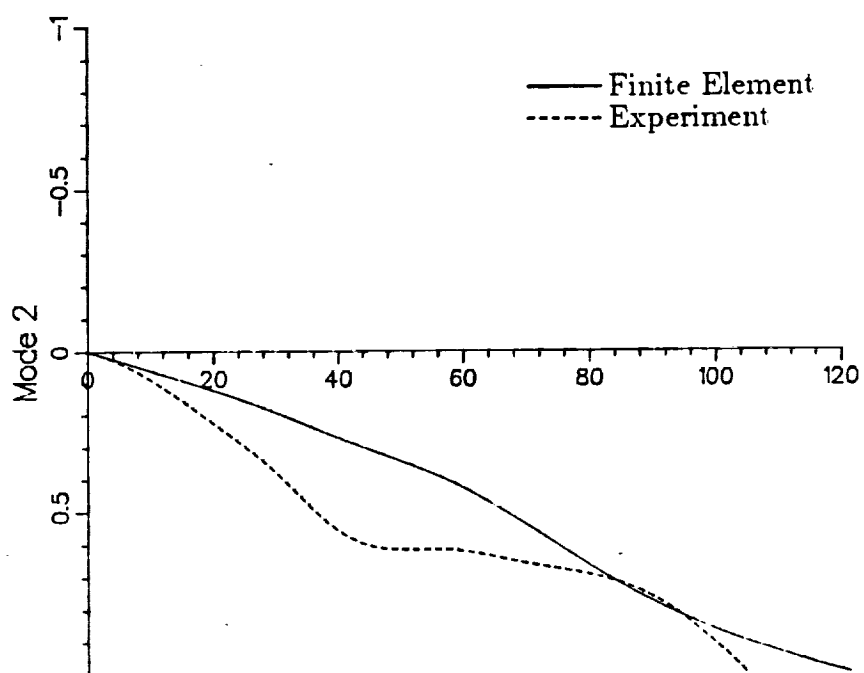
Figure 3.11 Second mode shape of lower link.
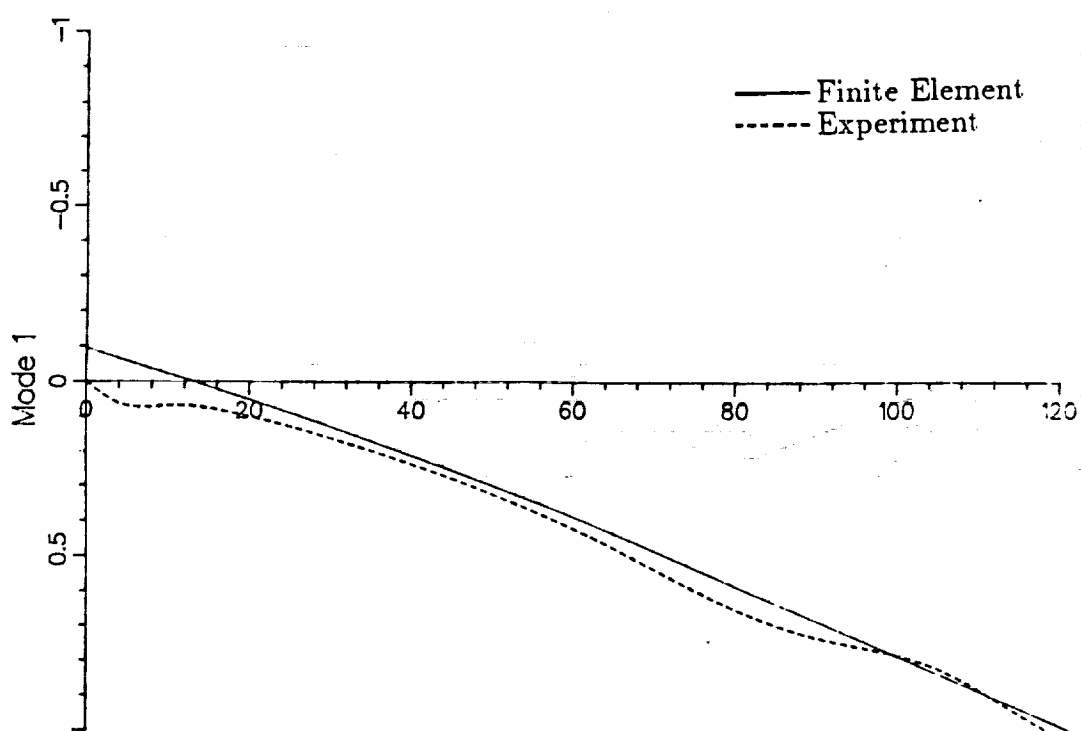
Figure 3.12 First mode shape of upper link.
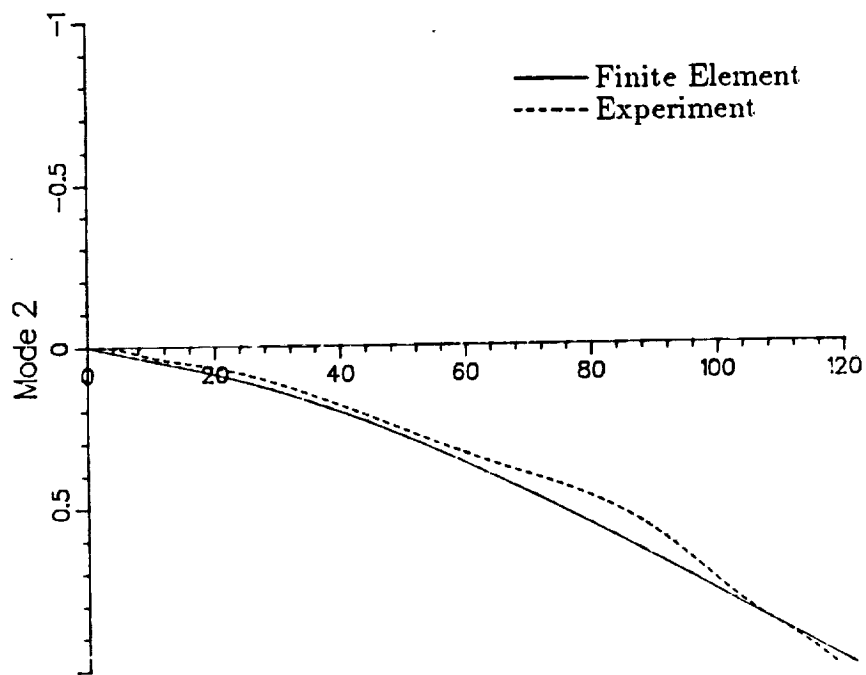
Figure 3.13 Second mode shape of upper link.
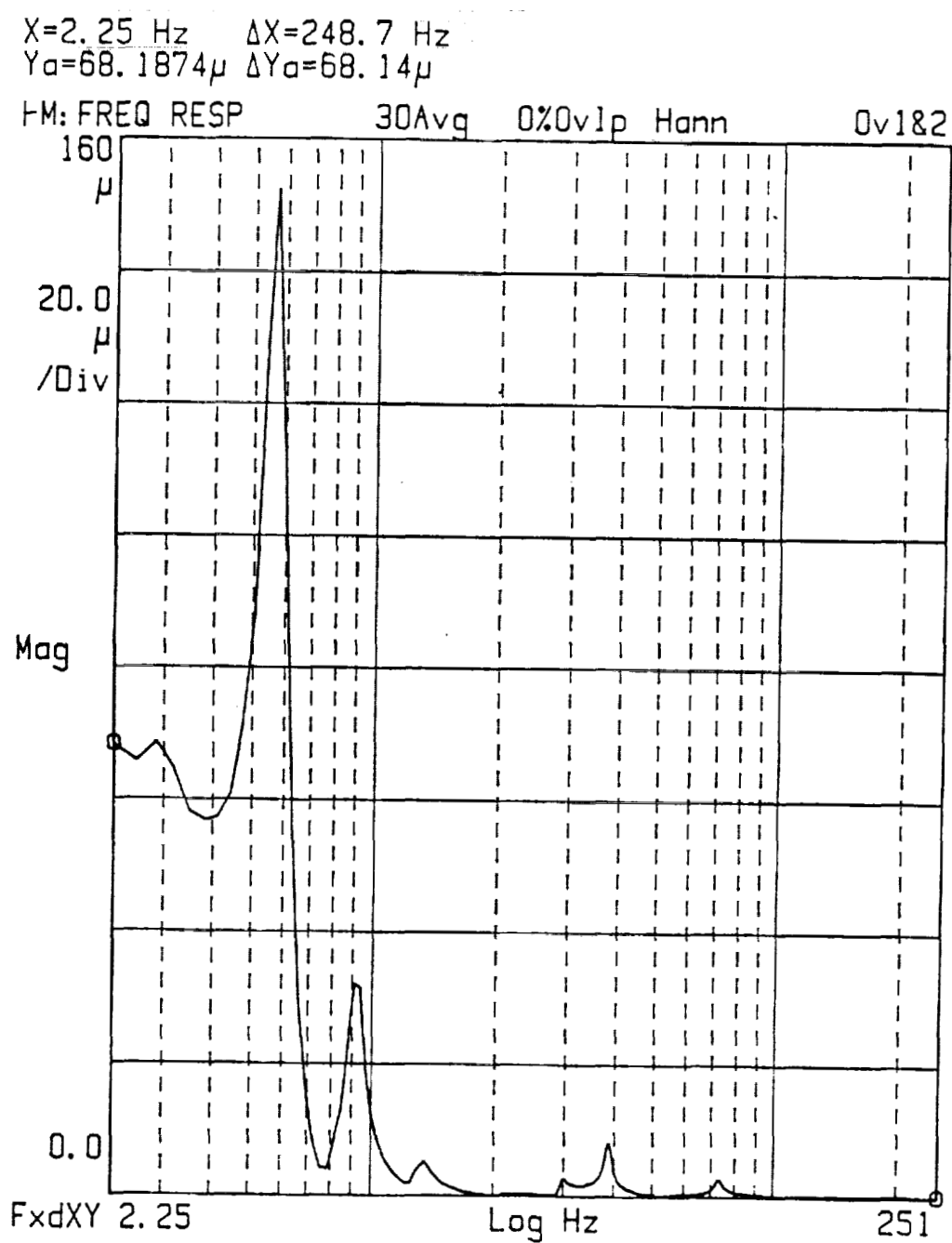
Figure 3.14 Frequency response of lower link.
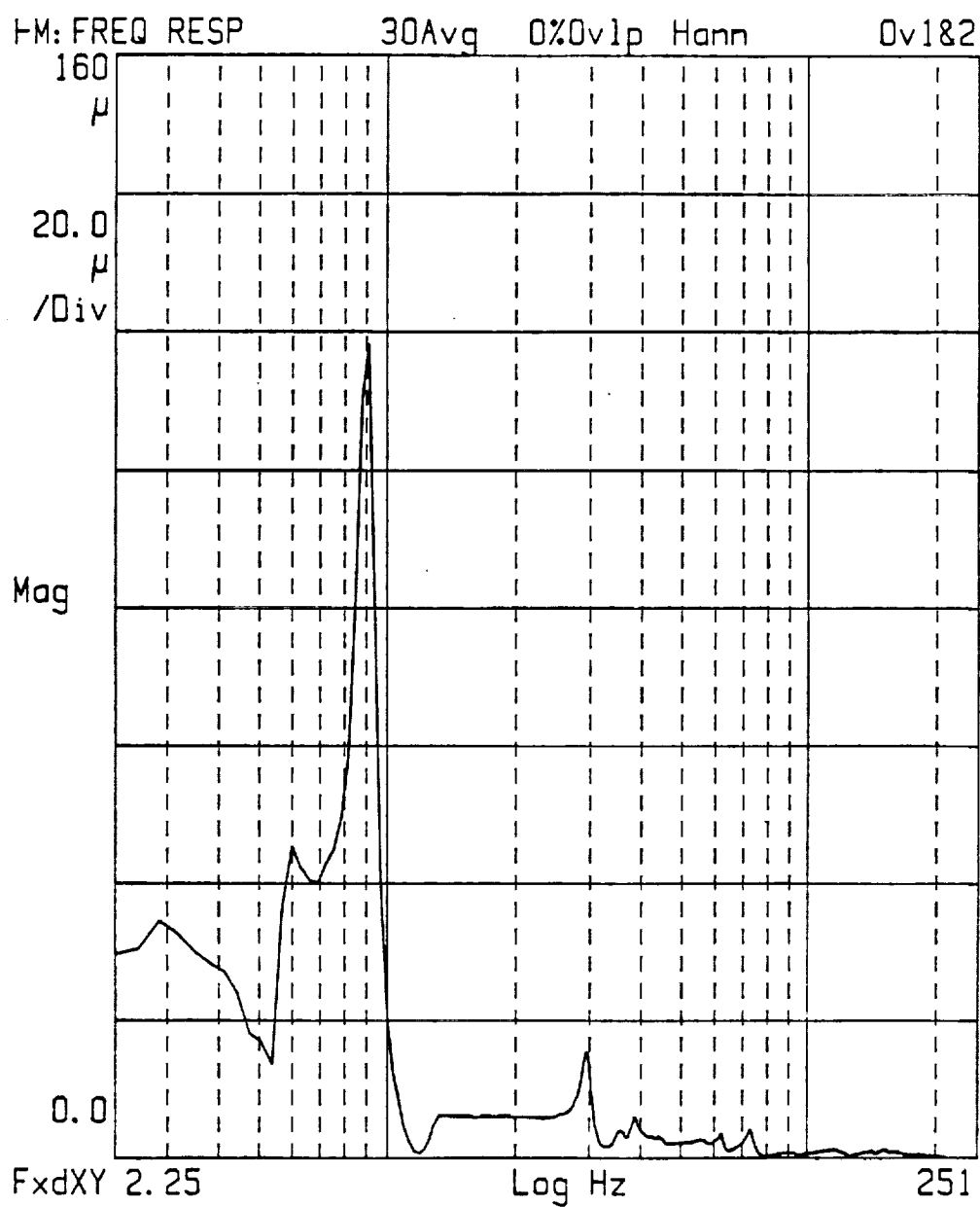
Figure 3.15 Frequency response of upper link.
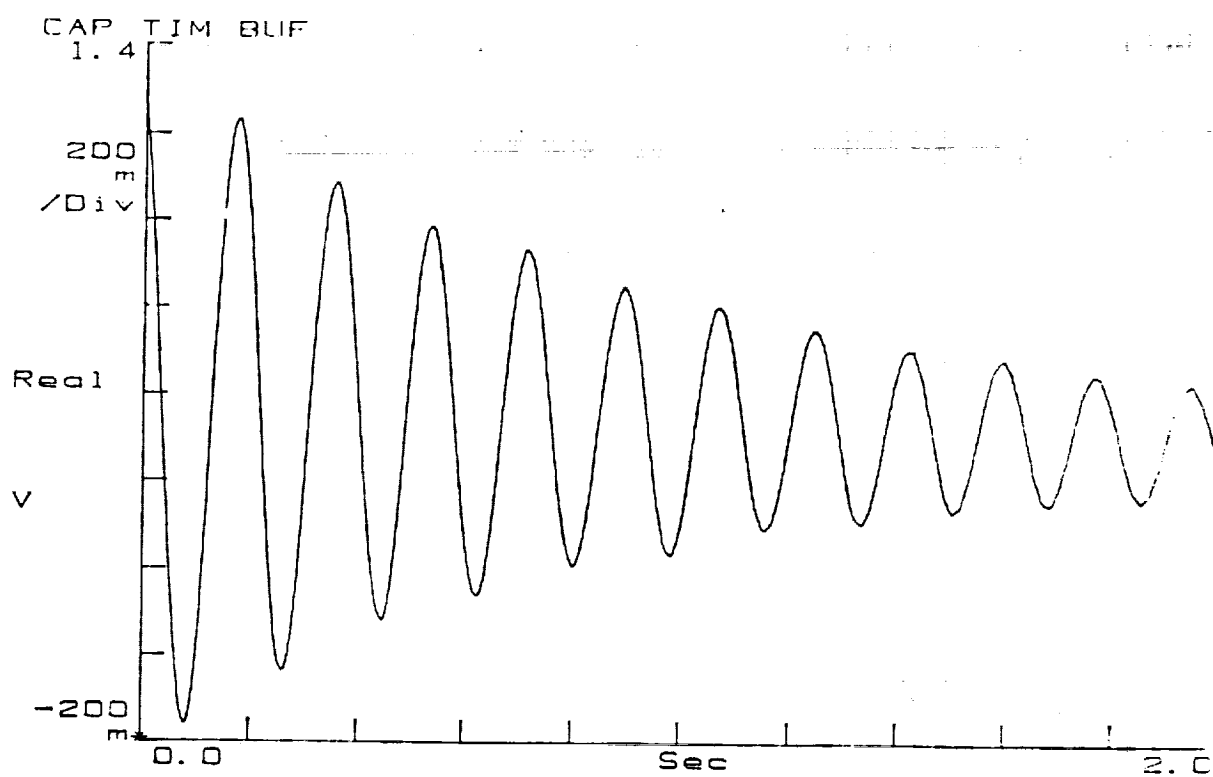
Figure 3.16 Experimental strain response at the mid-point of lower link.

CAP TIM BUF
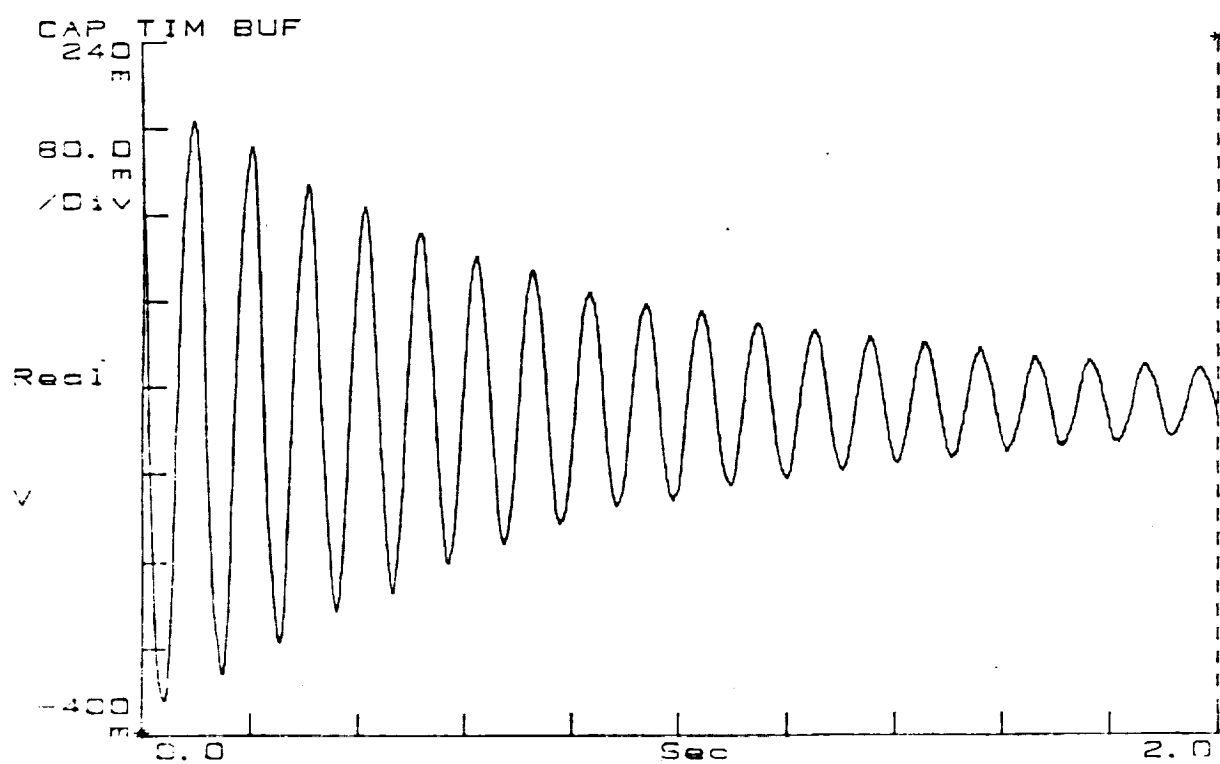
Figure 3.17 Experimental strain response at the mid-point of upper link.
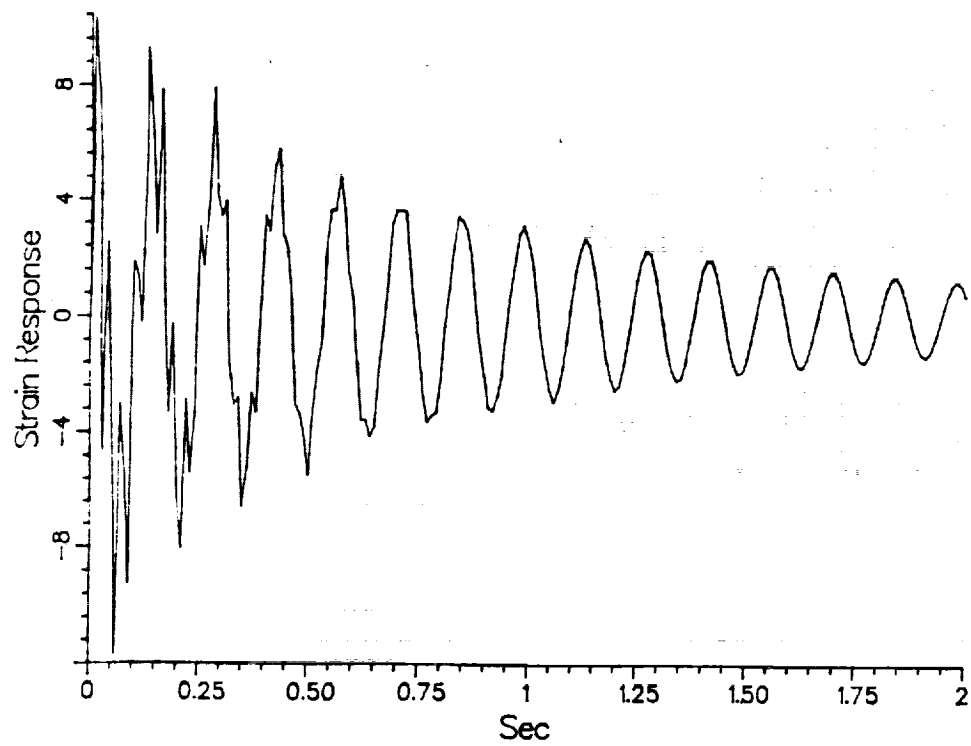
Figure 3.18 Simulated strain response at the mid-point of lower link.
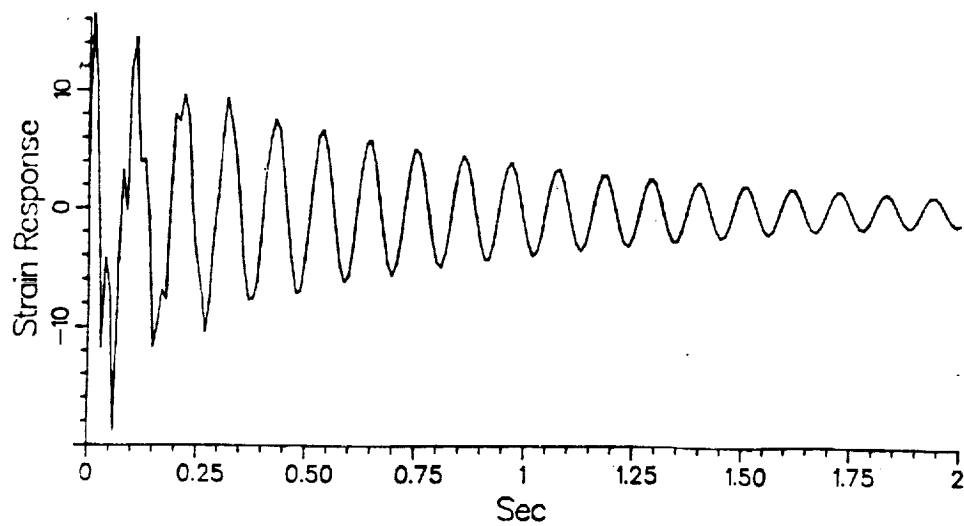
Figure 3.19 Simulated strain response at the mid-point of upper link.

CAP TIM BUF

4.5

500
m
/0.V

Real

V

500
m
X

Sec

Fxd X
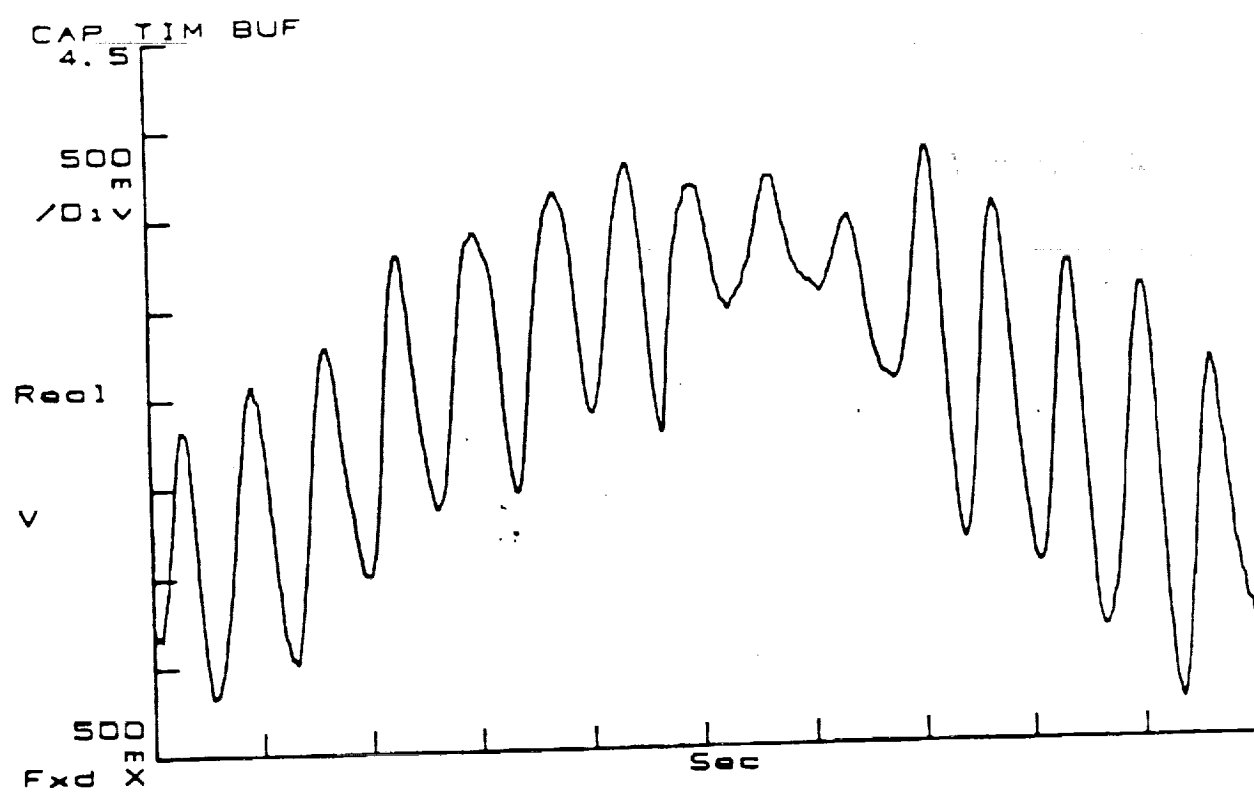
Figure 3.20 Experimental strain response of lower link (sine wave).
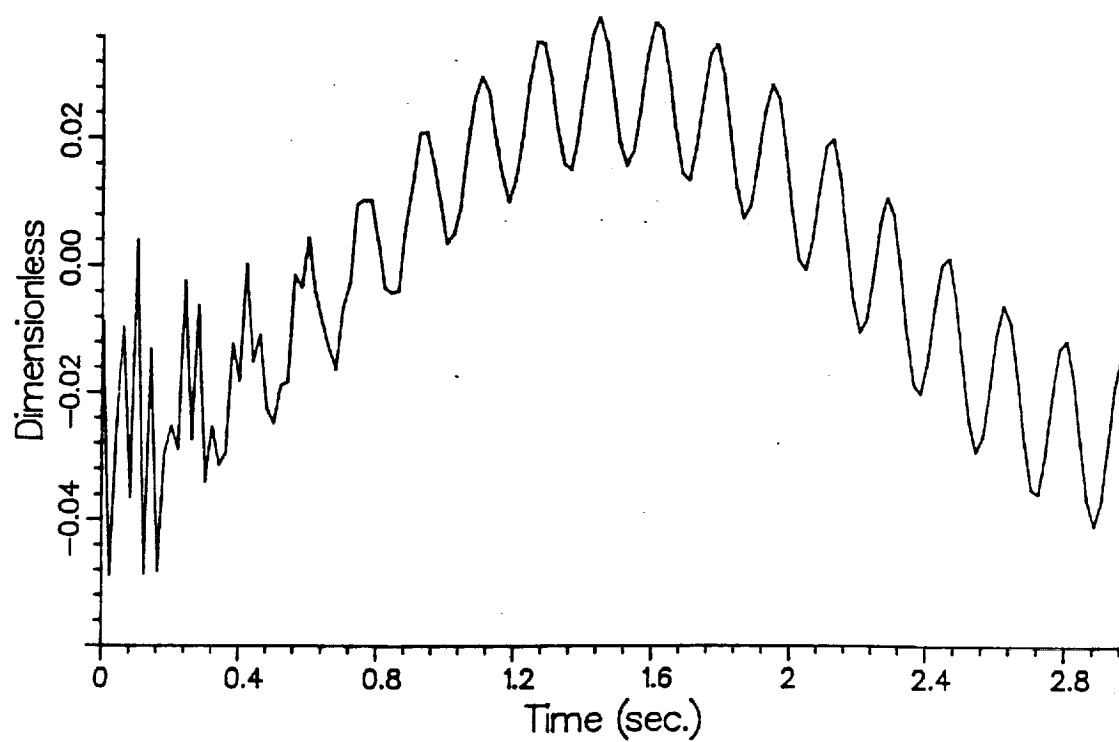
Figure 3.21 Simulated strain response of lower link (sine wave).
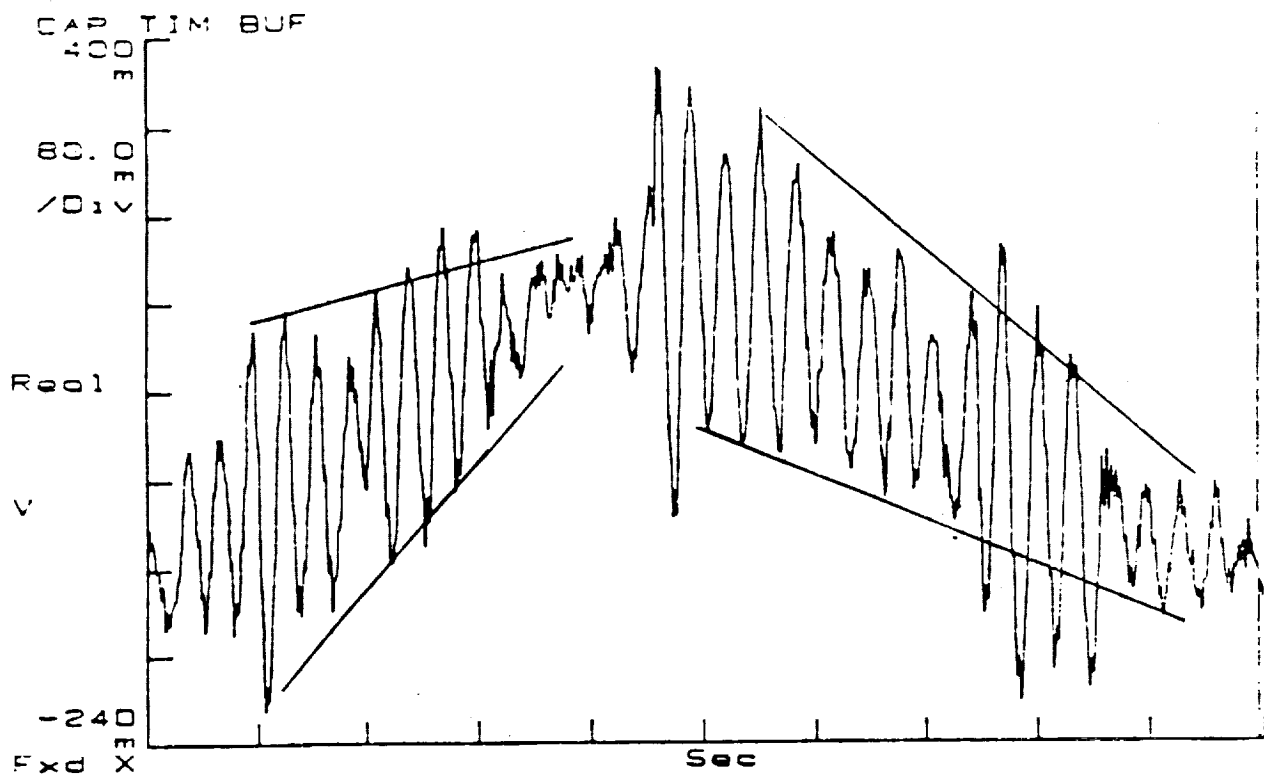
Figure 3.22 Experimental strain response of upper link (sine wave).
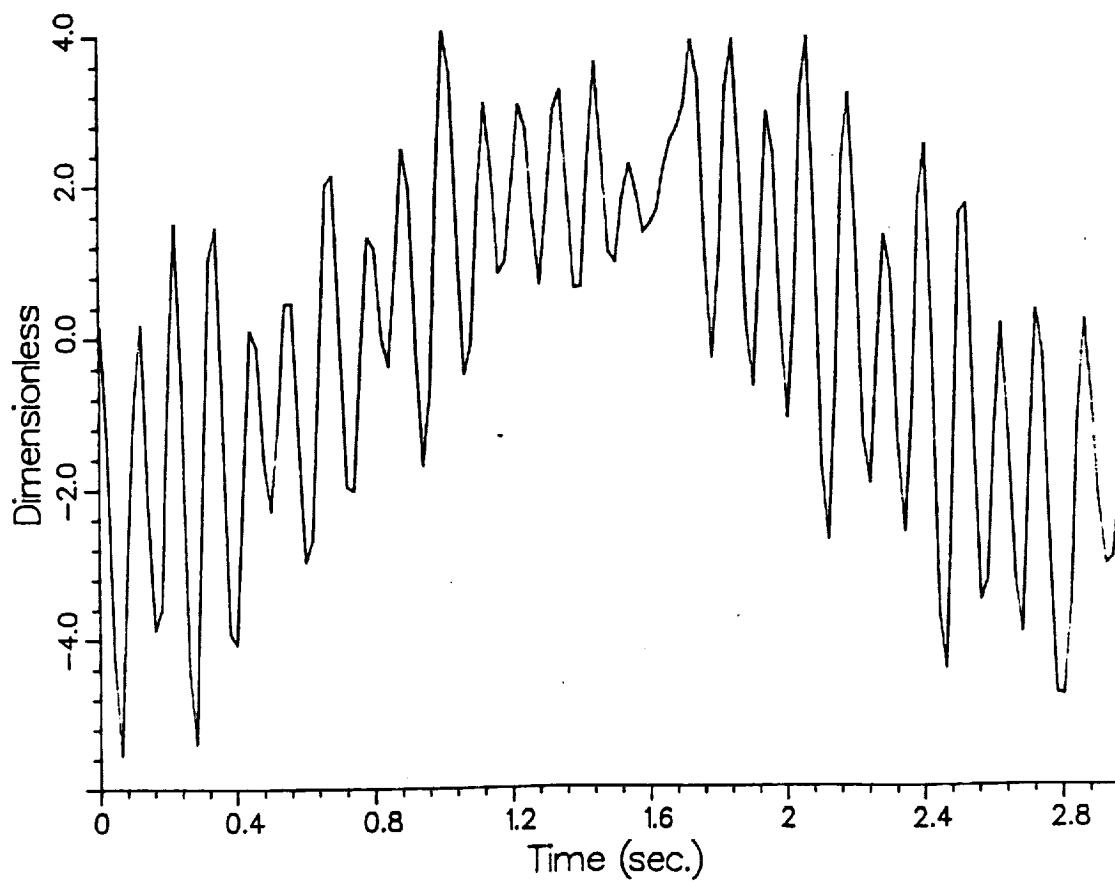
Figure 3.23 Simulated strain response of upper link (sine wave).

CHAPTER IV

THEORY OF CONTROL ALGORITHM

The light weight manipulator is a challenging research topic with potential to improve performance over today's robot. The main problem with light-weight structures is the flexible vibrations which are naturally excited as the arm is commanded to move or is disturbed. Control is one key to efficient use of lighter arms, but its capability is limited by uncertainties in the arm's behavior and in the environment.

The first step in designing a control system consists of establishing a dynamic model for the flexible arms. This has already been discussed in the two previous chapters. In the following, the theory of a control algorithm will be developed. The application to the flexible manipulator under different conditions is presented in the next chapter to illustrate its performance.

4.1 Mathematical Prelimiary

One great concern in control is the problem of stability of the dynamic system. The so-called "second method" of Lyapunov has been applied as the principal mathematical tool in tackling linear and nonlinear stability problems of the most varied type, particularly in the theory of control systems. However, the importance of the Lyapunov method lies primarily in its point of view of system stability rather than in its application as a design tool. The name "second method" is a philosophy of approach rather than a systematic method [Kalman].

The intuitive concept of stability is that a dissipative system perturbed from its equilibrium state will always return to it. In other words, from the energy point of view, if the rate of change $dE(X)/dt$ of the energy $E(X)$ of an isolated physical

system is negative for every possible state X, except for a single equilibrium state X_e, then the energy will continually decrease until it finally assumes its minimum value $E(X_e)$. However, the above explanation is based on the physical concept of energy, and in general there is no natural way of defining energy when the equations of motion are given in a purely mathematical form. The following statement is considered as its mathematical equivalent: A dynamic system is stable (in the sense that it returns to equilibrium after any perturbation) if and only if there exists a "Lyapunov function," i.e., some scalar function $V(X)$ of the state with the properties: (a) $V(X) > 0$, $\dot{V}(X) < 0$ when $X \neq X_e$, and (b) $V(X) = \dot{V}(X) = 0$ when $X = X_e$. For instance, let $V(X)$ be a measure of the "distance" of the state X from the origin in the state space, that is, $V(X) > 0$ when $X \neq 0$ and $V(0) = 0$. Suppose the distance between the origin and the instantaneous state $X(t)$ is continually decreasing as $t \to \infty$, that is, $\dot{V}(X) < 0$. Therefore, $X(t) \to 0$ [Kalman].

4.2 Definitions of Stability

In the mathematical formulation, the dynamics relates the state X and the control function (or forcing function) u of the system. Continuous-time dynamic systems will be treated here, but the concept of stability is analogous to discrete-time dynamic systems. Briefly, the dynamics of systems are given by the vector differential equation:

$$\frac{d}{dt}X = f(X,u,t) \qquad t \geq 0, \qquad (4.1)$$

where $X \in R^n$, $u \in R^m$ and $f : R_t \times R^m \times R^n \to R^n$.

If $u = 0$ for all t, the form of (4.1) is free (unforced):

$$\frac{d}{dt}X = f(X,t) \qquad t \geq 0, \qquad (4.2)$$

where $f : R_t \times R^n \to R^n$. Without loss of generality, the equation of (4.2) is used to illustrate the definition of stability, while the input function u is usually bounded and does not change the characteristic of system [Jordan & Smith].

It is always assumed that the function f in (4.2) is sufficiently smooth so that it has a unique solution over $[0, \infty)$ and this solution depends on the initial condition $X(0)$. If an $X_o \in R^n$ is said to be an equilibrium state of the system (4.2), at time t_o, then

$$\lim_{t \to \infty} \frac{d}{dt} X_o(t) = f(X_o, t) = 0 \qquad \forall \, t \geq t_o. \tag{4.3}$$

That the equilibrium state X_o is set to be 0 does not result in any loss of generality. Therefore, the stability of the system (4.2) at an equilibrium state $X = 0$ (the origin) is defined as follows:

[Definition 4.2.1] The equilibrium state 0 at time t_o of (4.2) is said to be stable at time t_o if, for each $\epsilon > 0$, there exists a $\delta(t_o, \epsilon) > 0$ such that

$$\|X(t_o)\| < \delta(t_o, \epsilon) \implies \|X(t)\| < \epsilon \qquad \forall \, t > t_o, \tag{4.4}$$

where $\|X\|$ is called the norm of X.

In graphic representation, it is shown in Figure 4.1 that there exists a radius for every ϵ such that if a trajectory starts at a point X_o inside the hyperspherical region of radius δ, then it will always remain in the hyperspherical region of radius ϵ.

Furthermore, in Figure 4.1, if every trajectory starting inside some hyperspherical region in the state space converges to the origin as time increases indefinitely, an equilibrium state 0 is asymptotically stable (AS).

[Definition 4.2.2] The equilibrium state 0 at time t_o is asymtotically stable at time t_o, if (4.2) is stable at time t_o and there exists a number $\delta(t_o) > 0$ such that

$$\|X(t_o)\| < \delta(t_o) \implies \|X(t)\| \to 0 \quad \text{as} \quad t \to \infty. \tag{4.5}$$

Conversely, the system (4.2) is said to be unstable whenever, for some arbitrarily large ϵ inside R and any arbitrarily small δ, there is always a starting point X_o within the hyperspherical region of radius δ such that the trajectory from X_o passes beyond the boundary hypersphere of radius ϵ (Figure 4.1).

In the last section, the scalar function $V(X)$ to be called a Lyapunov function is used to determine the stability of the system. If the system is of nth order, $V(X)$ may not be identified with energy level. From the definition of stability, another interpretation of the candidate Lyapunov function $V(X)$ results from a geometric pattern in the state space. Therefore, we must first define some properties of scalar functions [Takahashi]. A scalar function $V(X)$ is said to be positive definite when

1. $V(0) = 0$, and

2. $V(X) > 0$ in some region of X outside the origin. Let us represent the region in state space by S. Then

$$V(X) > 0, \qquad X \in S; \qquad X \neq 0 .$$

3. $V(X)$ is continuous in S, and

4. $\partial V(X)/\partial x_i$, $i = 1, 2, \ldots, n$ are also continuous.

The partial derivative for condition 4 creates a gradient vector

$$grad\ V(X) = \nabla V(X) = \begin{pmatrix} \frac{\partial V(X)}{\partial x_1} \\ \vdots \\ \frac{\partial V(X)}{\partial x_n} \end{pmatrix} . \qquad (4.6)$$

The time derivative $dV(X)/dt$ along any trajectory of a system (4.2) is given by

$$\dot{V}(X(t)) = \frac{\partial V(X(t))}{\partial t} + \nabla V(X(t))\, f(X, t) . \qquad (4.7)$$

4.3 The Lyapunov's Direct Method

In this section, the stability of systems in the sense of Lyapunov is given. The proof is not discussed here and has been given in many works [Kalman] [Yoshizawa] [Vidyasagar]. The theorem is that if there exists a Lyapunov function $V(X)$ in some region S (say a hyperspherical ball) around the origin, then the origin is stable for all X contained in S. Therefore, some requirements need to be met before $V(X)$ is called a Lyapunov function.

Referring to the last section, the following theorem is the basic stability theorem of Lyapunov's direct method with the system (4.2).

[Theorem 4.3.1] The equilibrium state 0 at time t_o of (4.2) is stable if there exists a continuously differentiable positive definite function V such that

$$\dot{V}(X(t)) \leq 0, \qquad \forall\, t \geq t_o \quad \forall\, X \in S, \qquad \text{for some ball } S\,.$$

The state is said to be uniformly stable, if V is strictly decreasing in the theorem. The theorem above provides sufficient conditions for stability but may not yield necessary conditions. To apply them to a particular system, it is a fairly simple matter to find a function V satisfying the requirements.

There is a more restrictive definition of stability than the previous one in that the condition $\dot{V}(X) = 0$ is not allowed. This means that a trajectory will not be allowed to stall on a closed hyperspherical ball of $V(X)$ containing the origin, but will always be required to approach the origin with a monotonic decrease in V along the trajectory. Precisely,

[Theorem 4.3.2] The equilibrium state 0 at time t_o of (4.2) is uniformly asymptotically stable over the interval $[t_o, \infty)$ if there exists a continuously differentiable decreasing positive definite function such that $-\dot{V}$ is a positive definite function.

4.4 Boundedness

The stability properties of the dynamical system have been recognized, under the conditions mentioned before. However, the time responses are not easily obtained, when the system (4.1) is nonlinear or uncertainty is included. A Lyapunov function candidate, which is chosen from a Lyapunov function of a stable nominal system, is utilized for the real system with uncertainties, and a control function is then obtained such that the Lyapunov function decreases along every possible trajectory of the uncertain system, at least outside a neighborhood of the zero state [Chen]. Therefore, two definitions need to be specified [Leitmann] [Yoshizawa].

[Definition 4.4.1] Given a solution $X(t) : [t_o, t_1] \longrightarrow R^n, X(t_o) = X_o$, of (4.1), we say it is uniformly bounded if there is a positive constant $d(X_o) < \infty$, possibly dependent on X_o but not on t_o, such that

$$\|X(t)\| \leq d(X_o), \ \forall \ t \in [t_o, t_1] \, .$$

[Definition 4.4.2] Given a solution $X(t) : [t_o, \infty) \longrightarrow R^n, X(t_o) = X_o$, of (4.1), we say that it is uniformly ultimately bounded with respect to set S, if there is a non-negative constant $T(X_o, S) < \infty$, possibly dependent on X_o and S but not on t_o, such that $X(t) \in S$ for all $t \geq t_o + T(X_o, S)$.

Stability properties have been illustrated so that the controller can be synthesized in the following sections to stabilize the system. This is the main task in this study.

4.5 Decentralized Joint Feedback

In this section, we will explain why decentralized controls can demonstrate adequate feedback performance for flexible manipulators. Independent linear controllers at each joint, commonly called joint proportional-derivative (PD) con-

trollers, which are based on the local measurements of joint positions (q_i) and velocities ($\dot{q}_i$) are described as follows:

$$\tau_i = -K_{pi}\bar{q}_i - K_{Di}\dot{\bar{q}}_i, \tag{4.8}$$

where K_{pi} and K_{Di} are positive constants. $\bar{q}_i = q_i - q_{ri}$ and $\dot{\bar{q}} = \dot{q}_i - \dot{q}_{ri}$, ($\dot{\bar{q}} = \dot{q}_i$), while q_{ri} is the reference state and assumed to be constant. Physically, the feedback system effectively equips each joint with equivalent rotary spring and damper. The frequency domain approach has been taken with the linearized system in previous works [Book, 1975], while the case of a rigid-link manipulator has been illustrated by Asada and Slotine [1986]. A Lyapunov approach is applied here to show the resulting stability.

Because the torques (τ) only act on each joint, the following equality exists,

$$\dot{X}^T Q = \dot{q}^T \tau, \tag{4.9}$$

where X, Q are given in (2.40). $q^T = [q_1, \cdots, q_n]$ represents the joint coordinate in (2.40). $\tau = [\tau_1, \cdots, \tau_n]^T$ and $\tau_i = Q_{io}$. In the absence of gravity and uncertainties such as friction and disturbances, the dynamics (2.40) becomes

$$M(X)\ddot{X} + H(X, \dot{X})\dot{X} + K\bar{X} = Q. \tag{4.10}$$

Lemma 4.5.1: Given a proper Lyapunov candidate (V) associated with the system (4.10) with feedback (4.8), the time derivative of V can be shown to be negative.

Proof: Consider a Lyapunov candidate V associated with the total mechanical energy of the feedback system [Slotine]:

$$V(X, \dot{X}, q) = \frac{1}{2}\left[\dot{X}^T M \dot{X} + \frac{1}{2}\bar{X}^T K \bar{X} + \frac{1}{2}\bar{q}K_p\bar{q} \right], \tag{4.11}$$

$C - 2$

where $K_p = \text{diag}\,[K_{pi}]$ and K is a positive constant matrix. Differentiating V with respect to time gives,

$$\dot{V} = \dot{q}^T K_p \tilde{q} + \dot{X}^T M \ddot{X} + \frac{1}{2}\dot{X}^T \dot{M}\dot{X} + \dot{X}^T K \bar{X}$$

$$= \dot{q}^T K_p \tilde{q} + \dot{X}^T (M\ddot{X} + K\bar{X}) + \frac{1}{2}\dot{X}^T \dot{M}\dot{X}, \qquad (4.12a)$$

By substituting (4.8), (4.9), (4.10) and $(\dot{M} - 2H)$ which is skew-symmetric into the above,

$$\dot{V} = \dot{q}^T K_p \tilde{q} + \dot{X}^T (Q - H\dot{X}) + \frac{1}{2}\dot{X}^T \dot{M}\dot{X}$$

$$= \dot{q}^T K_p \tilde{q} + \dot{X}^T Q + \frac{1}{2}\dot{X}(\dot{M} - 2H)\dot{X}$$

$$= \dot{q}^T K_p \tilde{q} + \dot{q}^T \tau$$

$$= -\dot{q}^T K_D \dot{q} \leq 0, \qquad (4.12b)$$

where $K_D = \text{diag}[K_{Di}]$ is a positive matrix.

Now, the system with the local joint PD control is stable. This leads to the development of an advanced control algorithm using the decentralized scheme which is restrictive on information transfer from one group of sensors and actuators to others.

4.6 Decentralized System

A system with a great multiplicity of measured outputs and inputs is commonly characterized as the Large-Scale system. This situation arising in a control system design may be treated with decentralization techniques. The designer for such systems determines a structure for control which assigns system inputs to a given set of local controllers, each of which observes only local system outputs. Figure 4.2 shows a two-controller decentralized system.

The advantages of this approach include ease in data gathering, computer program debugging and geographical separation of system components.

4.6.1 Decentralized Dynamics

In the flexible robot, unlike the conventional (rigid) robot, oscillations due to link elasticity need to be stabilized in addition to controling the joints. Therefore, the flexible manipulator system becomes a large scale system. Each link can be considered as a subsystem of the overall system.

In the absence of actuator dynamics, the system dynamics (2.40) of an n-link flexible manipulator combined with friction and other disturbances treated as uncertainties $R(\xi, \dot{\xi})$ are given in the following equation:

$$M(\xi)\ddot{\xi} + H(\xi, \dot{\xi})\dot{\xi} + K\xi + G(\xi) + R(\xi, \dot{\xi}) = Q. \tag{4.13}$$

Again, $M(\xi)$, the inertia matrix, is square, symmetric and positive definite. Therefore, one can define a constant matrix β such that

$$\|\beta\| \geq \|M^{-1}(\xi) - \beta\|, \tag{4.14}$$

where $\| \ \|$ is an induced norm. Note that β is usually chosen to have zero elements corresponding to subsystem coupling.

Equation (4.13) can then be rewritten as

$$\ddot{\xi} = -M^{-1}(\xi)\left[H(\xi, \dot{\xi})\dot{\xi} + K\xi + R(\xi, \dot{\xi}) + G(\xi)\right] + \beta Q + (M^{-1}(\xi) - \beta)Q. \tag{4.15}$$

Now, take each link i as a subsystem and define state variables $x_i = [\xi_i, \dot{\xi}_i]^T$, where ξ_i includes one joint coordinate and m_i generalized deflection coordinates for link i (2.38). Equation (4.15) is divided into n equations for the n interconnected subsystems. Therefore, each subsystem is described by a first-order differential equation of the form

$$\dot{x}_i = A_i x_i + b_i u_i + F_i(X) + f_i(X)u_i, \tag{4.16}$$

where $i = 1, 2, \ldots, n$; $X^T = [x_1, x_2, \ldots, x_n]^T$ and $u_i = Q_{io}$ in (2.39); $f_i(X)u_i =$ the coupling terms of $(M^{-1}(\xi) - \beta)Q$ for subsystem i. A_i is a constant matrix which represents the linear time invariant part of $-M^{-1}(\xi)K$.

$$A_i = \begin{pmatrix} 0 & I \\ a_{i1} & a_{i2} \end{pmatrix}, \tag{4.17}$$

while $F_i(X)$ represents the rest of $-M^{-1}K$ and the nonlinear terms of $-M^{-1}(\xi)[H(\xi, \dot{\xi})\dot{\xi} + R(\xi, \dot{\xi}) + G(\xi)]$. b_i becomes a vector form with zero elements on the upper half.

(i) $F_i(X)$ and $f_i(X)$ are assumed to be bounded and are modeled as system uncertainties assumed to have the properties [Leitmann]

$$F_i(X) \stackrel{\text{def}}{=} F_i(X, \sigma), \tag{4.18a}$$

$$f_i(X) \stackrel{\text{def}}{=} f_i(X, \sigma), \tag{4.18b}$$

where $\sigma \in R^p$ represents the system uncertainty and is continuous on R^p as well as the uncertainty bounding set.

(ii)
$$(A_i, b_i) \text{ is controllable.} \tag{4.19}$$

(iii) Moreover, there exist matrix functions $D_i(\ )$ and $E_i(\ )$ such that

$$F_i(X, \sigma) = b_i D_i(X, \sigma), \tag{4.20a}$$

$$f_i(X, \sigma) = b_i E_i(X, \sigma), \tag{4.20b}$$

where $\|E_i\| < 1$ from (4.14).

The dynamic system of flexible links is composed of rigid body modes and flexible modes, with the linear combination of flexible modes used to specify the deflection of any point along the arm from the position specified by the assumed

rigid body modes. If the dominant dynamics is related to the rigid body modes, for example the one-link flexible arm, then the flexible modes will contribute the most to the system uncertainties which are assumed continuous and bounded.

The control schemes implemented here assume the satisfaction of the matching conditions (4.20) [Leitman]. These conditions guarantee that the uncertainty vector does not influence the dynamics more than the control input does [Gutman]. However, the uncertainties (4.18) which do not satisfy (4.20) can be tolerated if they do not exceed the mismatch threshold [Chen, 1987].

Therefore, the overall system by the above assumptions will take the following matrix form

$$\dot{X} = AX + BU + BD(X,\sigma) + BE(X,\sigma)U , \qquad (4.21)$$

where for $i = 1, 2, \ldots, n$

$A = $ diagonal (A_i),

$B = $ diagonal (B_i),

$D(X,\sigma) = $ diagonal $(D_i(X,\sigma))$,

$E(X,\sigma) = $ diagonal $(E_i(X,\sigma))$ and

$U^T = [u_1, u_2, \ldots, u_n]$.

4.7 Reference Model

The objective of model reference adaptive control is to eliminate the state error between the plant and the reference model so that the behavior of the plant follows the model. Consider the reference model first.

$$\dot{x}_{mi} = A_{mi} x_{mi} + b_{mi} r_i , \qquad (4.22a)$$

where for $i = 1, 2, \ldots, n$

$x_{mi} = [\xi_{mi}, \dot{\xi}_{mi}]^T ,$

r_i is the reference input;

and let

$$A_{mi} = A_i + b_i K_{xi} , \qquad (4.22b)$$

$$b_{mi} = b_i K_{bi} , \qquad (4.22c)$$

where K_{xi} and K_{bi} are constant matrices with the corresponding dimension.

Also, A_{mi} which is a stable matrix satisfies the Lyapunov equation

$$A_{mi}^T P_i + P_i A_{mi} = -L_i , \qquad (4.23)$$

where P_i and L_i are positive definite and symmetric matrices.

4.8 Decentralized Robust Control

The signal-synthesis method [Landau] [Balestrino] implemented here seeks to control the system by adjusting the input u_i which is as described in the following equation

$$u_i = K_{xi} X_i + K_{bi} r_i + \psi_i(e_i) , \qquad (4.24)$$

where $e_i = x_{mi} - x_i$ is referred to as state error and the function ψ_i is the control input to compensate the system uncertainty. Thus, let ψ_i be

$$\psi_i(e_i) = \begin{cases} \frac{b_i^T P_i e_i}{\|b_i^T P_i e_i\|} \rho_i(X, e_i, r_i), & \text{when } \|b_i^T P_i e_i\| > \delta_i; \\ \frac{b_i^T P_i e_i}{\delta_i} \rho_i(X, e_i, r_i), & \text{when } \|b_i^T P_i e_i\| \le \delta_i, \end{cases} \qquad (4.25)$$

where δ_i is a prescribed positive constant and ρ_i is a positive constant which will be specified subsequently.

As a result, the error dynamics of the subsystem is derived from the difference between equation (4.16) and (4.22a) along with (4.24) and (4.20):

$$\dot{e}_i = \dot{x}_{mi} - \dot{x}_i$$

$$= A_{mi} e_i - b_i(\psi_i + v_i) , \qquad (4.26a)$$

where

$$v_i = D_i + E_i(K_{xi}x_i + K_{bi}r_i + \psi_i). \qquad (4.26b)$$

Given the boundedness of the state variable x_i and the reference input r_i, equations (4.26b) and (4.25) give the following inequality:

$$\|v_i\| \le \rho_i(X, e_i, r_i), \qquad (4.27a)$$

where

$$\rho_i(X, e_i, r_i) \stackrel{\text{def}}{=} \|D_i(X)\| + \|E_i(X)\| (\|K_{xi}x_i\| + \|K_{bi}r_i\| + \|\psi_i(e_i)\|). \qquad (4.27b)$$

This definition involves ρ_i on both sides of the equation. The definition of ρ_i in (4.27b) is valid, i.e., (4.27) can be solved since (4.14) is satisfied. Therefore, we have

$$\rho_i = (1 - \|E_i\|)^{-1} [\|D_i\| + \|E_i\|(\|K_{xi}\|\|x_i\| + \|K_{bi}r_i\|)]. \qquad (4.28)$$

Now, consider a closed ball, $B(\eta)$, centered at 0 with radius η,

$$\eta = \left[\frac{4\delta_i\rho_i}{\lambda_{\min}(L_i)}\right]^{1/2}. \qquad (4.29)$$

where $\lambda_{\min}$ represents the minimum eigenvalue. Since $L_i > 0$ from (4.23), one can define

$$\varepsilon(k) \stackrel{\text{def}}{=} \{e_i \in R^{m_i+1} \mid e_i^T P_i e_i \le k\}. \qquad (4.30)$$

Let

$$k > \underline{k}, \qquad (4.31a)$$

$$\underline{k} = \lambda_{\max}(P_i)\eta^2, \qquad (4.31b)$$

where $\lambda_{\max}$ represents the maximum eigenvalue; and let

$$k_o = e_i^T(t_o) P_i e_i(t_o). \qquad (4.31c)$$

Finally, if $e_i(t_o) \notin \varepsilon(k)$, define

$$C_o \overset{\text{def}}{=} \inf \{ e_i^T L_i e_i - 4\delta_i \rho_i \} . \qquad (4.32)$$

Theorem 4.8.1: For subsystem i, consider the system (4.16) and the reference model (4.22) with control (4.24). Conditions (i) - (iv) are met, then given any $k > \underline{k}$, every solution corresponding to initial condition $(e_i(t_o), t_o) \in R^{m_i+1} \times R^1$ is uniformly bounded with

$$d(e_i(0)) = \begin{cases} \|e_i(0)\| \left(\dfrac{\lambda\max(P_i)}{\lambda\min(P_i)} \right)^{1/2} , & \text{for } e_i(t_o) \notin \varepsilon(k); \\ \left(\dfrac{k}{\lambda\min(P_i)} \right)^{1/2} , & \text{for } e_i(t_o) \in \varepsilon(k), \end{cases} \qquad (4.33)$$

and time T to enter $\varepsilon(k)$ is uniformly ultimately bounded with respect to $\varepsilon(k)$ with

$$T(e_i(t_o), \varepsilon(k)) = \begin{cases} \frac{k_o - k}{C_o}, & \text{for } e_i(t_o) \notin \varepsilon(k); \\ 0 & \text{for } e_i(t_o) \in \varepsilon(k). \end{cases} \qquad (4.34)$$

Proof:

Since $P_i > 0$, the function $V(\ ) : R^{m_i+1} \rightarrow R_+$ given by

$$V(e) = e_i^T P_i e_i \qquad \forall \ e_i \in R^{m_i+1} \qquad (4.35)$$

is a Lyapunov function candidate.

To show that it is indeed a Lyapunov function for the system (4.26a) with any possible uncertainties, one needs to consider the time derivative of the Lyapunov candidate (4.35) as described before in (4.7).

$$\dot{V}(e_i) = \dot{e}_i^T P_i e_i + e_i^T P_i \dot{e}_i . \qquad (4.36)$$

$$\begin{aligned} \dot{V}(e_i) &= e_i^T (A_{m_i}^T P_i + P_i A_{m_i}) e_i - 2 e_i^T P_i b_i (\psi_i + v_i) \\ &= -e_i^T L_i e_i - 2 e_i^T P_i b_i (\psi_i + v_i) \\ &\leq -e_i^T L_i e_i - 2 [b_i^T P_i e_i]^T \left[\psi_i - \frac{b_i^T P_i e_i}{\|b_i^T P_i e_i\|} \rho_i \right] . \end{aligned} \qquad (4.37)$$

With control (4.25), thus

if $\|b_i^T P_i e_i\| > \delta_i$,

$$\dot{V}(e_i) \leq -e_i^T L_i e_i \, ;$$

if $\|b_i^T P_i e_i\| \leq \delta_i$,

$$\dot{V}(e_i) \leq -e_i^T L_i e_i + 4\delta_i \rho_i \, . \tag{4.38}$$

Consequently, $\dot{V} < 0$ is a necessary condition to satisfy the Lyapunov function for all $t \in R^1$ and all e_i. Then,

$$e_i^T L_i e_i - 4\delta_i \rho_i > 0 \, . \tag{4.39}$$

From the definition of matrix norm,

$$\lambda_{\min}(L_i)\|e_i\|^2 \leq e_i^T L_i e_i \leq \lambda_{\max}(L_i)\|e_i\|^2 \, . \tag{4.40}$$

Since L_i is positive definite, (4.39) and (4.40) give the following inequality:

$$\lambda_{\min}(L_i)\|e_i\|^2 - 4\delta_i \rho_i > 0 \, . \tag{4.41}$$

Therefore, $\dot{V} < 0$ is assured for all $t \in R^1$ and all $e_i \notin B(\eta)$, where η is given in (4.29). Now, consider the boundedness of all solutions for (4.26a). (a) If $e_i(t_o) \in \varepsilon(k)$, then $e_i(t) \in \varepsilon(k_o)$, and (b) if $e_i(t_o) \notin \varepsilon(k)$, then $e_i(t) \in \varepsilon(k)$ for all $t \in [t_o, t_1]$. The Lyapunov candidate gives boundedness.

$$0 < \lambda_{\min}(P_i)\|e_i(t)\|^2 \leq e_i^T P_i e_i \leq e_i^T(t_o) P_i e_i(t_o) \leq \lambda_{\max}(P_i)\|e_i(t_o)\|^2 \, , \tag{4.42}$$

for case (a), which leads to

$$\|e_i(t)\| \leq \|e_i(t_o)\| \left[\frac{\lambda_{\max}(P_i)}{\lambda_{\min}(P_i)}\right]^{1/2} \, ;$$

$$0 < \lambda_{\min}(P_i)\|e_i(t)\|^2 \leq e_i^T P_i e_i \leq k$$

for case (b), which leads to

$$\|e_i(t)\| \leq \left[\frac{k}{\lambda_{\min}(P_i)} \right]^{1/2} .$$

This proof shows the uniform boundedness result (4.33).

The ultimate boundedness result also follows conditions (4.38) and (4.39). If $e_i(t_o) \in \varepsilon(k)$, it is an immediate consequence of the boundedness result, and $T(e_i(0), \varepsilon(k)) = 0$. If $e_i \notin \varepsilon(k)$, then $V(e_i)$ decreases and $e_i(t)$ reaches the boundary $\partial \varepsilon(k)$ of the ball $\varepsilon(k)$ in a finite time interval. An upper bound of this interval is obtained by considering

$$\dot{V}(e_i(t)) \leq -C_o , \tag{4.43}$$

where C_o is given in (4.32).

Define t' and $e_i(t') \in \partial \varepsilon(k)$. It means that t' is the time when e_i crosses the boundary of $\varepsilon(k)$. So,

$$V(e_i(t')) - V(e_i(t_o)) \leq -C_o(t' - t_o)$$

$$k - k_o \leq -C_o(t' - t_o)$$

$$t' - t_o \leq \frac{k_o - k}{C_o} \overset{\text{def}}{=} T(e_i(t_o), \varepsilon(k))$$

Then, this is uniformly ultimately bounded with (4.34).

4.8.1 Physical Interpretation of the Control System

Some fundamental control techniques such as pole placement, optimal control, state feedback and state estimation require complete information from all system sensors for the sake of feedback control. However, these schemes are inadequate for feedback control of large-scale systems. Due to the physical configuration and high dimensionality of such systems, a centralized control is neither economically feasible nor even necessary. Therefore, a total decentralization is employed, that is, every local control is obtained from the local output and possible external input. In many applications, some degree of restriction, however, needs to be assumed. The control input here includes the linear and the nonlinear parts. The local and linear feedback controller is used to stabilize the subsystem when isolated from the rest of the system. Then, regarding the interactions among the subsystems as uncertainties, a nonlinear controller is utilized to minimize the coupling effects.

The "matching conditions" embodied in condition (iii) assures that the range space of the input, BU in (4.21), contains that of the uncertainties. Thus, there is an input that can cancel the possible uncertainties. The nonlinear controller given in (4.25) is a type of saturation control and a constant is imposed to determine the saturated level. However, the feedback gain can generally expressed by

$$\psi_i(e_i) = \begin{cases} \frac{b_i^T P_i e_i}{\|b_i^T P_i e_i\|} \rho_i, & \text{when } \|b_i^T P_i e_i\| > \delta_i; \\ \|\psi_i(e_i)\| \le \rho_i, & \text{when } \|b_i^T P_i e_i\| \le \delta_i. \end{cases} \tag{4.44}$$

Note that the controller in (4.44) which may be a discontinuous control leads to the excitation of vibration modes in the case of application in a flexible structure.

Equation (4.14) needs to be satisfied so that condition (iii) is assured. This means that a given control acts in the desired "direction".

However, as distinct from other decentralized control schemes, the scheme presented in this chapter attempts to stabilize a large linear system by manipulating

only subsystem matrices. Besides a considerable saving in the numerical aspects of control, the presented scheme produces systems which are dynamically reliable with respect to structural perturbations and which can tolerate a wide class of nonlinearities in the interactions among the subsystems. As a matter of fact, by this scheme systems can be stabilized in cases where we have no information about the actual shape of the nonlinear interactions among the subsystems, and only their bounds are available to the designer.

In the previous section, the uniform boundedness of each subsystem has been proven. However, uniform boundedness of individual subsystems does not constitute boundedness of the total system. Thus, one must consider the total system and establish uniform boundedness and uniformly ultimate boundedness.

Theorem 4.8.2: The system (4.13) represented by (4.21) is uniformly bounded, if the reference model (4.22a) of each subsystem is stable and the error dynamics (4.26a) of subsystem is uniformly bounded with the control input (4.24).

Proof:

Let us assume that a Lyapunov function V_i for the error dynamics (4.26a) of subsystem i is known and consider the use of a weighted sum as a candidate for the Lyapunov function of the error dynamics of the total system:

$$V = \sum_{i=1}^{n} d_i V_i \,, \tag{4.45}$$

where the coefficients $d_i, i = 1, \ldots, n$, are positive constants. Thus, $\dot{V} = \sum_{i=1}^{n} d_i \dot{V_i}$.

From Theorem 4.8.1, $\dot{V_i}$ is negative, if all error states ($e_i = x_{mi} - x_i$) are outside the ball region of (4.29). To choose the reference model to be stable and its subsystem as described in (4.22a).

$$\dot{X}_m = A_m X_m + B_m r \,, \tag{4.46}$$

where $A_m = \text{diag}\,[A_{m1} \cdots A_{mn}]$ and $B_m = \text{diag}\,[b_{m1} \cdots b_{mn}]$. Then, $\dot{V} < 0$ is assured for all $e(t)\,(e = [e_1 \cdots e_n]^T) \notin B(\eta)$, where a closed ball $B(\eta)$ centered at 0 has a radius η,

$$\eta = \left[4 \sum_{i=1}^{n} \frac{\delta_i \rho_i}{(d_i)\lambda_{\min}(L_i)} \right]^{1/2} . \qquad (4.47)$$

Therefore, the uniform boundedness of the total system is clearly shown.

From Theorem 4.8.2, it should be emphasized the system may become unstable if stability is not satisfied for any of the subsystems. In other words, the total system (4.21) is stable, only if the matching conditions are met for all subsystems given by (4.20).

4.9 Decentralized Adaptive Control

The controller design implemented here has not been specifying the state responses in the transient time; i.e., large state error and/or oscillation transients may occur. To overcome this problem and to improve convergence speed, an auxiliary input $w_i(t)$ is introduced and applied to the input u_i in (4.24). This input is effectively an integral action. Thus,

$$u_i = K_{zi} x_i + K_{bi} r_i + \psi_i(e_i) + w_i . \qquad (4.48)$$

The error dynamics (4.26a) then becomes

$$\dot{e}_i = A_{mi} e_i - b_i(\psi_i + v_i + w_i) , \qquad (4.49)$$

where v_i still has the same form as (4.26b) and is bounded in ρ_i.

The auxiliary signal $w_i(t)$ is expressed in the following:

$$\dot{w}_i = -\alpha_i(t)w_i + S_i^{-1} b_i^T P_i e_i , \qquad (4.50)$$

where $S_i > 0$ and

$$\alpha(t) \geq \frac{(4\delta_i \rho_i - \lambda_{\min}(L_i)\|e_i\|^2)}{2\lambda_{\min}(S_i)\|w_i\|^2} \qquad \forall\, t \in R^1 . \qquad (4.51)$$

With the feedback input in (4.48), the stability of the system needs to be analyzed. The next theorem therefore specifies the result.

Theorem 4.9.1: The error dynamics (4.49) between (4.22a) and (4.16) with control (4.48) is uniform bounded, if (4.23), (4.25), (4.27) and (4.50) are satisfied.

Proof:

The proof of this theorem is similar to that of Theorem 4.8.1. The only additional requirement to be considered is that there exists a Lyapunov function.

Define a candidate Lyapunov function which is positive definite,

$$V = e_i^T P_i e_i + w_i^T S_i w_i .\qquad(4.52)$$

Taking the derivative of (4.52) along with (4.49) yields

$$\dot{V} = -e_i^T (A_{mi}^T P_i + P_i A_{mi}) e_i - 2 e_i^T P_i b_i (\psi_i + v_i + w_i) + 2 \dot{w}_i^T S_i w_i$$

$$= -e_i^T L_i e_i - 2 [b_i^T P_i e_i]^T (\psi_i + v_i) + [2 S_i \dot{w}_i - 2 b_i^T P_i e_i]^T w_i .\qquad(4.53)$$

From Theorem 1 and (4.50), $\dot{V}$ in (4.53) gives the following inequality:

$$\dot{V} \leq -e_i^T L_i e_i + 4 \delta_i \rho_i - 2\alpha w_i^T S_i w_i .\qquad(4.54)$$

And by satisfying (4.51), one obtains $\dot{V} \leq 0$. Consequently, the system is evidently uniformly bounded.

The auxiliary signal w_i imposed here is to improve the system performance. In the Lyapunov synthesis, convergence speed of a dynamic system can be compared by a positive value $\gamma = -\dot{V}/V$ [Kalman]; i.e., the convergence rate in the feedback system is faster, if the value γ is larger. Obviously, the system with control (4.48) has a larger value of γ than that with control (4.24), if α satisfies the following inequality.

$$\alpha > \frac{\lambda(L_i)\|e_i\|^2 - 4\delta_i \rho_i}{\lambda(P_i)\|e_i\|^2} .\qquad(4.55)$$

This can be seen by comparing (4.35) and (4.38) with (4.52) and (4.54). Note that (4.51) and (4.55) are not conflicting conditions since (4.51) gives a necessary condition on $\alpha(t)$ for the system with uniform boundedness.

4.9.1 Design Procedure

This section summarizes the procedure for this decentralized adaptive control design. The inertia matrix can be acquired from the dynamic equation (4.13) so that β is determined from (4.14) to form b_i in equation (4.16). A_i is obtained by linearizing the equation (4.13). According to equations (4.22), the constant feedback gains K_{zi} and K_{bi} are calculated and the reference model A_{mi} and b_{mi} can be chosen to be stable. P_i and L_i are obtained from the matrix Lyapunov equation (4.23). The reference input r_i can be directly derived from inverse dynamics of the reference model with the values associated with the deflection states assumed to be zero; i.e., the reference input comes from the "rigid" dynamics only. Finally, the control input u_i is given by equation (4.24) and with an auxiliary signal given by equation (4.49). Note that ρ_i satisfies the inequality (4.27) and those bounds can be determined from the workspace domain of robot manipulators and the state region of the reference model. A case study is provided in Appendix 3 and the block diagram is shown in Appendix 6.

4.10 Summary

The joint PD controller has been proven to stabilize the system, while the decentralized adaptive control with robust stabilization has been proven for motion control of large structures and flexible manipulators. Under consideration of the uncertainty for interconnected terms of each subsystem, the dynamic system of the manipulator motion is illustrated to be bounded, while an auxiliary input with the update action should have faster convergence rate and smaller steady-state error.

The possible magnitude of the uncertainty is presumed known, making the statistical information for a stochastic approach unnecessary. Thus, the feedback systems are also insensitive to other uncertainties such as friction, backlash, measurement error, etc.

Without adaptation of parameters, this control has a simple control structure for reducing real-time calculation. This leads to an attractive option both to address complex tasks, and simplified high level programming of more standard operations. The control algorithm has superior performance for high-speed motion, when the manipulator is light-weight. However, the drawback of the signal synthesis method which may cause saturation of the control torque will be discussed in the next chapter. It will be shown that problems caused by such drawback can be eliminated by choosing a proper input matrix in the control algorithm.
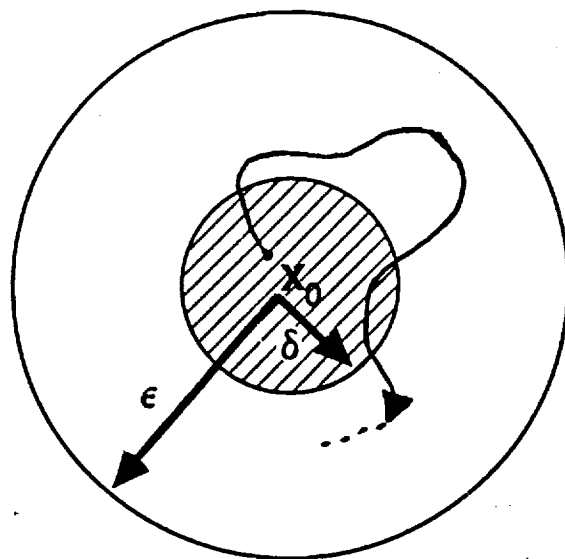
Definition of Stability
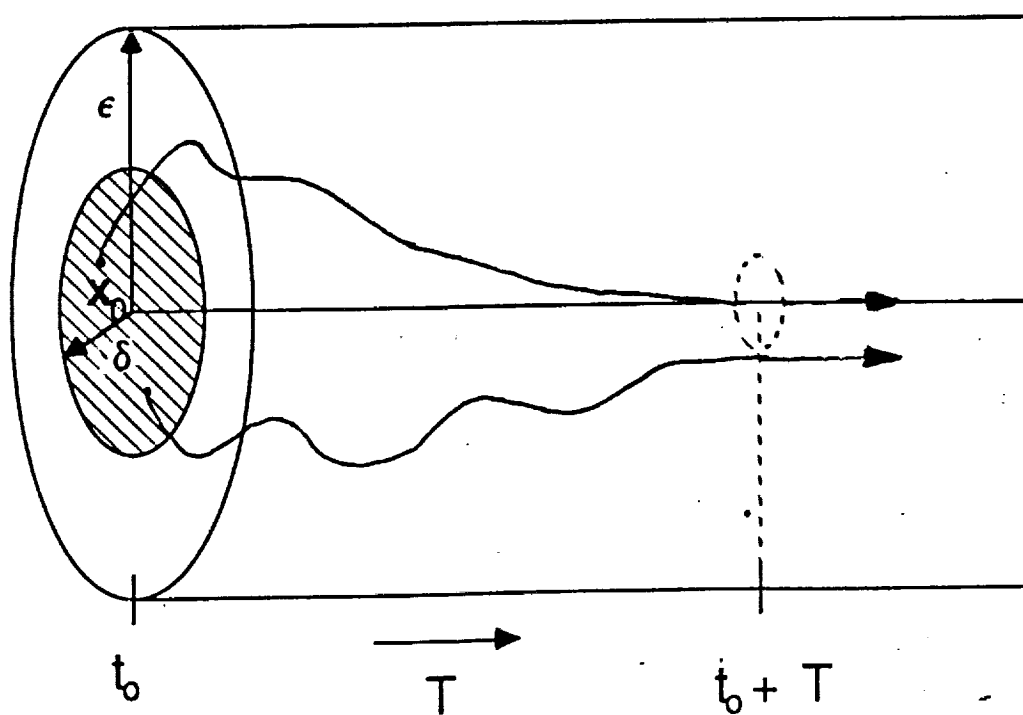
Definition of Asymptotic Stability

Figure 4.1 Definition of stability.
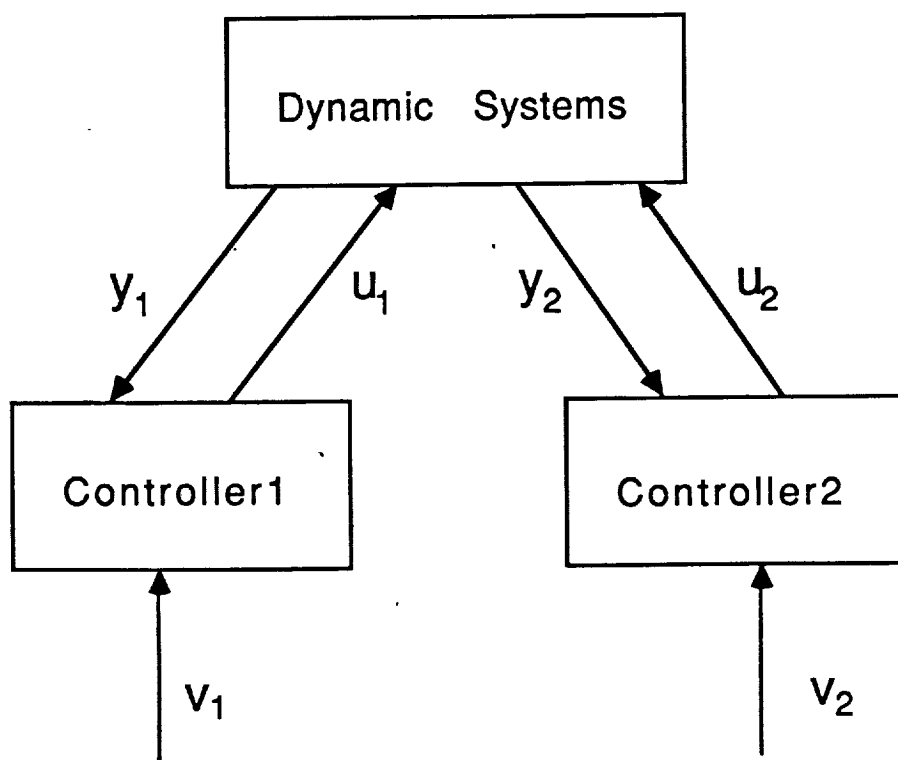
Figure 4.2 Decentralized control system (a two-controller case).

CHAPTER V

CONTROL IMPLEMENTATION
AND EXPERIMENTAL INVESTIGATION

In the previous chapters, the dynamic model of motion for flexible arms has been obtained by the recursive method and the control algorithm implemented here has been proven to be theoretically feasible. Therefore, computer simulations and physical experiments should be carried out to test the theoretical work. A computer-controlled prototype of a two link manipulator, RALF (Robotic Arm, Large and Flexible) driven by hydraulic cylinders is used to perform this verification. The experimental results show promise for the adaptive control algorithm.

5.1 Experimental Apparatus

To establish a point of reference for the following works and to set the physical scale of the experiment, the experimental facilities need to be described and illustrated. Chapter III has introduced the mechanical components of RALF. This section will specify measurement sensors, signal conditioning, and the computer system and its interface involved in the control experiment. Figure 5.1 shows the block diagram of the control implementation and software program, which is indicated in the dashed line. Figure 5.2 is the flow chart of the plot used to execute the computation of the controller.

A Micro Vax II running the VMS operating system is used to provide high-speed calculation during real-time control. The data acquisition and control signals use the analog to digital (A/D) and digital to analog (D/A) boards with 12-bit resolution. The control program is written in Fortran. It results in sampling and calculation

time of 7 ms. When the adaptive control algorithm is applied, computation time is increased by approximately 1 ms to a total of 8 ms. However, this sampling rate is feasible to control the RALF since the bandwidth of both hydraulic actuators is above 45 Hz and the lowest two frequencies of the RALF are 5.69 Hz and 9.12 Hz, while the higher mode frequencies are hardly measurable. The actuating link's slowest response is about 30 Hz, which cannot be controlled.

The measurement of the piston position is used for feedback instead of the joint angle. A linear variable differential transformer (LVDT) is the transducer. Because the LVDT is located at the same position as the actuator, the non-collocation problem existing in the feedback control of flexible structures may be avoided [Balas]. However, the transducer mounted at the joint reflects the flexible motion, while the LVDT does not reflect the flexibility of the link. Figure 5.3 shows the time responses of the angular transducer and the LVDT of both links.

Strain gages mounted near the base and midpoint of each link provide measurements of the link deflections. The relationship between strain gage and link deflection has been described in Chapter III. Bridge circuitry and amplification are used to augument the strain signal. The servo valve of the hydraulic actuator is driven by a power amplifier based on the voltage signal.

In this experiment, only the equivalent joint angle that is calculated from LVDT reading (Appendix 4) and the link strain are measured (Appendix 5). However, the control design applied here requires that all states be available; i.e., the joint angular velocity and the strain rate must be obtained. The estimator technique, however, may not easily be implemented due to the characteristic of the controller and the dynamical uncertainty. A low-pass digital filter is utilized as a pre-filter in the control program such that all feedback signals are not subject to sudden changes. Therefore, the difference of the angular position and the strain directly give their

rates. The low-pass digital filter design technique implemented here is such that an ideal low-pass filter in the s-plane with a cut-off frequency 0.3π is mapped to the z-plane by means of the bilinear transformation [Oppenheim]. A third order filter is used in this experiment and described as follows:

$$H(s) = \frac{0.12460\,(s^2 + 1.3040)}{(0.6498s + 0.2448)\,(s^2 + 0.2521s + 0.4313)} \,. \qquad (5.1)$$

A phase lag results, but it is small compared to the dominant frequencies of the RALF such that the feedback signals of all states are not wrapped and applicable to control the system.

5.2 Computer Simulation

A computer simulation has been conducted to evaluate the performance of the control schemes developed in the last chapter, which include joint PD feedback, decentralized control (with strain feedback) and adaptive control (also decentralized, with strain feedback). The detailed dimensions of flexible manipulators have been described in Chapter III. A one-link flexible manipulator which is considered a "quasi-linear" case has been studied by many workers so that it will not be discussed in this thesis. The control of RALF which represents a multi-link flexible manipulator operating in the gravitational field should lead to more contribution from the practical and theoretical points of view. Since the bandwidth of the hydraulic actuator is much higher than the first two frequencies of RALF, the dynamics of the actuator is assumed to be a constant. To compare the analysis with the experiment, time responses are simulated with payloads of 0 lb and 30 lb, while one flexible mode on each link is assumed. The controller design is carried out assuming no payload on the end and the configuration of the RALF at "home" position; i.e., the first joint of 35° and the second joint of 109°. Without modification of the controller and by adding a 30 lb payload to the configuration, one can illustrate the

robustness of the feedback system through the simulation.

Different sets of simulations have been carried out with point-to-point and trajectory tracking control of joints. The Runge-Kutta method using sampling time of 0.1 ms is utilized to solve the nonlinear dynamics. First, the control gains are derived from the LQR (Linear Quadratic Regulator) technique with a prescribed degree of stability (α) for the linearized dynamics. From the experimental results of Chapter III, the constants for the first and the second actuators are 5238 and 3374 respectively. In order to reduce the joint angular errors, the weighting matrix is selected to be diag [1E11, 1, 1E11, 1, ..., 1] and the joint torque penalty matrix is an identity matrix of order 2. Therefore, the gains associated with the joint positions and velocities turn out to be the joint PD controller as follows:

$$K_p = \begin{pmatrix} 2.8161E7 & 0. \\ 0. & 3.0015E7 \end{pmatrix} , \tag{5.2a}$$

$$K_D = \begin{pmatrix} 2.8031E5 & 0. \\ 0. & 7.7616E4 \end{pmatrix} , \tag{5.2b}$$

The decentralized controller given in (4.24) is then obtained as

$$K_{z1} = \begin{pmatrix} -2.8161E7 & -1.3518E4 & -2.8031E5 & -1.1384E3 \end{pmatrix} , \tag{5.3}$$

and

$$K_{z2} = \begin{pmatrix} -3.0015E7 & -1.0065E4 & -7.7616E4 & -268.2405 \end{pmatrix} . \tag{5.4}$$

Equation (4.14) needs to be satisfied in deriving b_i such that β^{-1} is here chosen as the inertia matrix with the interconnecting terms of zero. Therefore, b_1 and b_2 are

$$b_1 = \begin{pmatrix} 0. \\ 0. \\ 0.002 \\ -0.2589 \end{pmatrix} , \tag{5.5a}$$

and

$$b_2 = \begin{pmatrix} 0. \\ 0. \\ 0.0373 \\ -5.2673 \end{pmatrix}. \tag{5.5b}$$

By equation (4.22), the reference model is

$$A_{m1} = \begin{pmatrix} 0 & 0 & 1 & 0 \\ 0 & 0 & 0 & 1 \\ -6.6489E4 & 29.2705 & -573.9691 & -2.3310 \\ 8.4057E6 & -6.0265E3 & 7.2562E4 & 294.6916 \end{pmatrix}, \tag{5.6}$$

and

$$A_{m2} = \begin{pmatrix} 0 & 0 & 1 & 0 \\ 0 & 0 & 0 & 1 \\ -1.1877E6 & 151.1719 & -2.8961E3 & -10.0089 \\ 1.6765E8 & -2.8189E4 & 4.0883E5 & 1.4128E3 \end{pmatrix}. \tag{5.7}$$

Substituting the above into (4.23) with $L_i = \text{diag}[1E9, 1E4, 1, 1]$, the Lyapunov equation gives

$$P_1 = \begin{pmatrix} 1.7177 & 0.0084 & 0.0111 & 0.0001 \\ 0.0084 & 0.0001 & 0. & 0. \\ 0.0111 & 0. & 0.0006 & 0. \\ 0.0001 & 0. & 0. & 0. \end{pmatrix} \times 1.E7, \tag{5.8}$$

and

$$P_2 = \begin{pmatrix} 2.9435 & 0.0143 & 0.0069 & 0. \\ 0.0143 & 0.0001 & 0. & 0. \\ 0.0069 & 0. & 0.0003 & 0. \\ 0. & 0. & 0. & 0. \end{pmatrix} \times 1.E7, \tag{5.9}$$

The value of ρ_i in (4.25), which is determined by (4.28), is here set to be 3.0E5 from the engineering viewpoint; and the value of δ_i is then 2.0. For the decentralized adaptive controller, S_i, is chosen to be 3.33E-3, while α_i is simply set to zero.

The various simulation conditions are outlined in Table 5.1. First, the end point of each link is moved about 8.5 inches in 0.4 seconds for joint point-to-point control. Figures 5.4a and 5.4b show the typical position and velocity profiles of the reference joint angle. Without payload, time responses are illustrated for three different controllers (PD, Decentralized and Adaptive) in Figures 5.5a-d. It is noticed in

Fig. 5.6a-d that the system with payload has lower vibrational frequency on the upper and lower links. Obviously, the decentralized adaptive control results in the best performance in joint position tracking as well as link flexibility, while the joint PD control expresses the stability of the feedback system. Figures 5.6a-d show the results of each state for the case of a 30 lb payload but using the same controllers as in Fig. 5.5. The state responses of the decentralized control are convergent, but worse than those of the case of no payload due to nonadaptive action. Therefore, it is noted that all of the three controllers demonstrate the robustness with the addition of the payload.

For a longer travel, the reference joint position and velocity are shown in Figures 5.7a-b. The tip ends of both the lower and the upper links are moved approximately 24.3 inches in 1 second. Therefore, the nonlinear effect and the inertia variation have more impact on the dynamical system. But the joint angle change is still small. Figures 5.8a-d show the time responses of the feedback system with no payload, while Figures 5.9a-d show those of the system with 30 lb payload. Note that better tracking and fast vibration-setting time of each link still occur with adaptation but that the link oscillations damp out slowly for the joint PD and the decentralized controls when the system has the payload on the tip. Some variations between experiment and simulation are expected since some vibrational energy is absorbed by the hydraulic actuators but not included in the simulation model.

For the tracking control of a joint trajectory, the reference signal for both joints is a sinusoid with the magnitude of 0.0167 radian and the frequency of 3 Hz, which is close to the first structural frequency of the system with payload. Error responses for both joints with and without payload are as shown in Figure 5.10. Time responses of the strain without and with payload are demonstrated in Figures 5.11a-b and Figures 5.12a-b respectively. The joint PD controller results in

the least accuracy in the path tracking of each joint and the greatest amplitude in the oscillation of each link among three controllers applied here. The decentralized adaptive control shows its adjustability to different conditions.

5.3 Experiments

In order to verify the effectiveness of control schemes implemented on flexible manipulators, several tests which are roughly parallel to the simulations have been carried out. The experimental conditions are outlined in Table 5.2. The control program has been discussed in Section 5.1. The values of the joint angle are converted from the measurements of the LVDT instead of the noisy signals measured directly from the joint. Due to the dimension of the hydraulic actuators and size of the valves, the speed of the manipulator will have some limit before saturating the actuators. This results in comparatively small oscillations on each link so that only one strain gage needs to be used in the experiments. However, the A/D range is ±10 Volts and may saturate on the strain signal with a constant saturation value substituted for the true one. The outputs from the reference model are off-line calculated and stored in computer memory. If the reference model has stability of a high degree, the reference outputs can be substituted by the states of the tracked path without increasing real-time computation. Again, the actuator is treated here as a constant signal-gain from the practical point of view.

The first set of plots (Figures 5.13a,b) show time responses of the strain from the lower link without and with the decentralized control, when an impulse force suddenly pushes the lower link. The strain responses of both links are then shown in Figures 5.14 and 5.15 for a step reference input to each joint. Obviously, the link oscillations damp out slowly if the system does not have strain feedback; i.e., the joint PD control. Figures 5.16a,b show the control inputs to the actuators.

Figures 5.17a,b demonstrates the pistons of both actuators moved one inch in 0.4 seconds. The case of the decentralized control with no adaptation is excluded in this experiment. Figures 5.18a,b and 5.19a,b show the results from strain gages with the joint PD control and the decentralized adaptive control respectively. Note that no payload is added to the manipulator. Figures 5.20-5.22 are for the case of the pistons being moved 3 inches in 1 second. In the decentralized adaptive control, the overshoot occurs when traveling longer distances, while the steady-state errors are reduced. It is noted that the gravitational effect provides the partial reason for the steady-state error in the joint PD control.

With 30 lb payload, two cases of motion described above have been executed. The plots of the resulting responses are given in Figures 5.23-5.28. The decentralized adaptive control always provides more accuracy on the joint tracking and much faster vibration-setting time, although the overshoot may appear on the end point of travel due to the different adaptive gain implemented. From these experiments, one can also conclude that the adaptive control is robust and self-adjustable so that it is insensitive to variations in the payload. Figures 5.29a-d show the strain responses from both links, when the manipulator moves several points in the workspace.

Figures 5.30a-d, and 5.31a-d illustrate the responses of the strains when the manipulator is controlled by the joint PD and when the decentralized adaptive scheme is utilized to follow a sinusoidal reference actuator position of 0.3 inches and 3.33 Hz. Note that frequencies other than 3.33Hz appears in the strain response of the upper link if the system is controlled by the joint PD scheme.

5.4 Summary

The work done in this chapter emphasizes verification of the control algorithms developed for the RALF by simulation and experiments. The experimental facility

has been introduced taking into account its equivalently mathematical value and restriction. Several cases have been studied to compare the results. Conditions similar to the experiments are imposed in simulations of the feedback system.

The results from simulation, which are based on the theoretical work, are compared with the experiments to illustrate agreement, while the cases of point-to-point and trajectory tracking are common in robot controls. Due to transducer limitations, the piston motion responses in the experiments need to be converted into the corresponding joint angle responses in the simulations. The conversion between the LVDT and the joint angle is shown in Appendix 4 and the strain calibration from the measurement voltage is found in Appendix 5 [Huggins]. However, the fact that the simplified model used in the simulation may cause small deviation from the measured experimental data is expected and acceptable from the engineering point of view.

By applying positive gains on individual joint position and velocity feedbacks, the system is shown to be stable. This agrees with the theoretical conclusion. The decentralized algorithm results in much improvement. To achieve insensitivity to variations of the payload and to large motion, the adaptive scheme of control is superior. Therefore, the fact that the interconnected action between subsystems is bounded and comparatively small also agrees with assumptions made in this work.
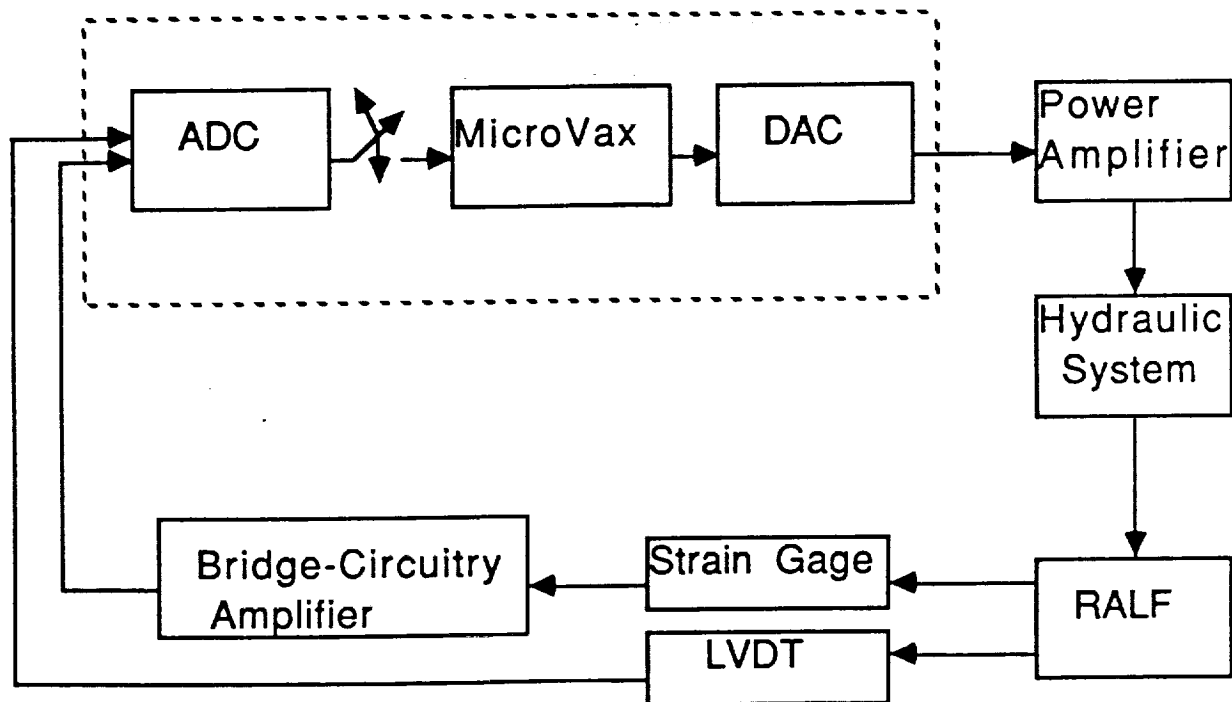
Figure 5.1 Block diagram of experimental control implementation.
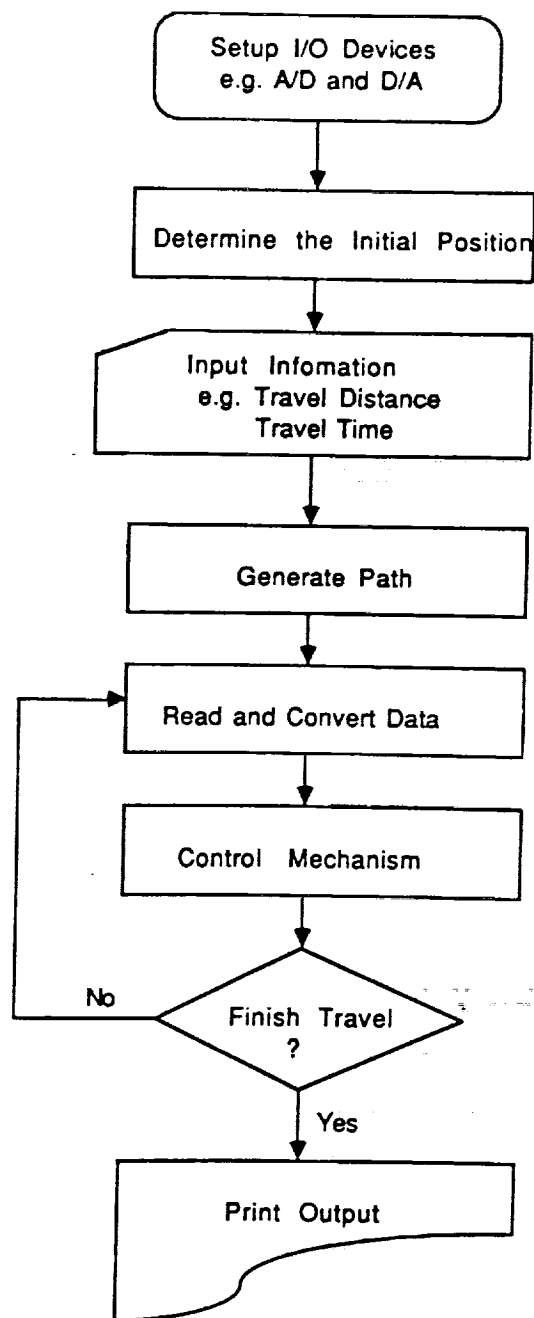
Figure 5.2 Block diagram of control algorithm.

(a)

(b)
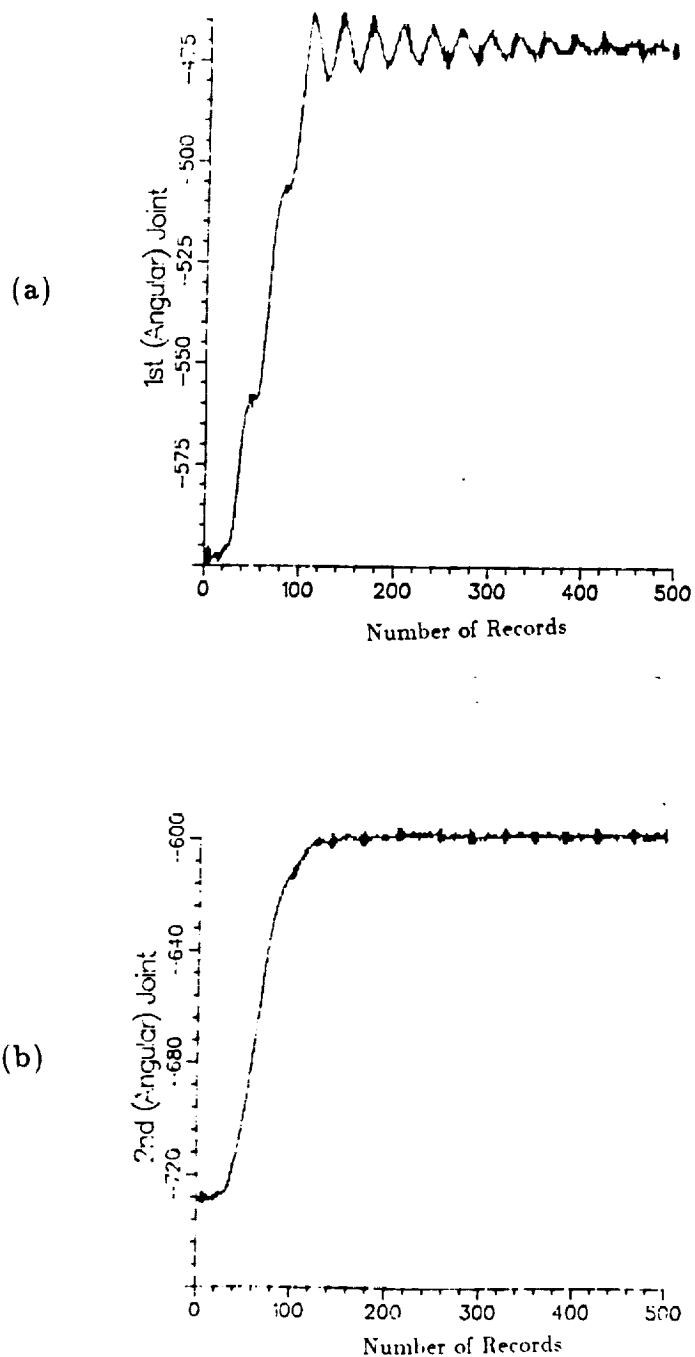
Figure 5.3a,b (a) Time response of the first joint angular transducer. (b) Time response of the second joint angular transducer.

(c)

1st (LVDT) Joint

Number of Records

(d)

2nd (LVDT) Joint

Number of Records
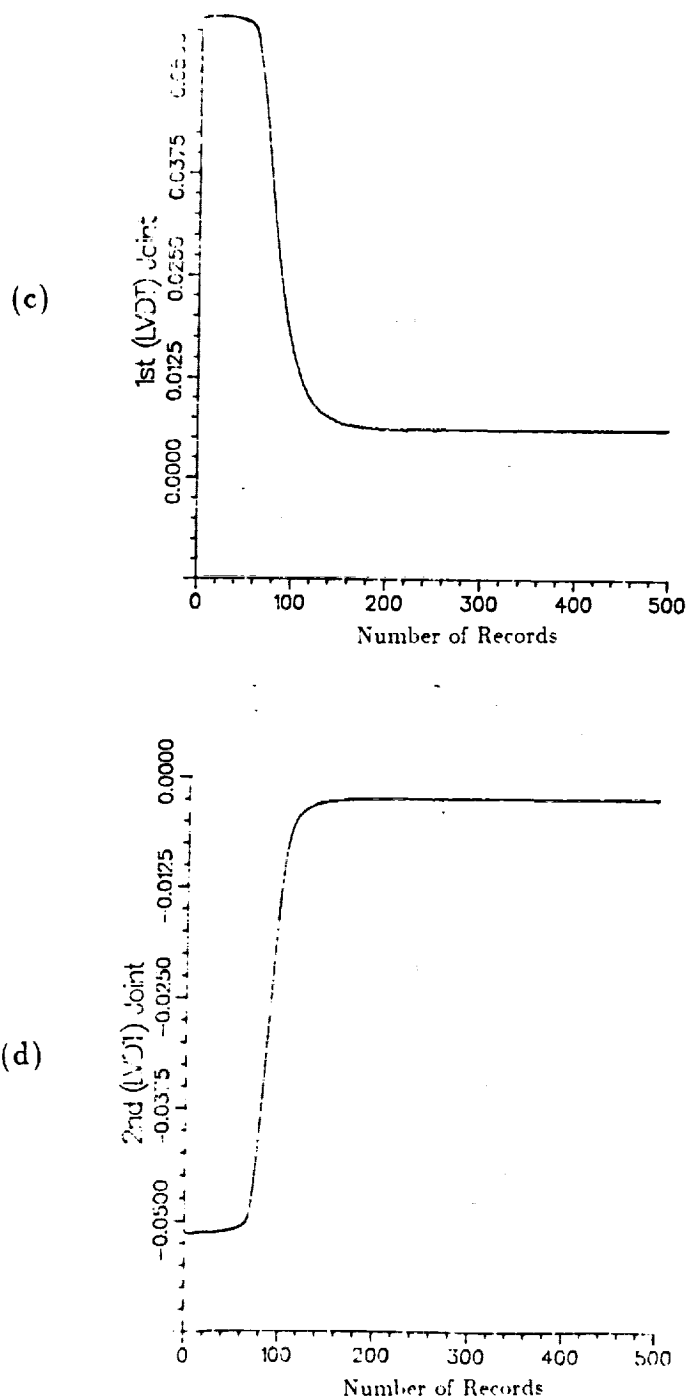
Figure 5.3c,d (c) Time response of the first LVDT. (d) Time response of the second
LVDT.

Reference Position

(a)

Reference Velocity

(b)
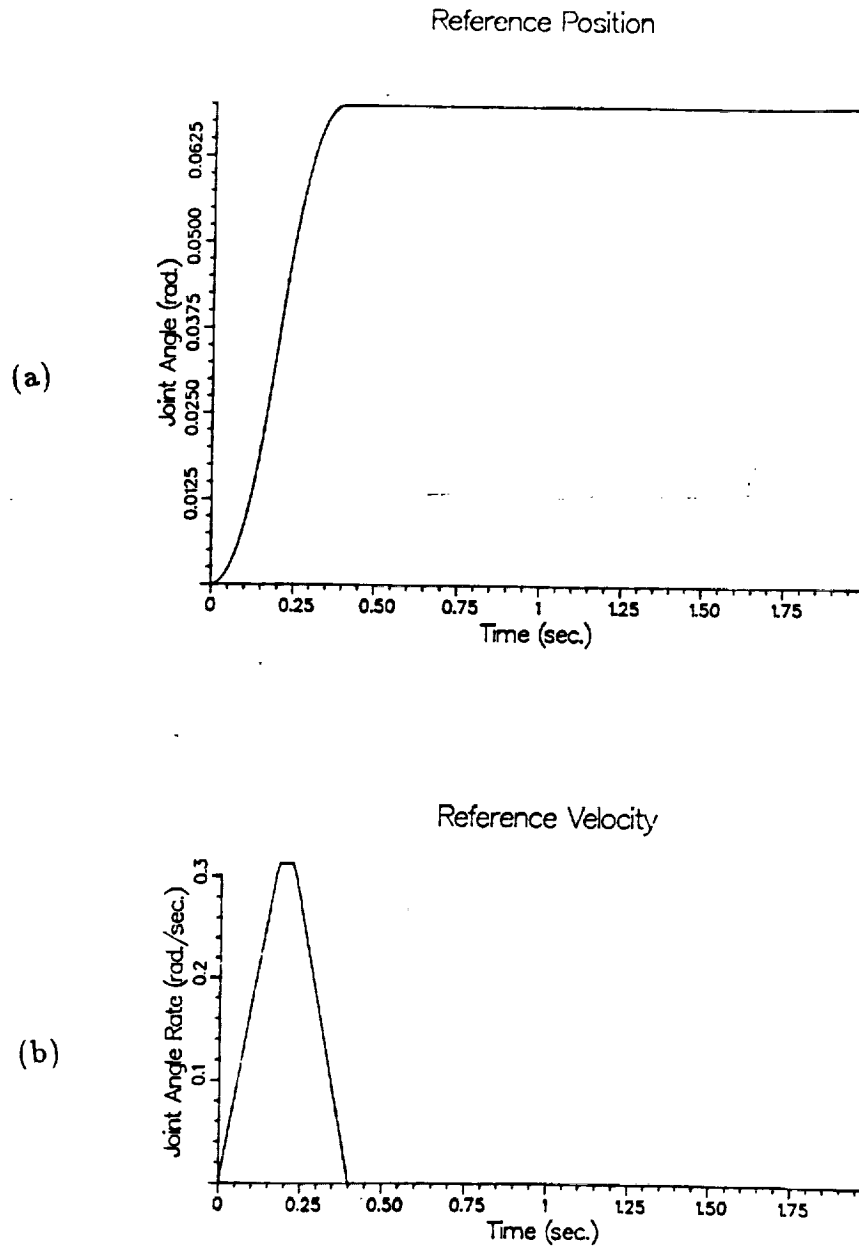
Figure 5.4 (a) Reference position profile. (b) Reference velocity profile.
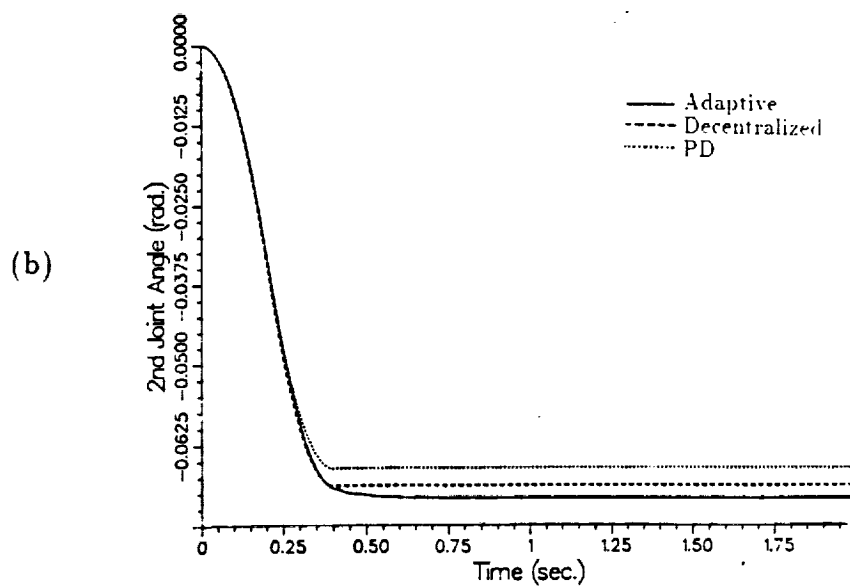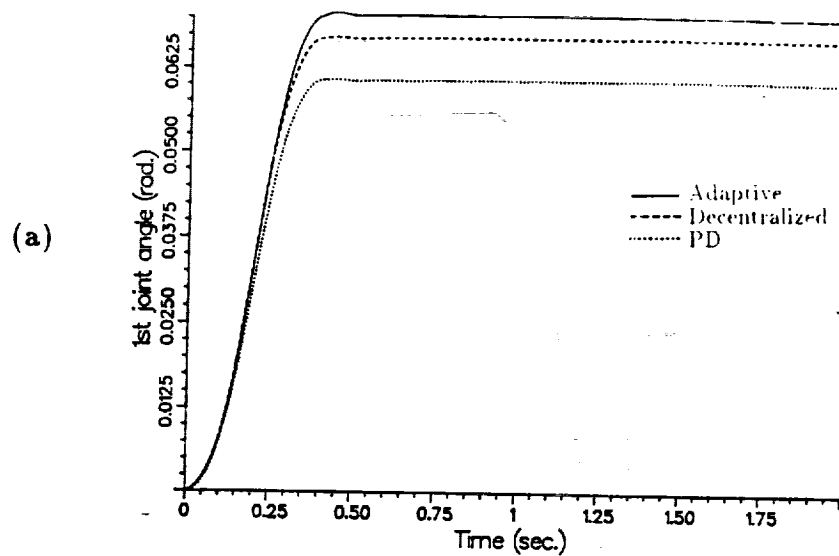
Figure 5.5a,b (a) First joint angular response. (b) Second joint angular response.

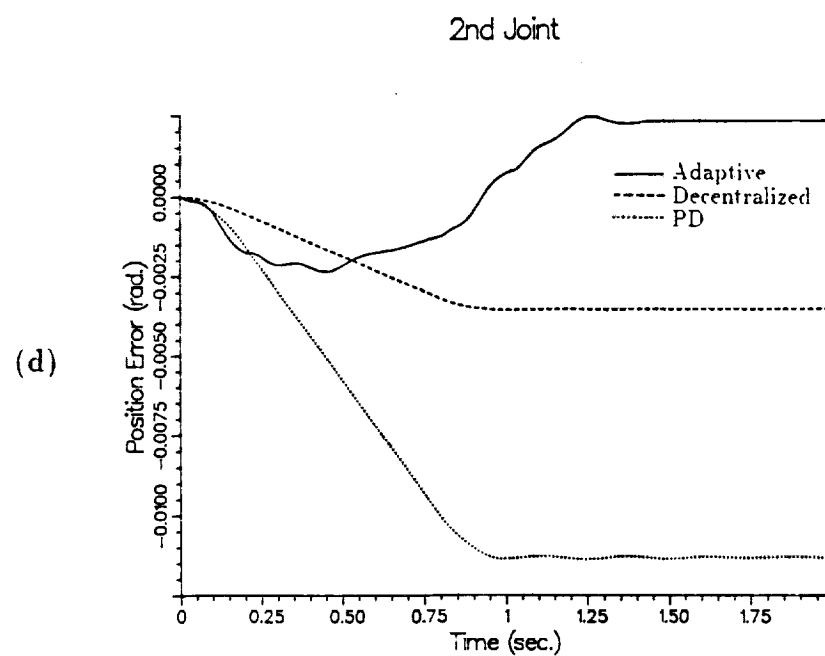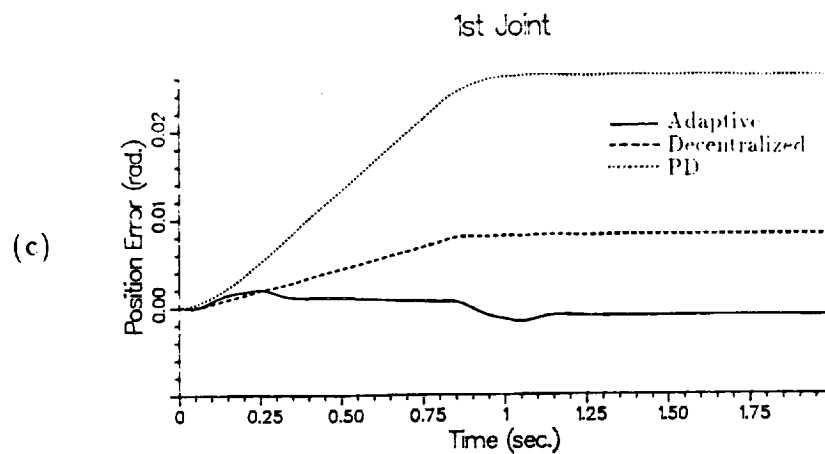1st Joint

(c)

2nd Joint

(d)
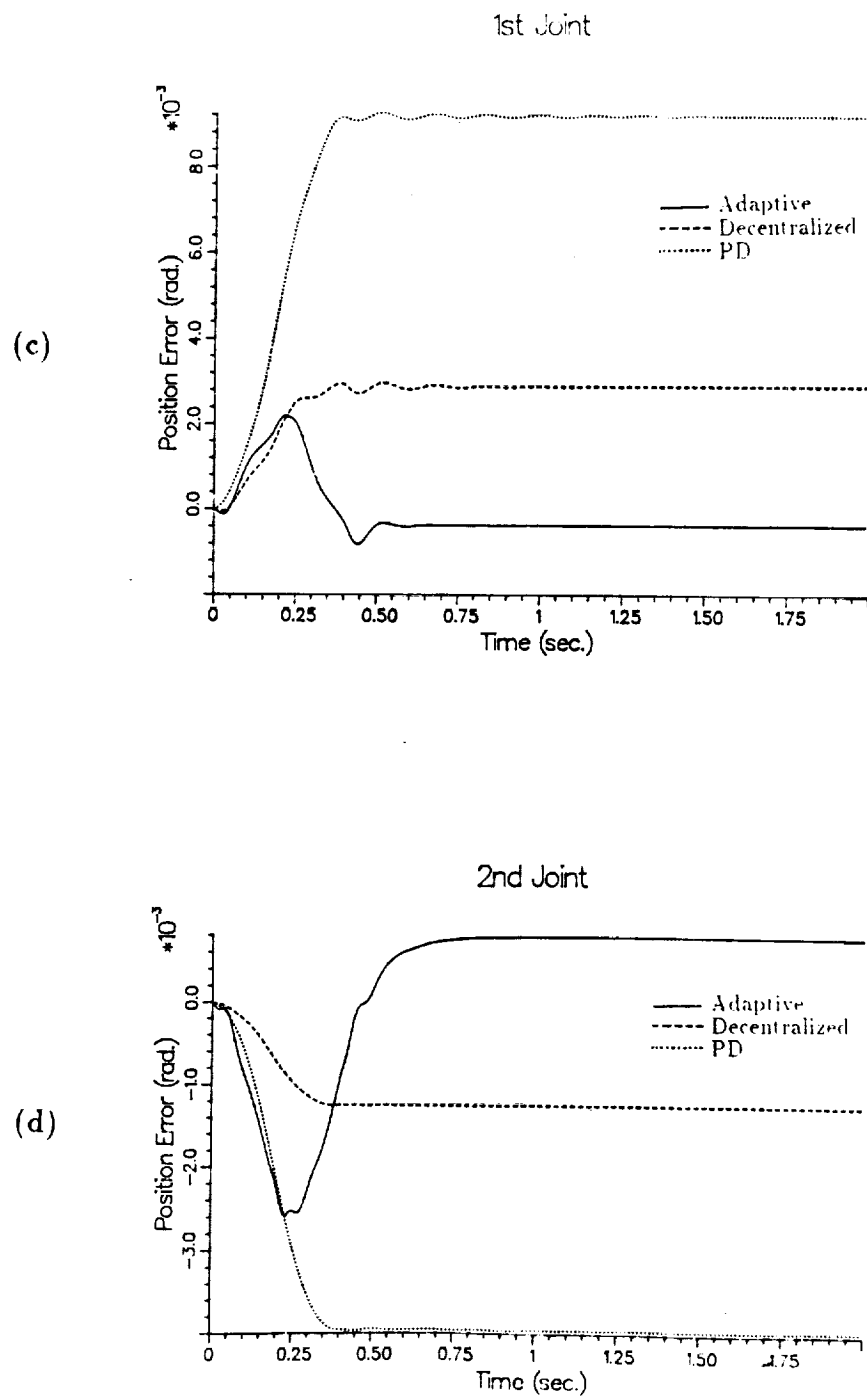
Figure 5.5c,d (c) Error response of first joint. (d) Error response of second joint.

Flexible Mode of Lower Link

(e)

Flexible Mode of Upper Link

(f)
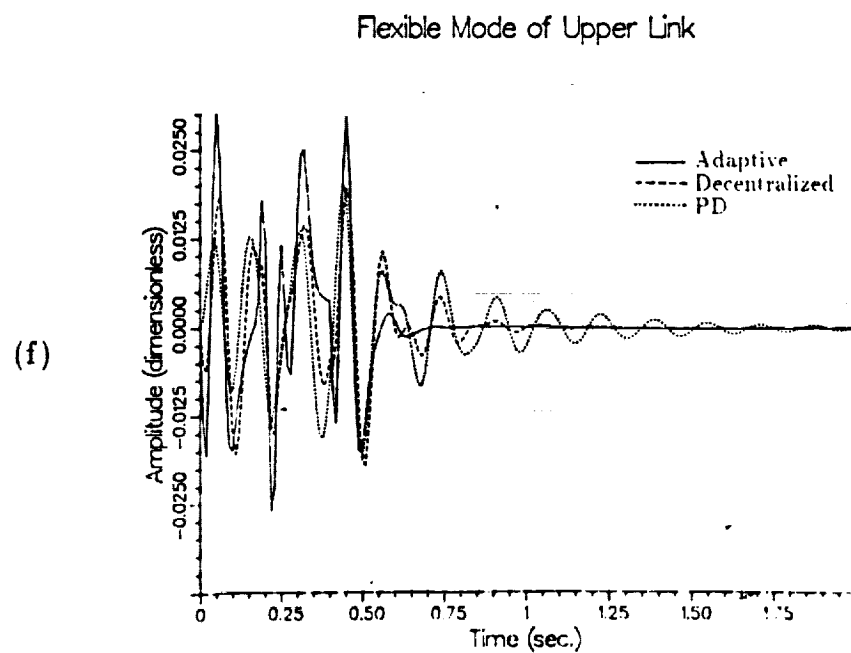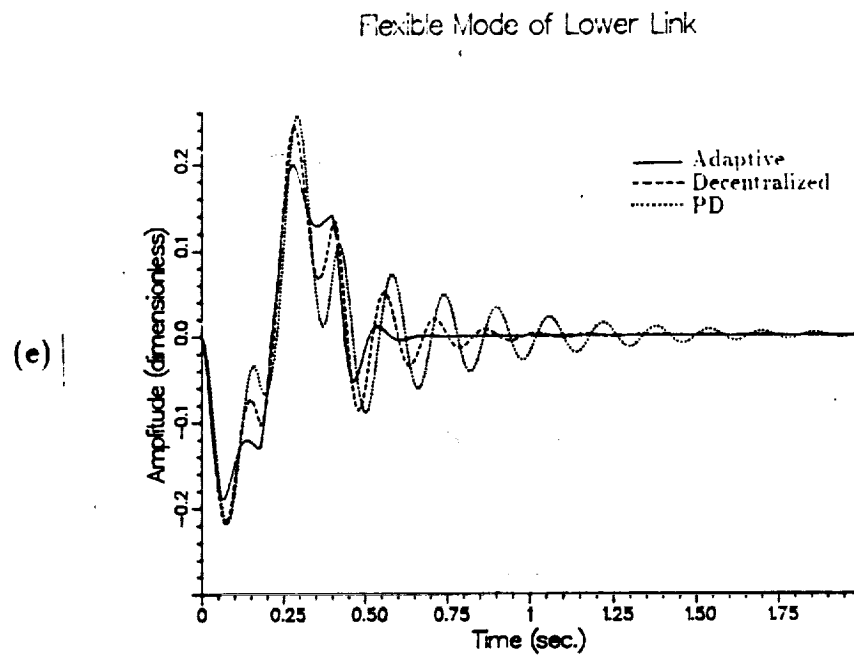
**Figure 5.5e,f** (e) Strain response of lower link. (f) Strain response of upper link.

(a)

(b)
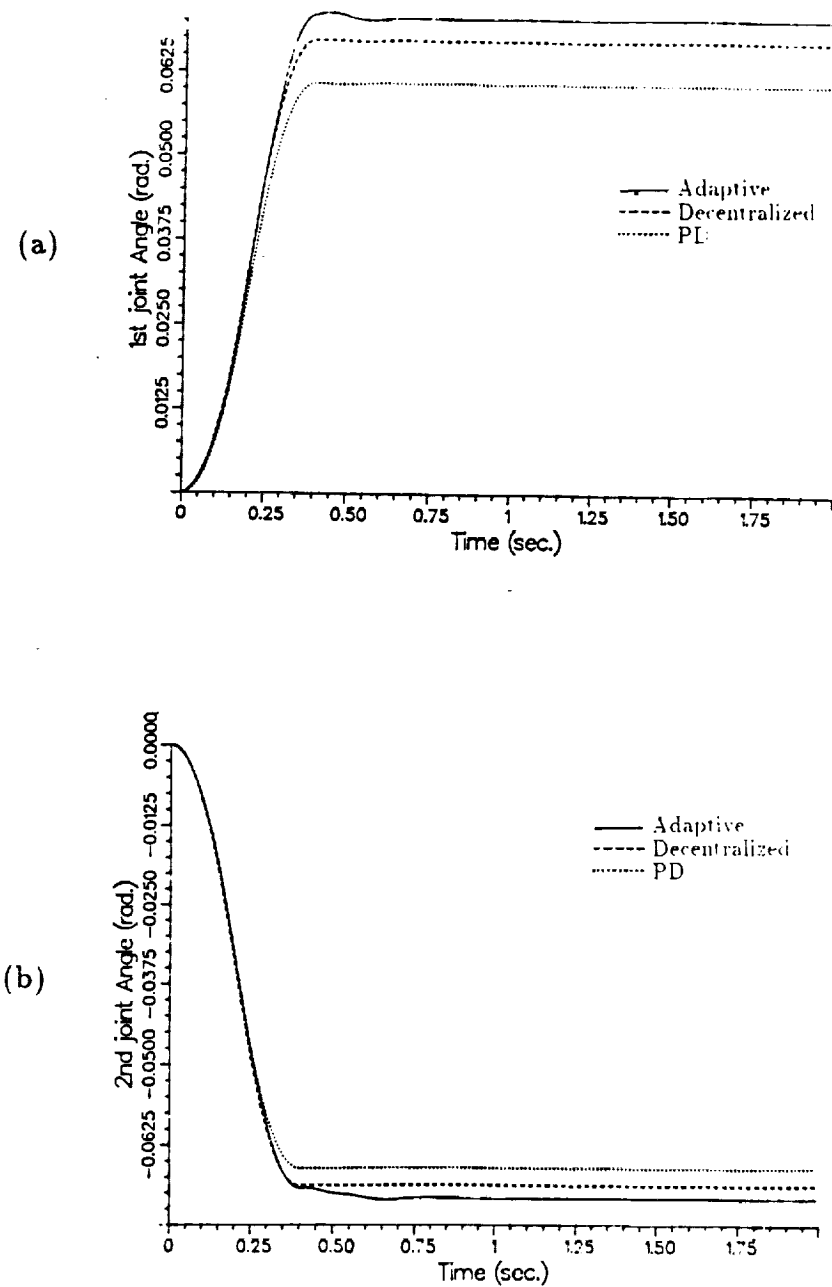
Figure 5.6a,b (a) First joint angular response. (b) Second joint angular response.

1st Joint

(c)

2nd Joint

(d)
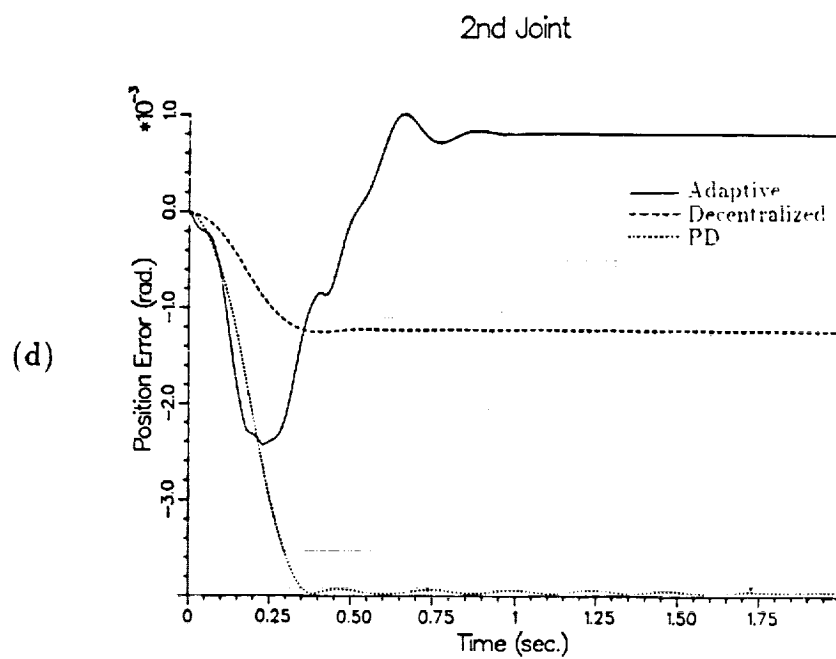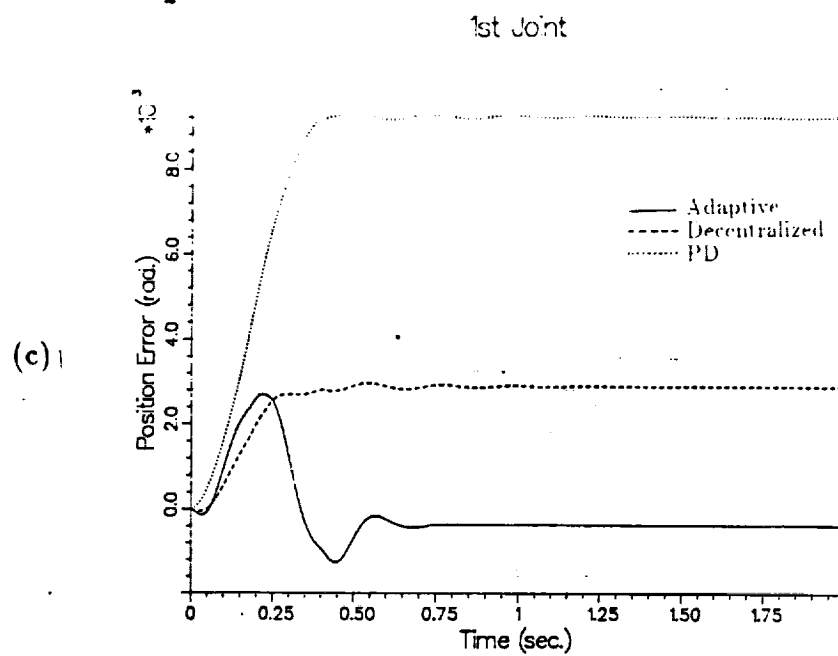
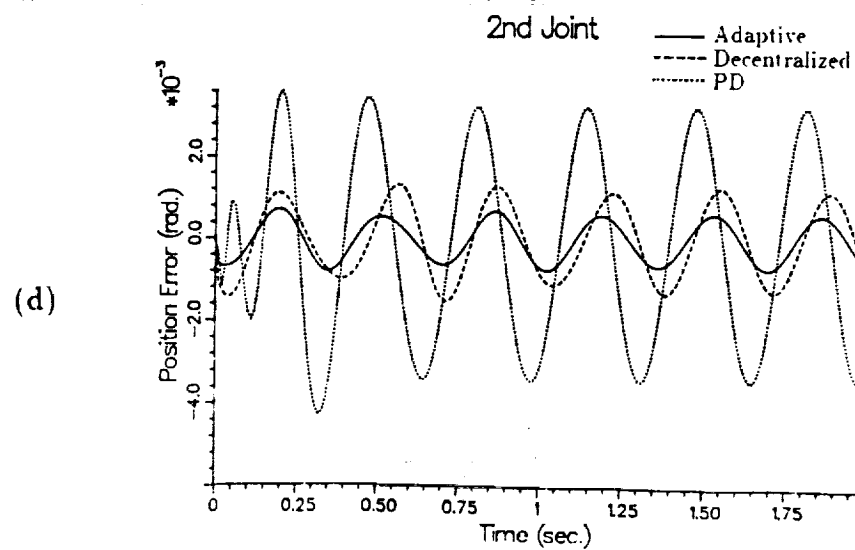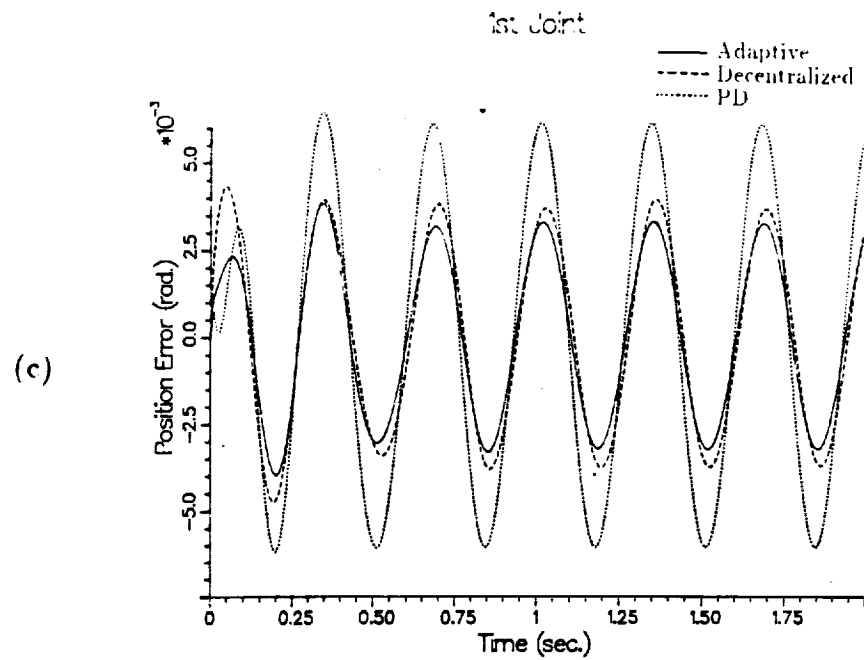**Figure 5.6c,d** (c) Error response of first joint. (d) Error response of second joint.

Flexible Mode of Lower Link

(e)

Flexible Mode of Upper Link

(f)
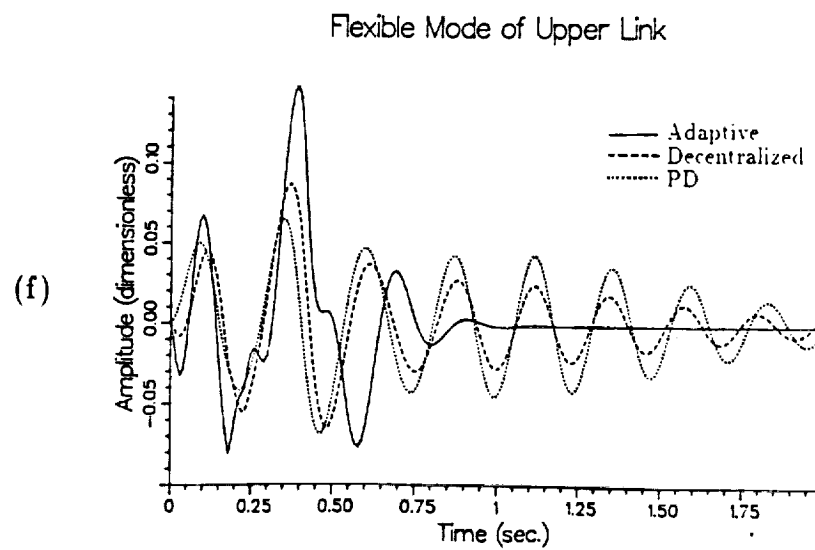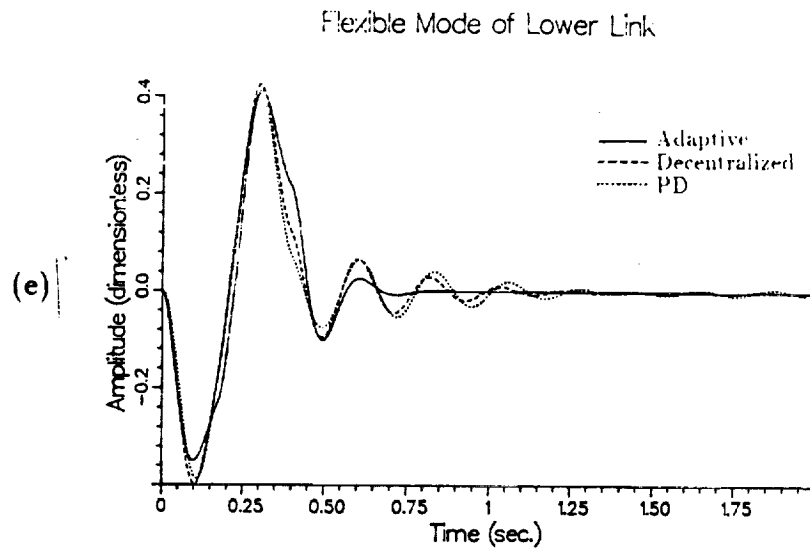
Figure 5.6e,f (e) Strain response of lower link. (f) Strain response of upper link.

Reference Position

Reference Velocity
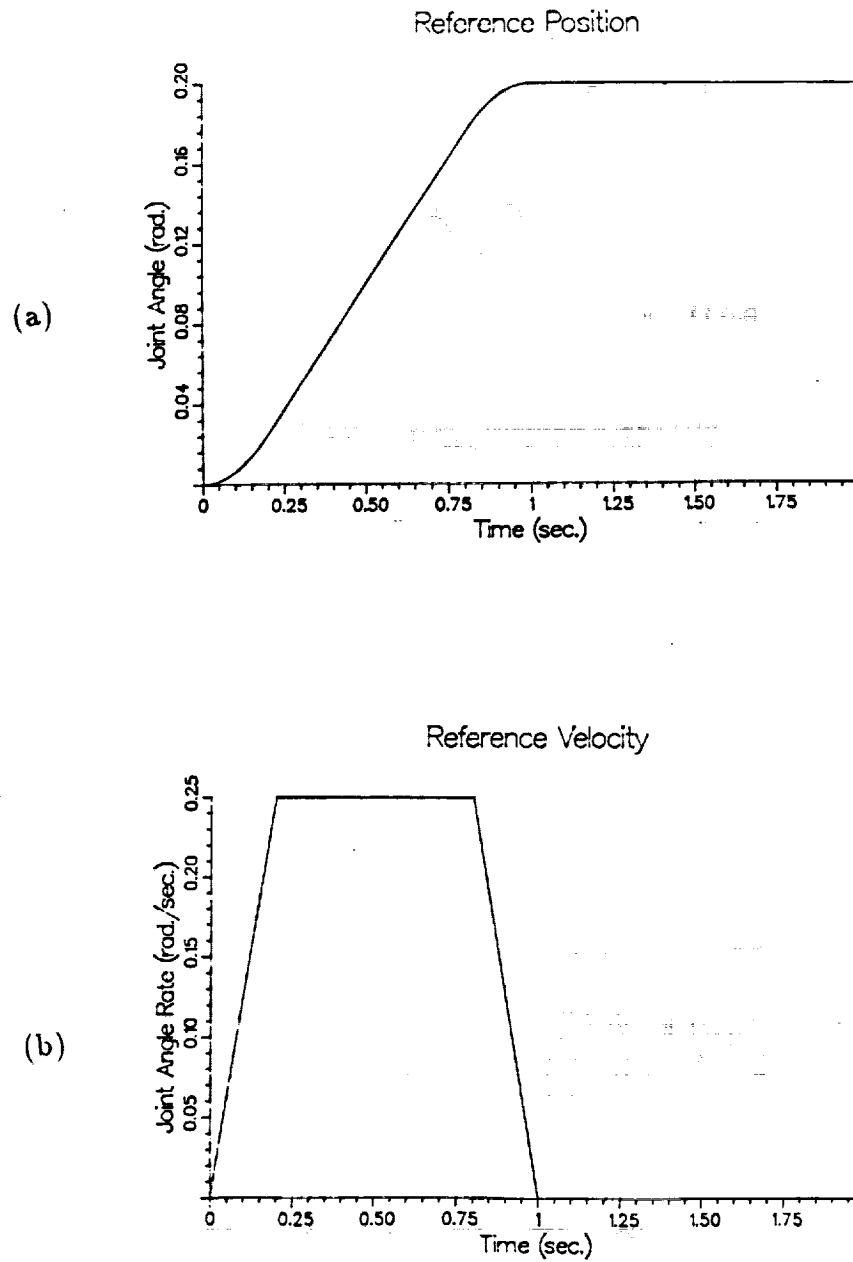
Figure 5.7 (a) Reference position profile. (b) Reference velocity profile.
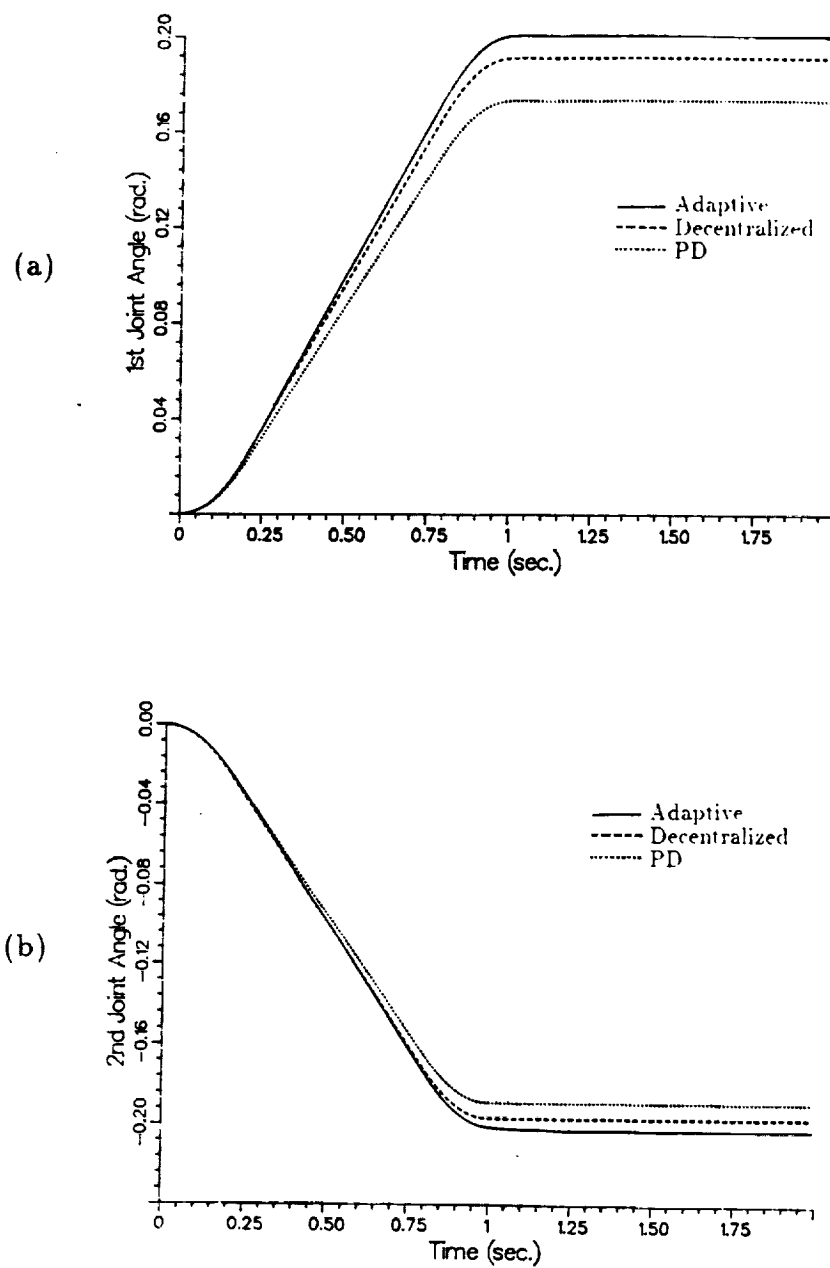
Figure 5.8a,b (a) First joint angular response. (b) Second joint angular response.

1st Joint

(c)

2nd Joint

(d)
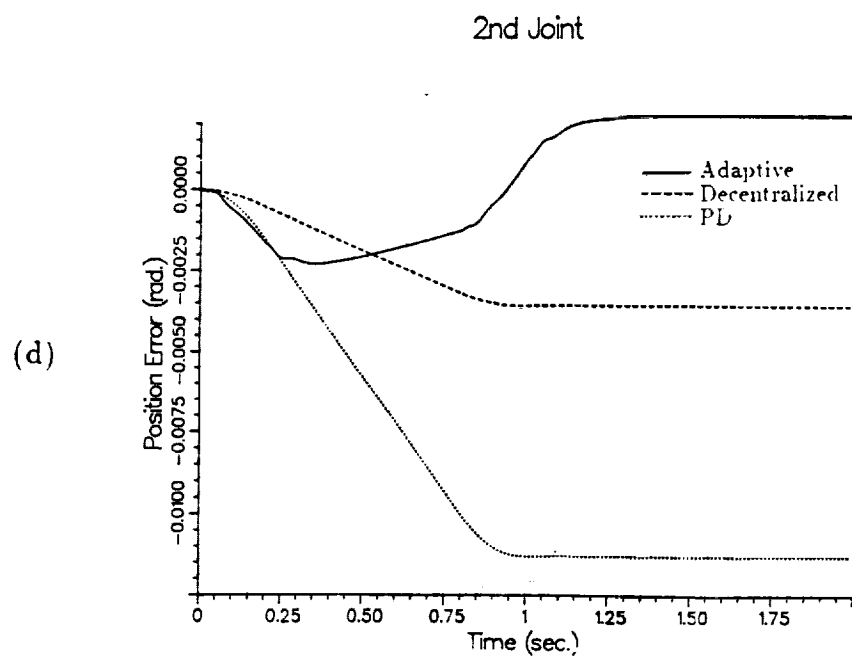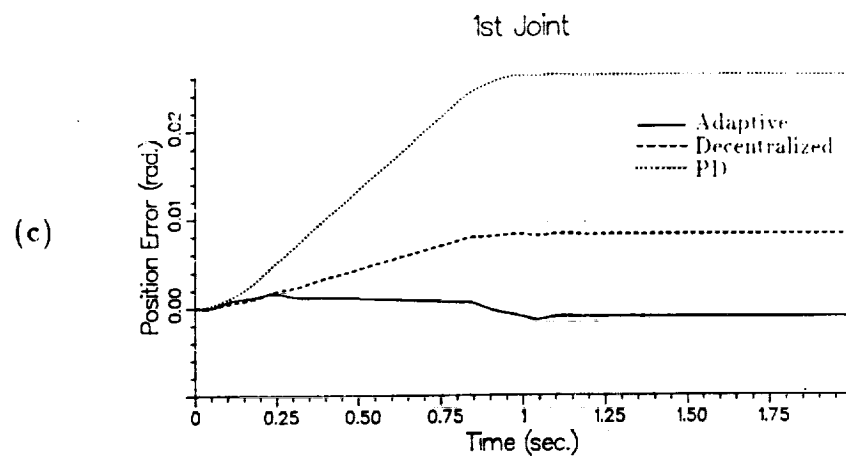
Figure 5.8c,d (c) Error response of first joint. (d) Error response of second joint.

Flexible Mode of Lower Link

(e)

Flexible Mode of Upper Link

(f)
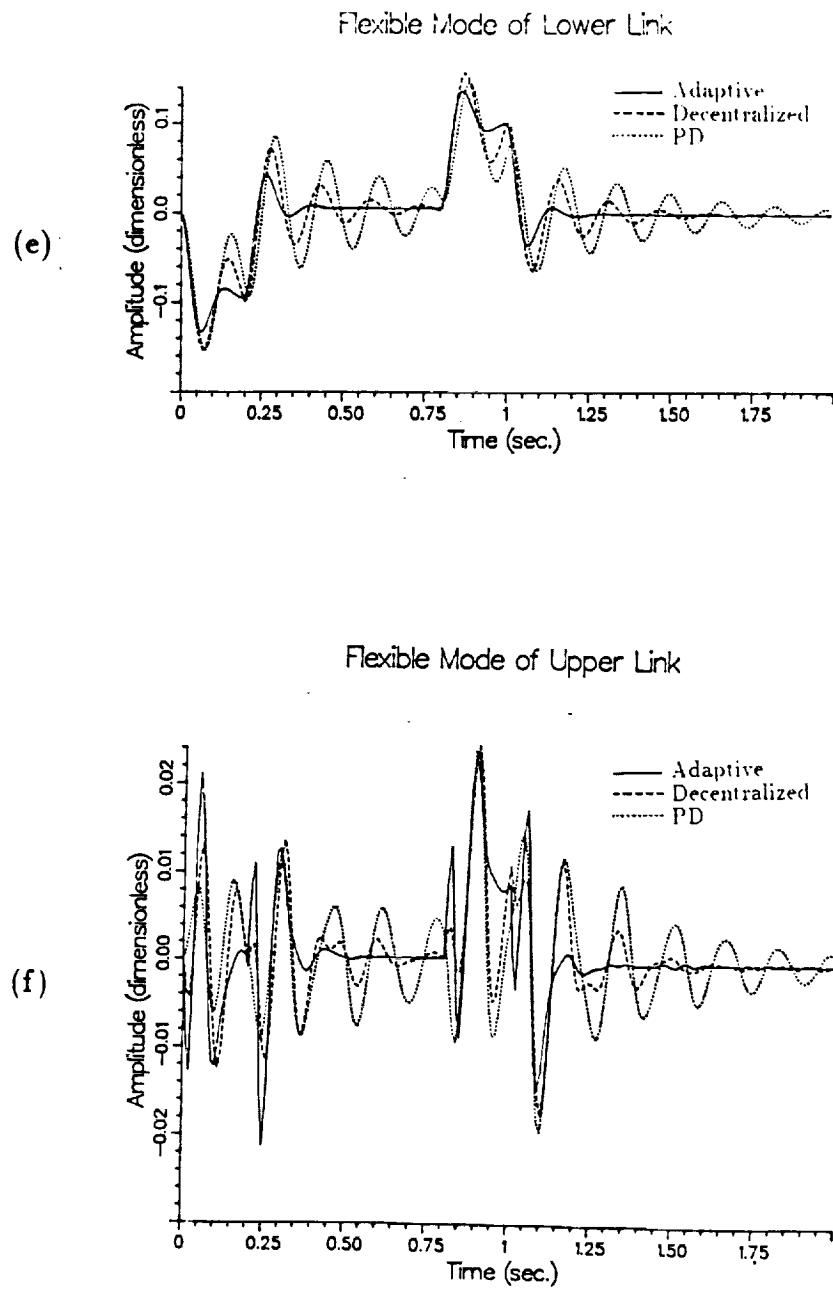
Figure 5.8e,f (e) Strain response of lower link. (f) Strain response of upper link.
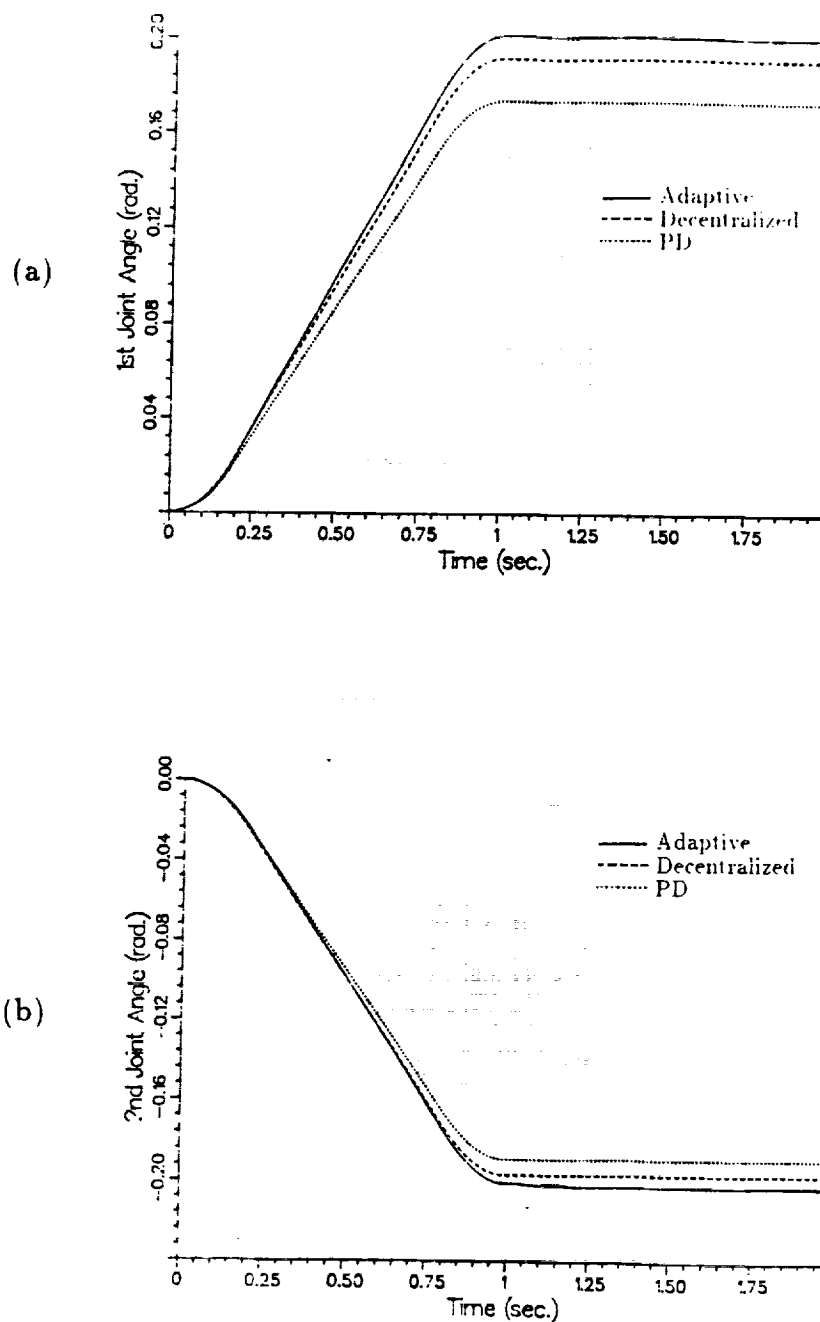
Figure 5.9a,b (a) First joint angular response. (b) Second joint angular response.

1st Joint

(c)

2nd Joint

(d)

Figure 5.9c,d (c) Error response of first joint. (d) Error response of second joint.

i lexible Mode of Lower Link

(e)

Flexible Mode of Upper Link

(f)
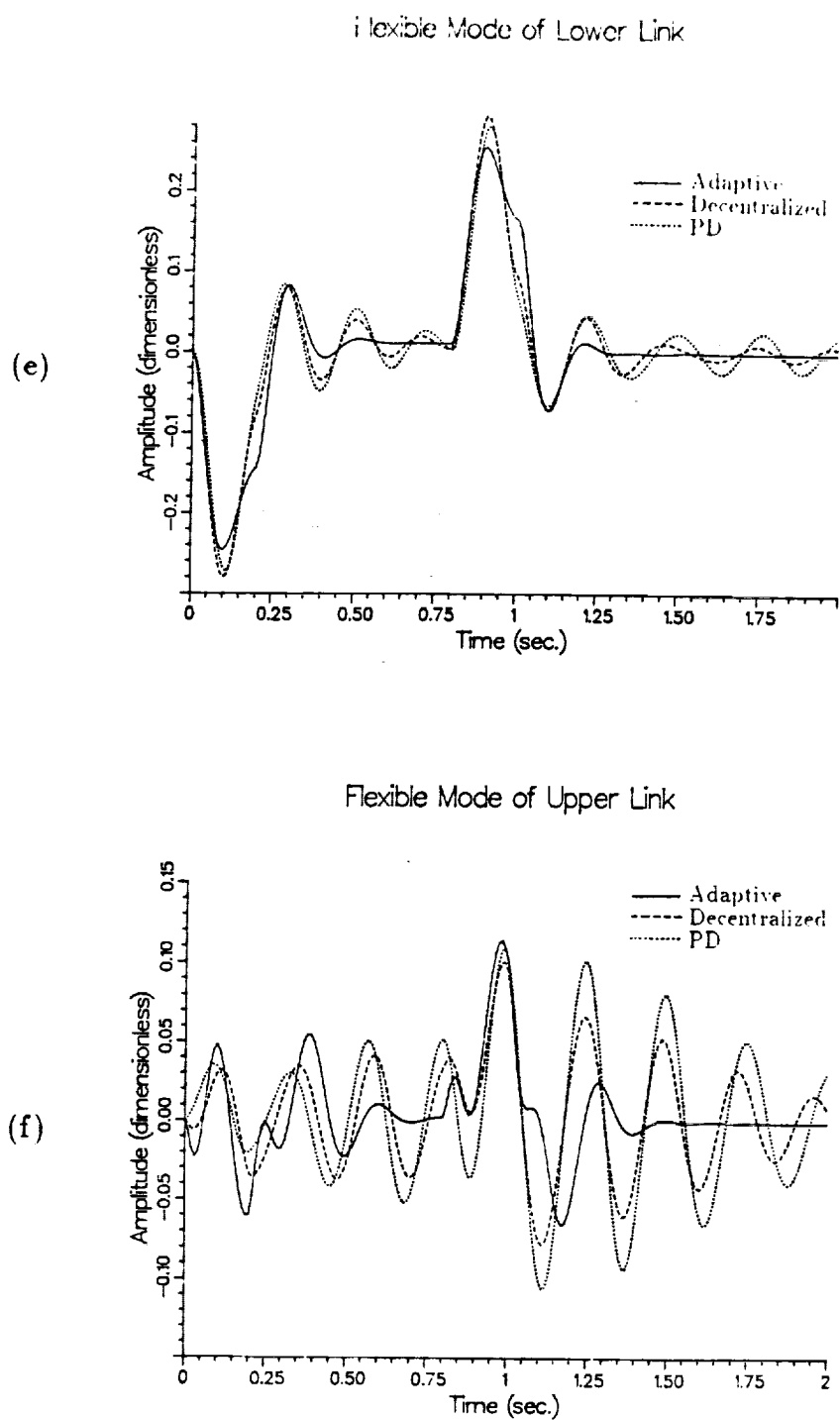
Figure 5.9e,f (e) Strain response of lower link. (f) Strain response of upper link.
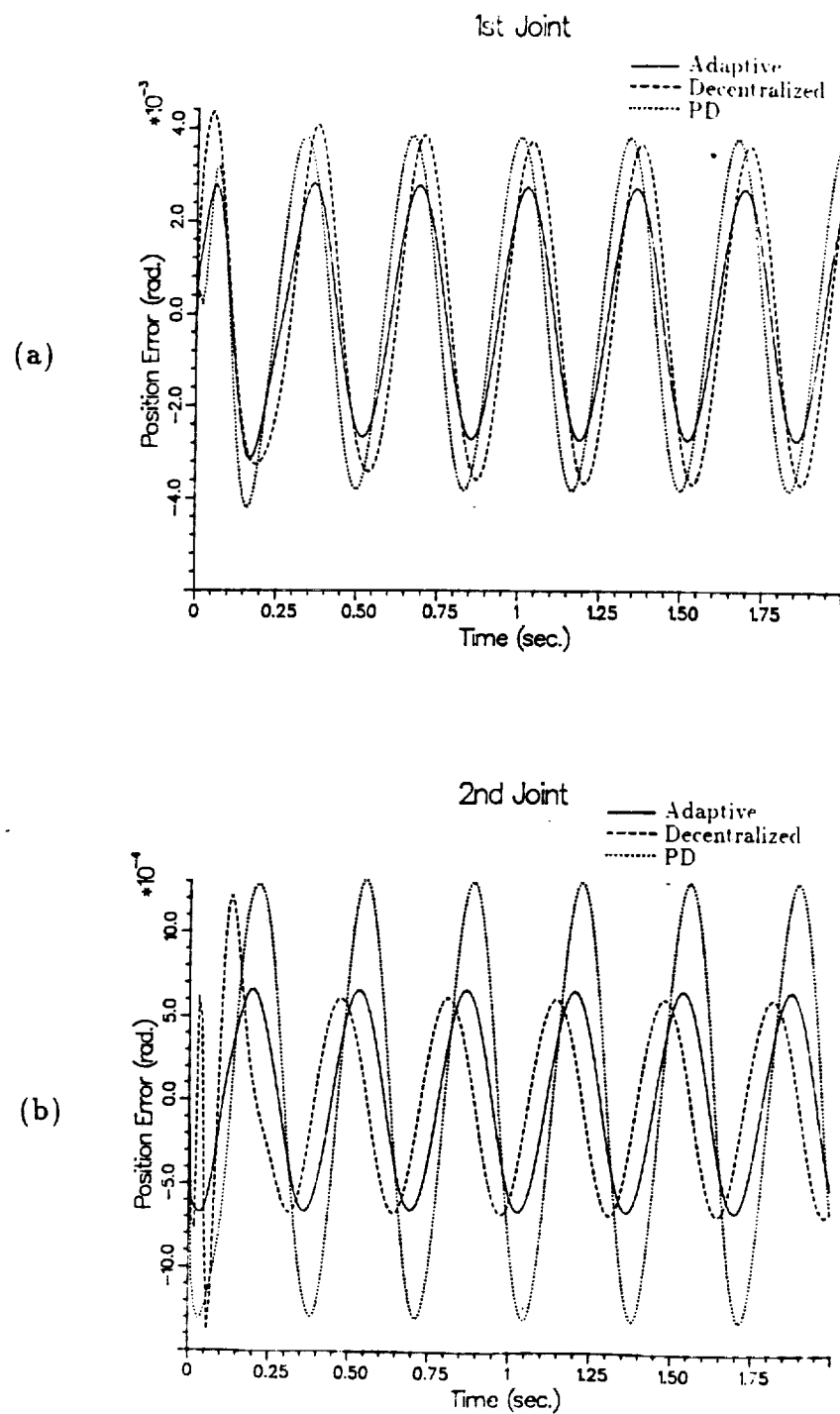
Figure 5.10a,b (a) Error response of first joint (without payload). (b) Error response of second joint (without payload).
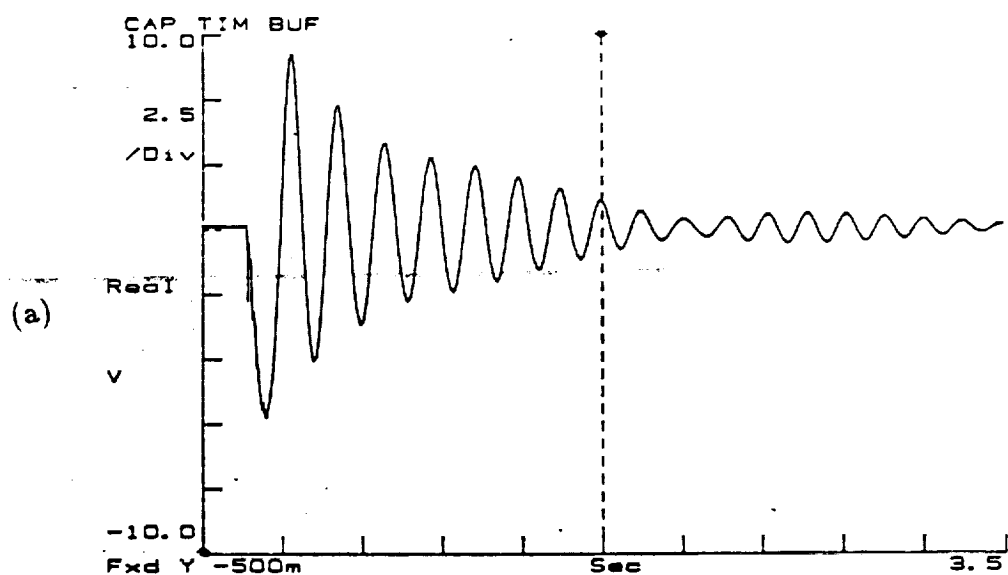
Figure 5.10c,d (c) Error response of first joint (with payload). (d) Error response of second joint (with payload).

Flexible Mode of Lower Link

(a)

Flexible Mode of Upper Link

(b)
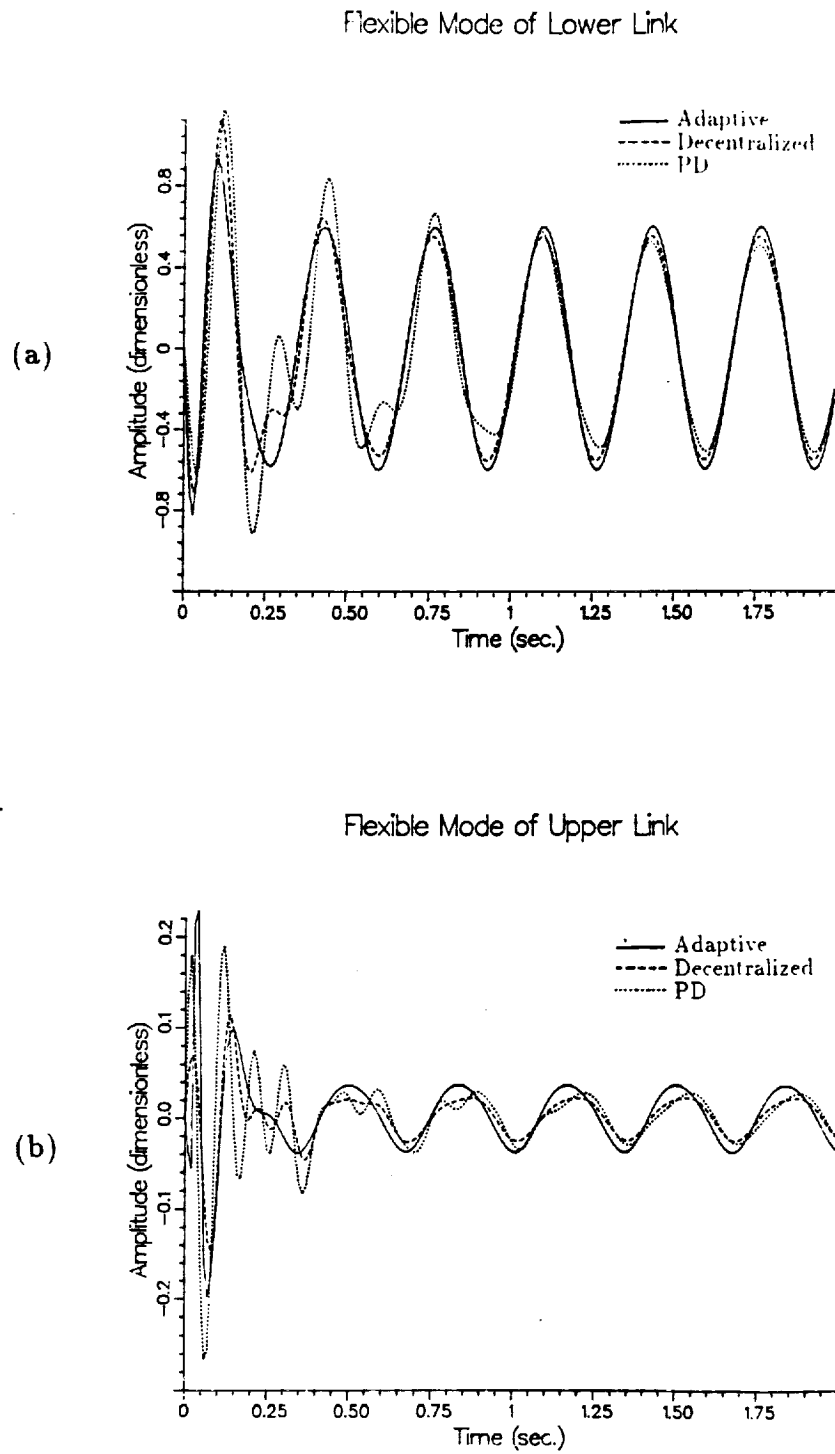
Figure 5.11 (a) Strain response of lower link (without payload). (b) Strain response of upper link (without payload).

Flexible Mode of Lower Link

(a)

Flexible Mode of Upper Link

(b)
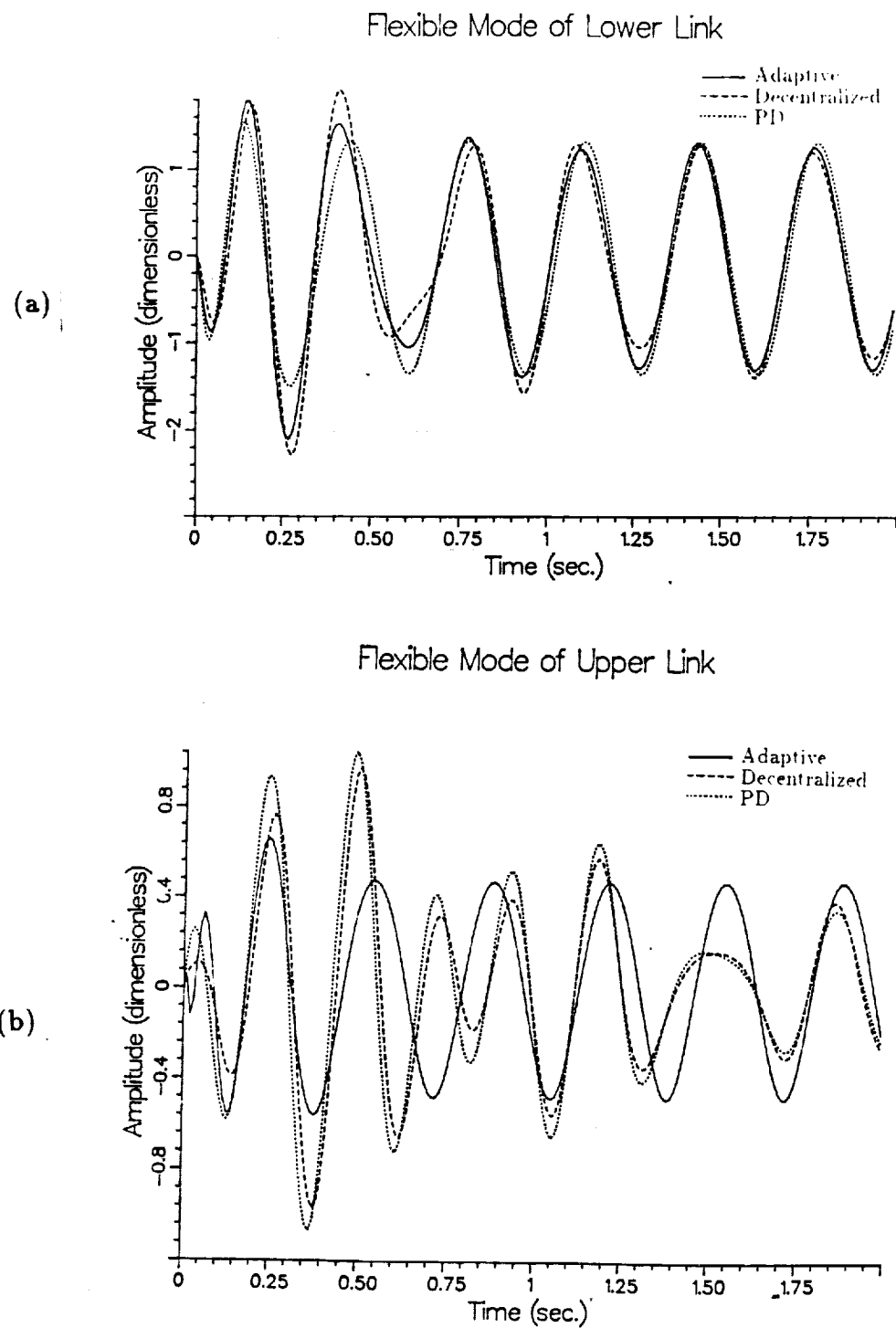
Figure 5.12 (a) Strain response of lower link (with payload). (b) Strain response of upper link (with payload).

(a)

CAP TIM BUF
10.0

2.5

/Div

Real

V

-10.0
Fxd Y -500m   Sec   3.5

(b)

CAP TIM BUF
10.0

2.5

/Div

Real

V

-10.0
Fxd Y -500m   Sec   3.5
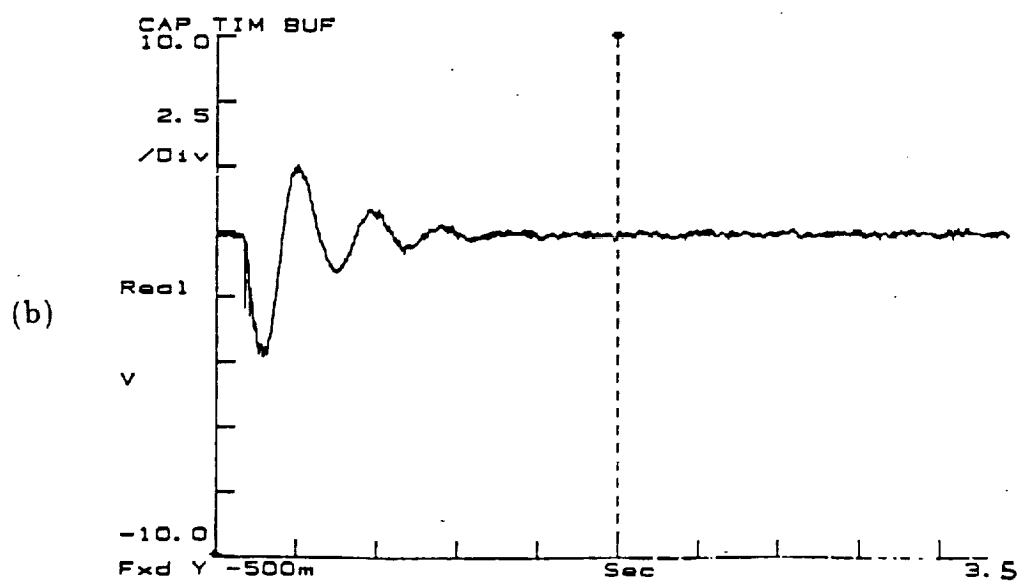
Figure 5.13 (a) Strain response of lower link (without control). (b) Strain response of lower link (with control).

Strain Response for Lower Link
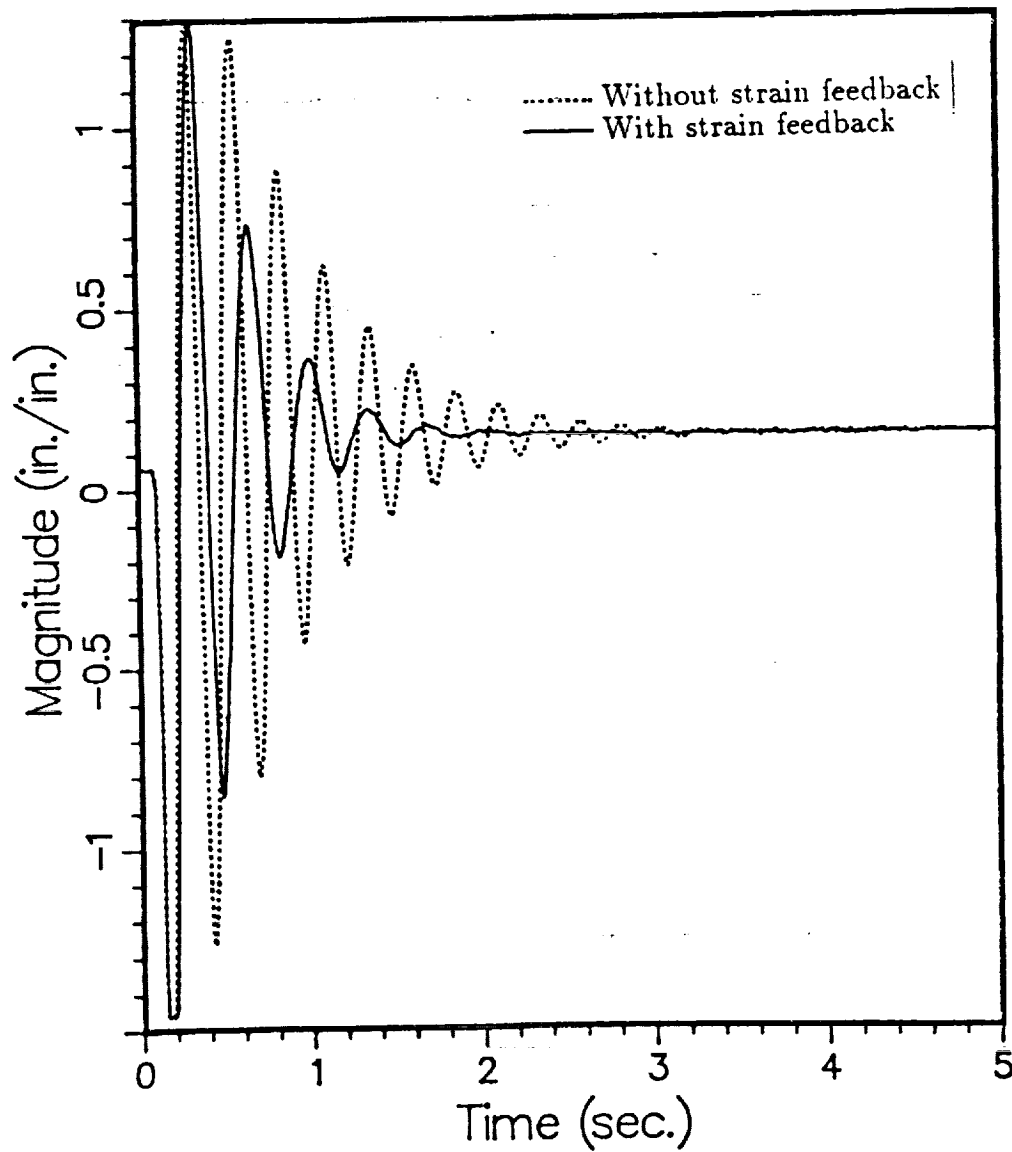
Figure 5.14 Strain response of lower link.

Strain Response for Upper Link
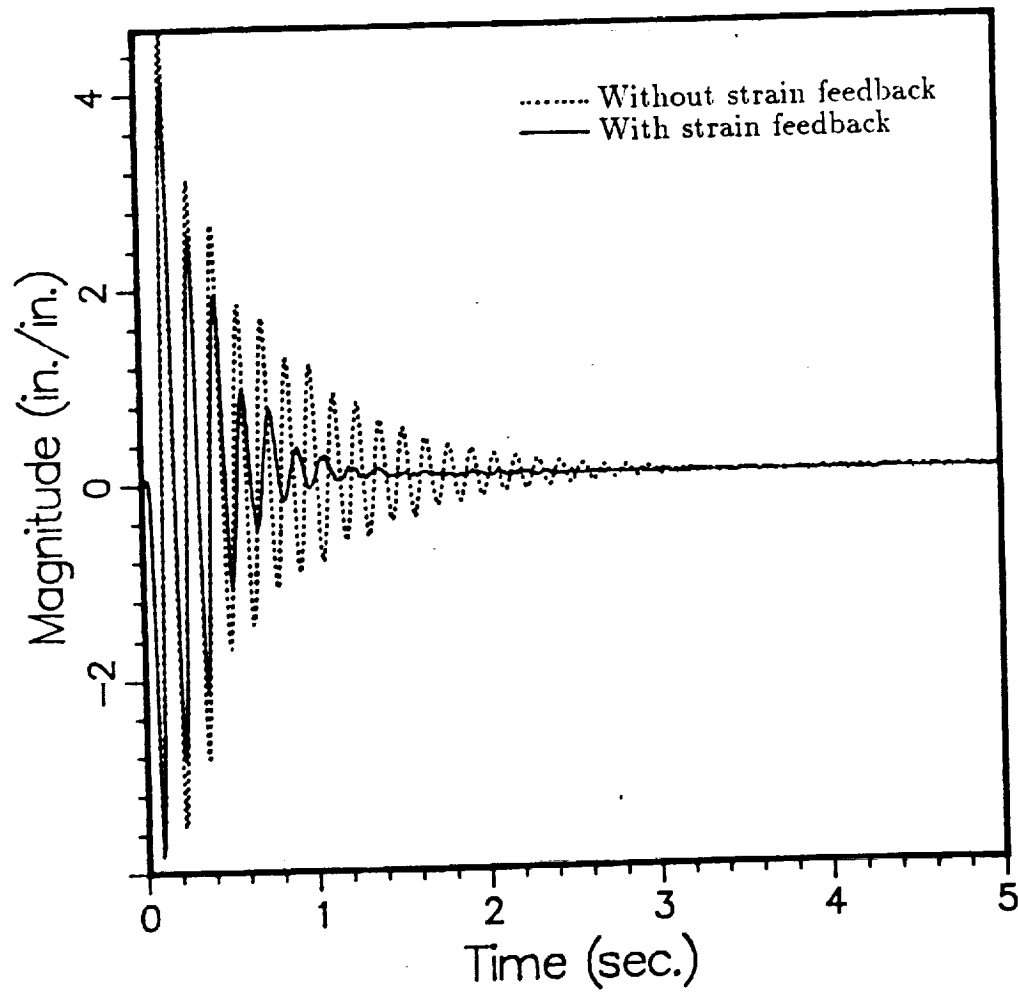
Figure 5.15 Strain response of upper link.

Control Torque for Actuator 1
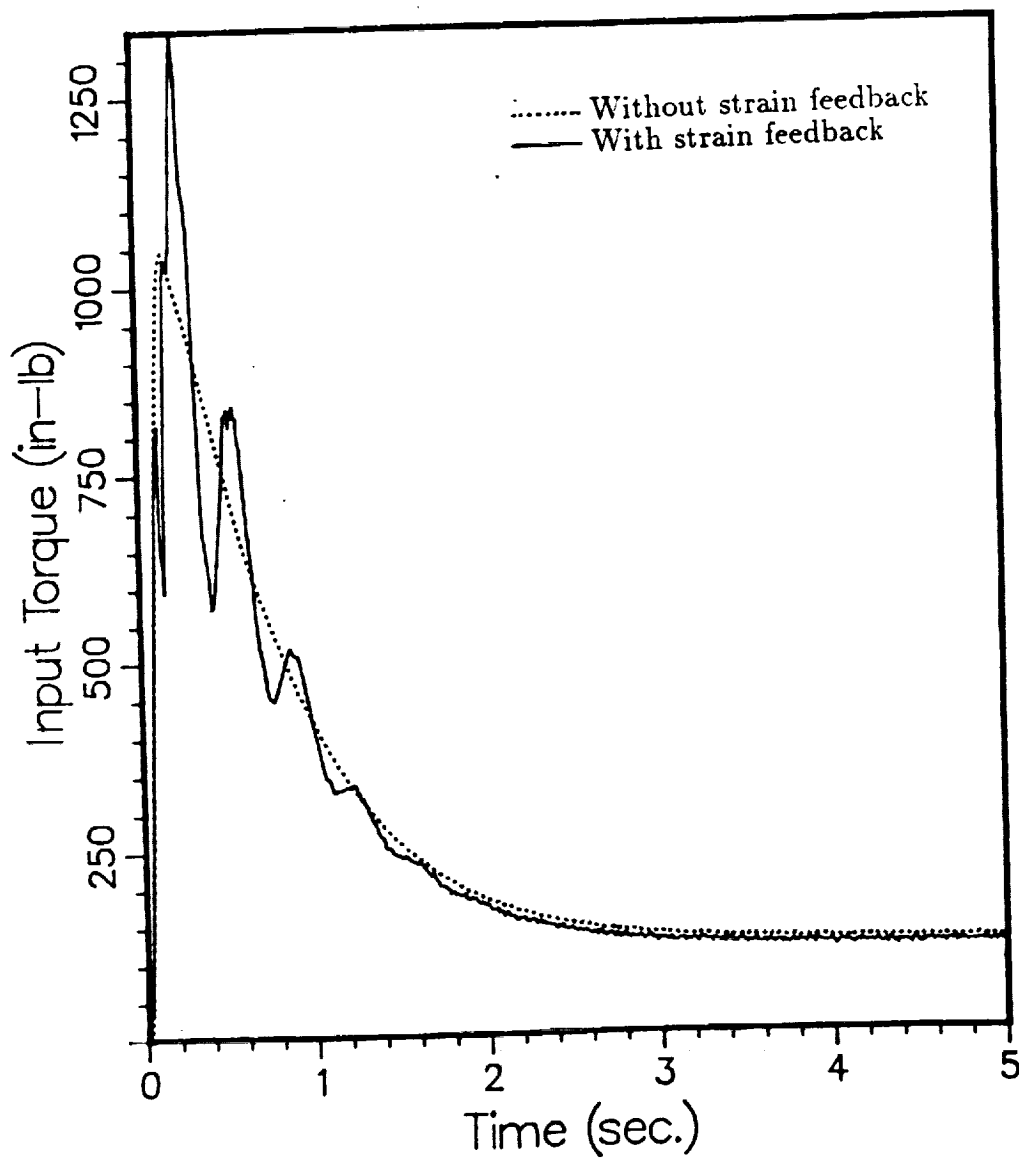
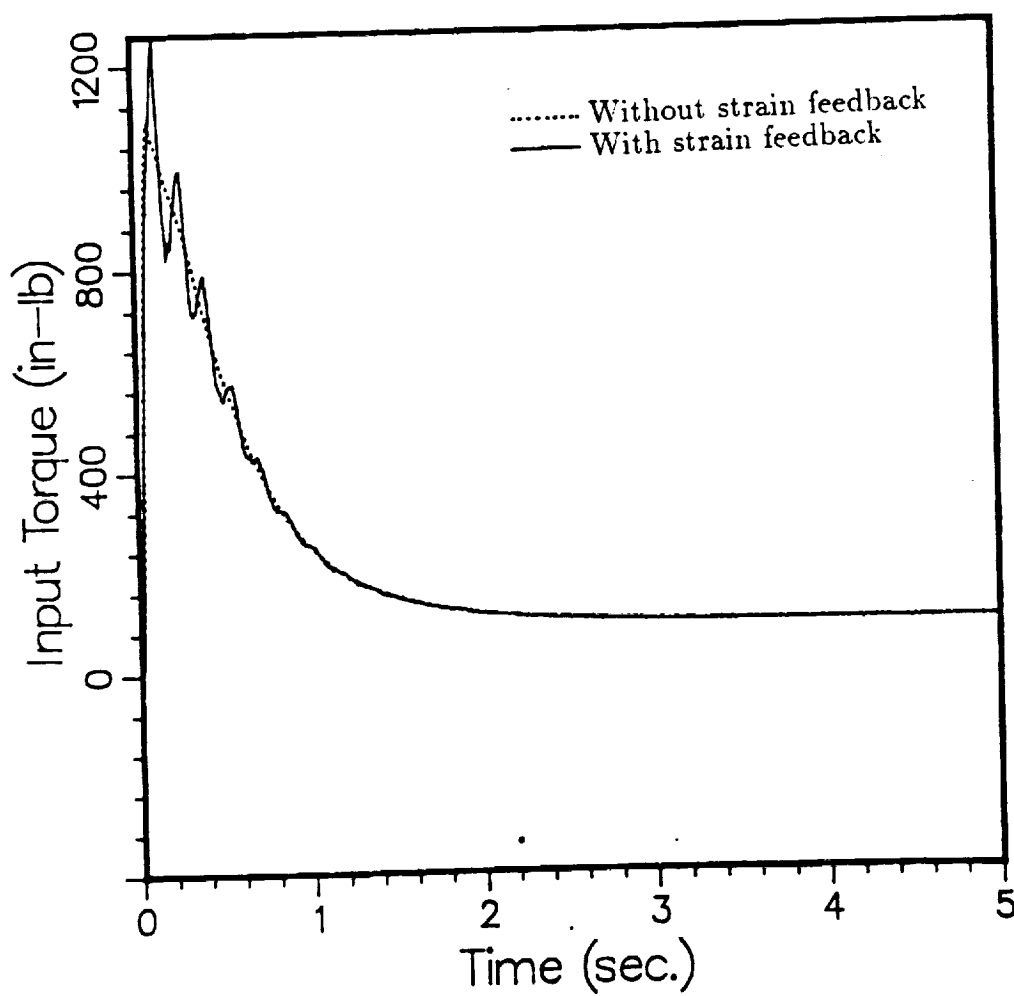**Figure 5.16a** Input to first actuator.

Control Torque for Actuator 2

········· Without strain feedback
——— With strain feedback

Input Torque (in–lb)

Time (sec.)

Figure 5.16b Input to second actuator.

CAP TIM BUF
5.0

1.25
/Div

Real

(a)

V

-5.0
Fxd Y -500m   Sec   3.5

CAP TIM BUF
3.0

1.62
/Div

Real

(b)

V

-10.0
Fxd Y -500m   Sec   .3.5
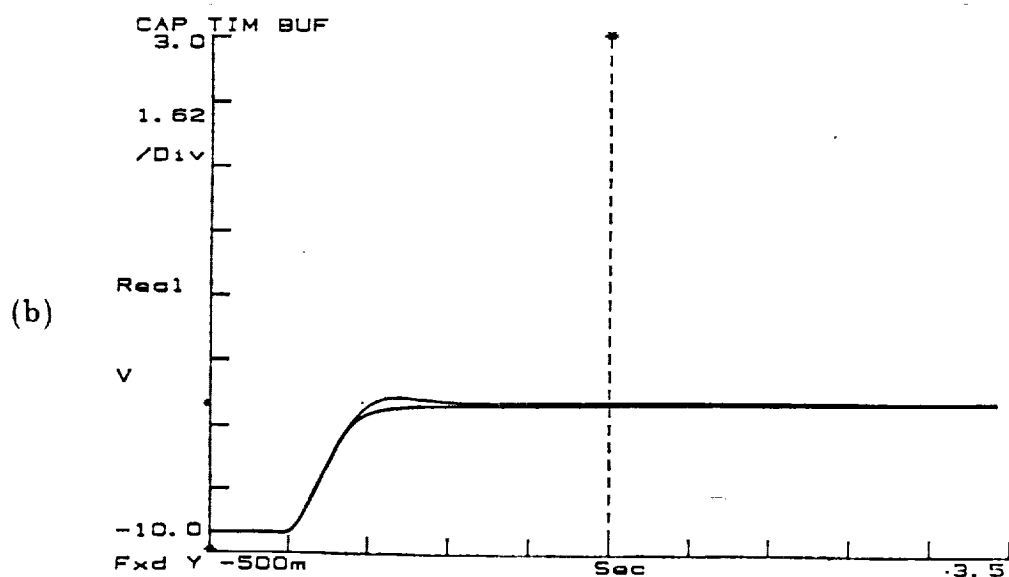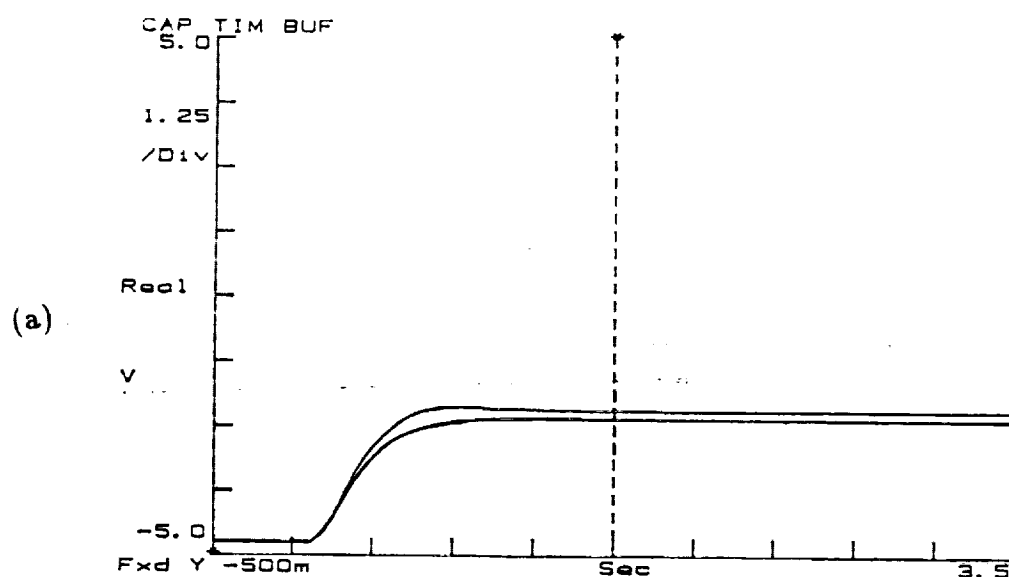
Figure 5.17 (a) LVDT response of first actuator.
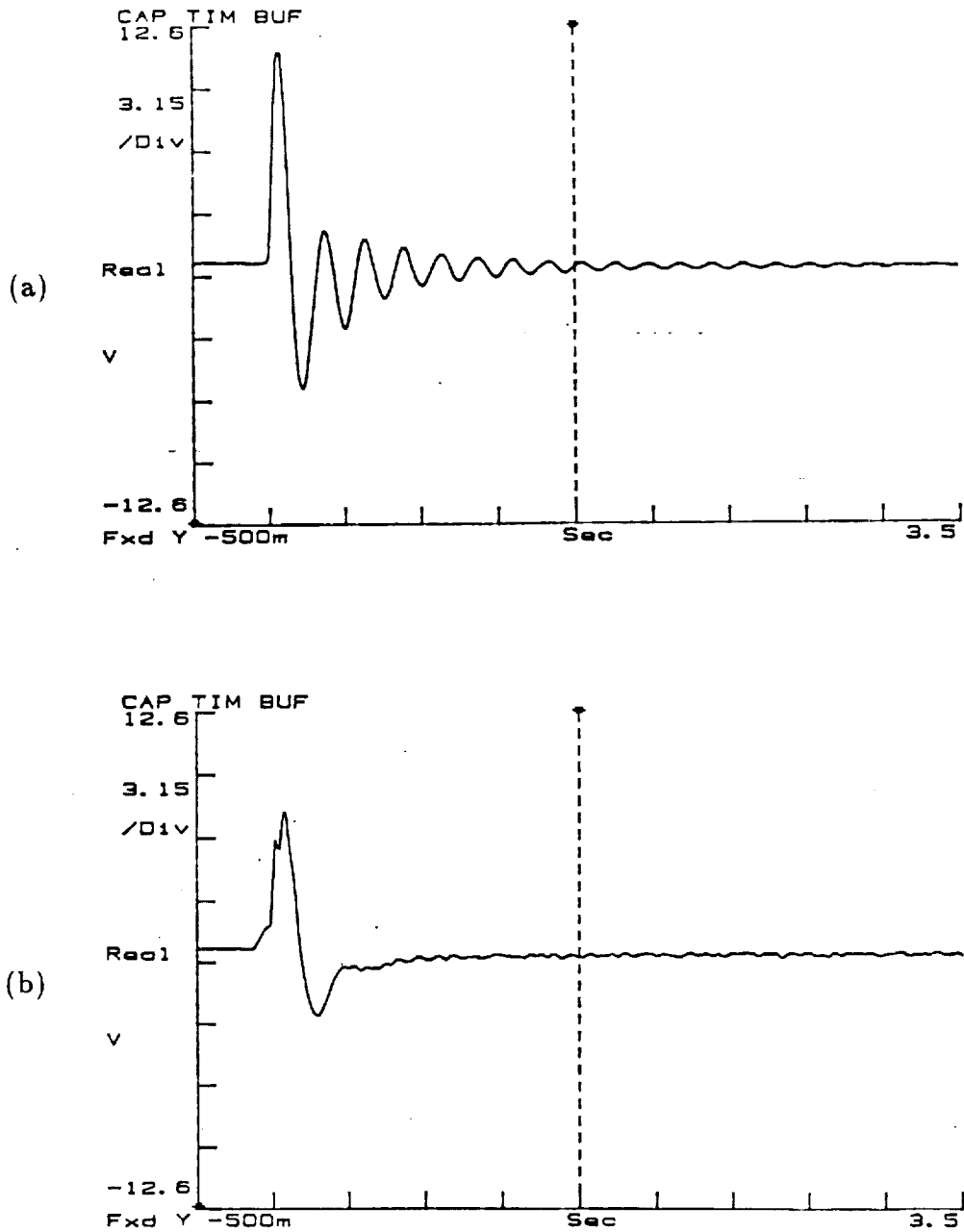
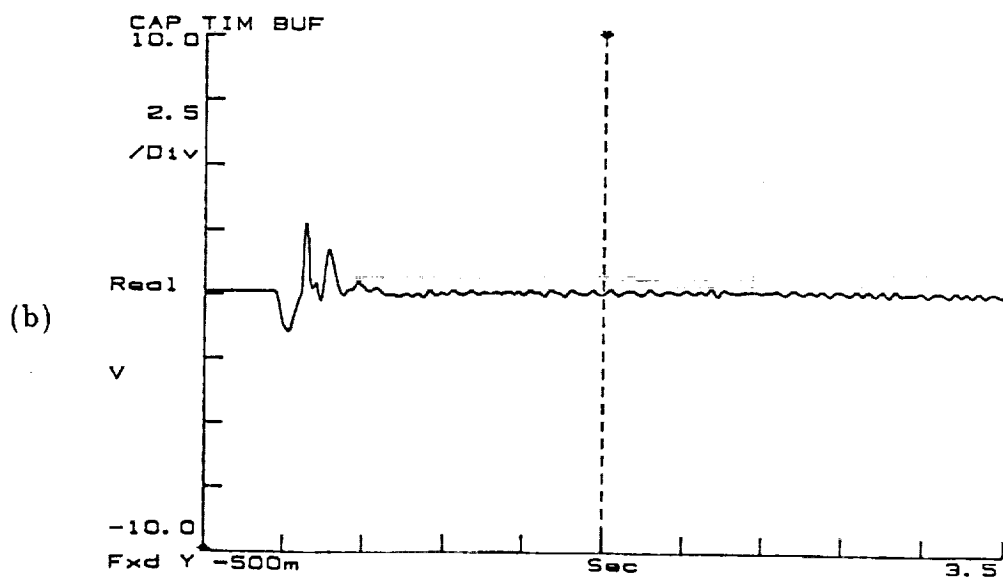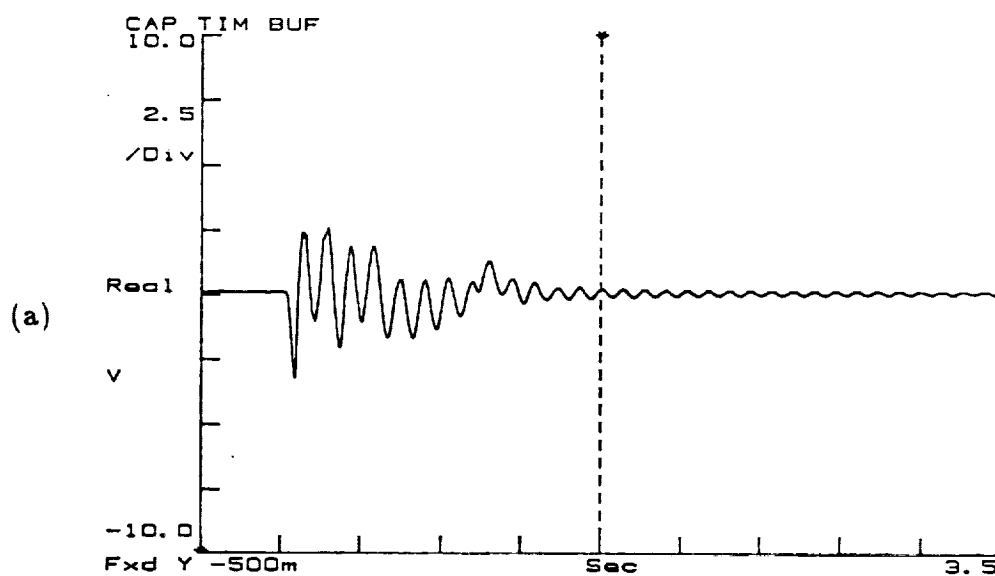(b) LVDT response of second actuator.

Figure 5.18 (a) Strain response of lower link (PD control). (b) Strain response of lower link (adaptive control).

Figure 5.19 (a) Strain response of upper link (PD control). (b) Strain response of upper link (adaptive control).

CAP TIM BUF
5.0

1.25
/Div

Real

V

-5.0

-500m   Sec   3.5

(a)

CAP TIM BUF
3.0

1.62
/Div

Real

V

-10.0

Fxd Y -500m   Sec   3.5

(b)

Figure 5.20 (a) LVDT response of first actuator. (b) LVDT response of second actuator.

Figure 5.21 (a) Strain response of lower link (PD control). (b) Strain response of lower link (adaptive control).

Figure 5.22 (a) Strain response of upper link (PD control). (b) Strain response of upper link (adaptive control).
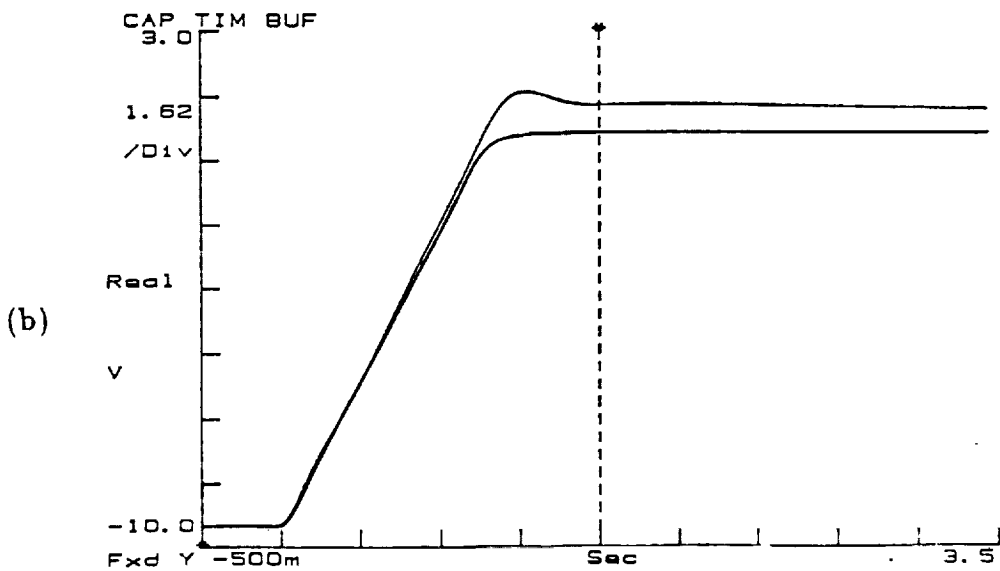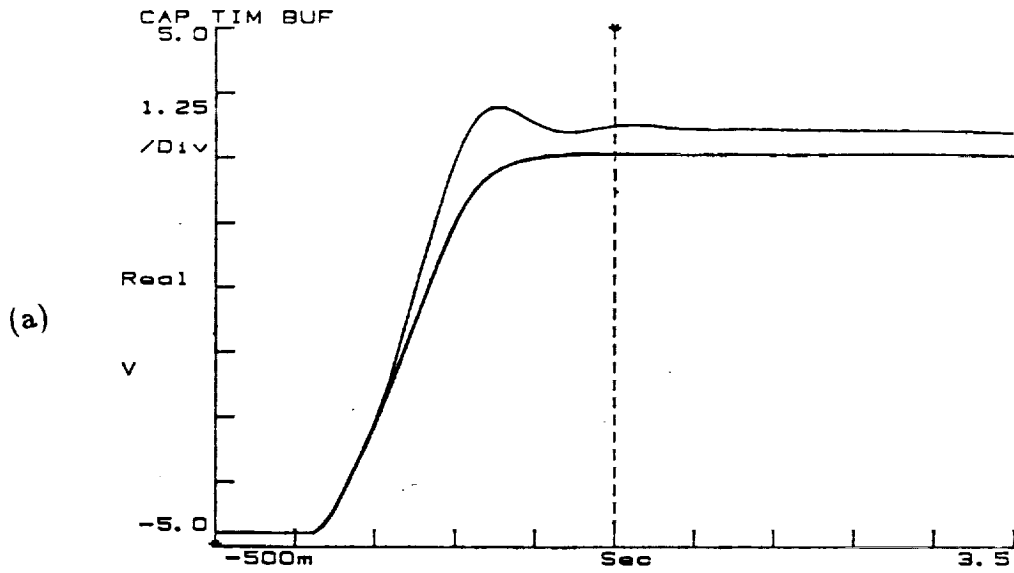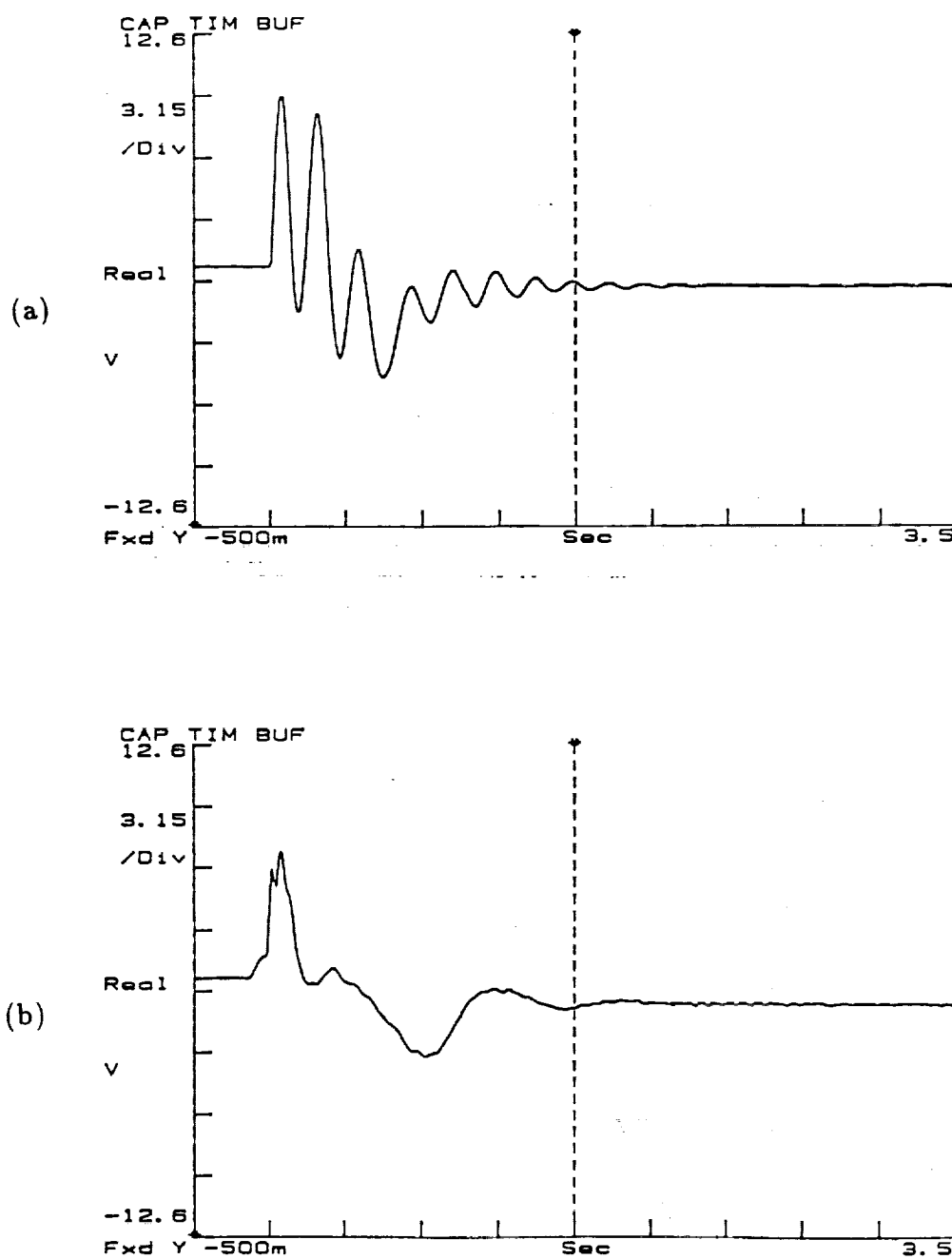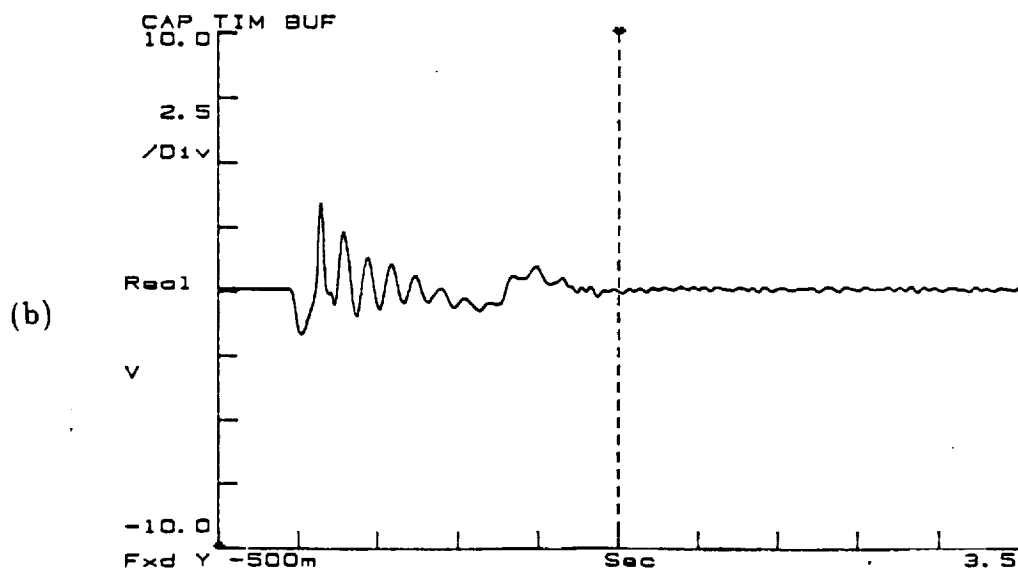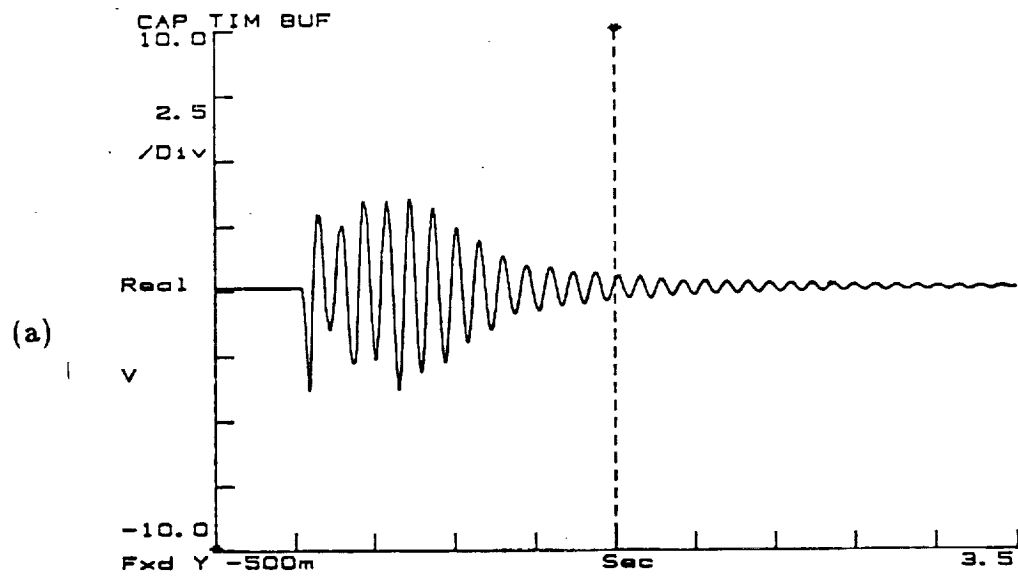
Figure 5.23 (a) LVDT response of first actuator (with payload). (b) LVDT response of second actuator (with payload).

Figure 5.24 (a) Strain response of lower link (PD control, with payload). (b) Strain response of lower link (adaptive control, with payload).

Figure 5.25 (a) Strain response of upper link (PD control, with payload). (b) Strain response of upper link (adaptive control, with payload).

(a)

(b)
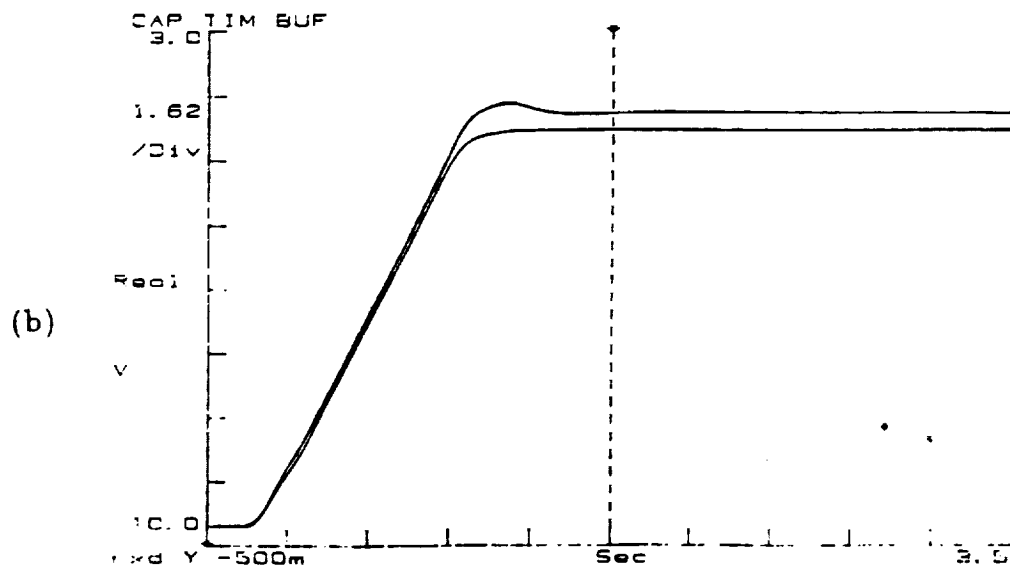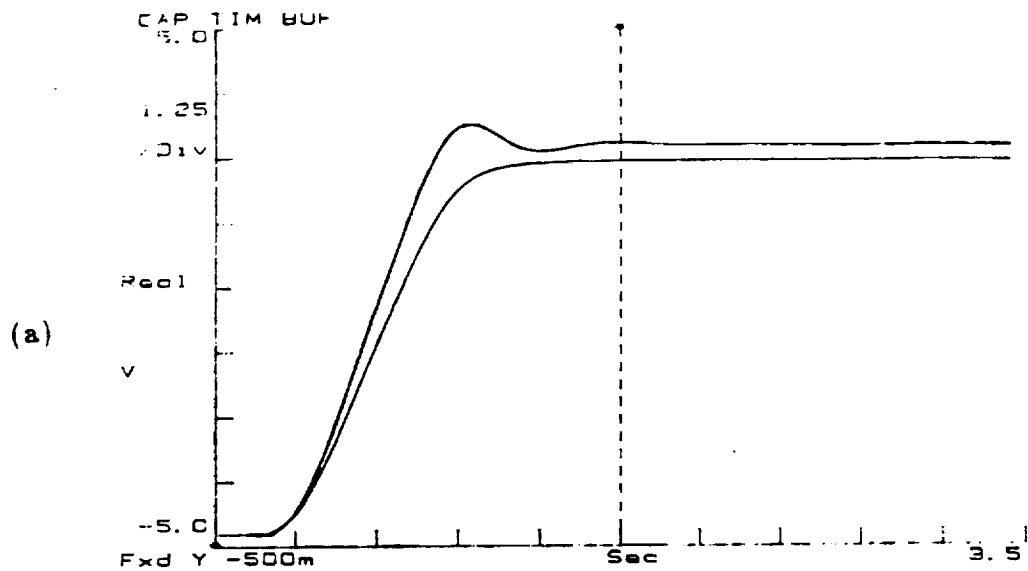
Figure 5.26 (a) LVDT response of first actuator (with payload). (b) LVDT response of second actuator (with payload).

(a)

(b)
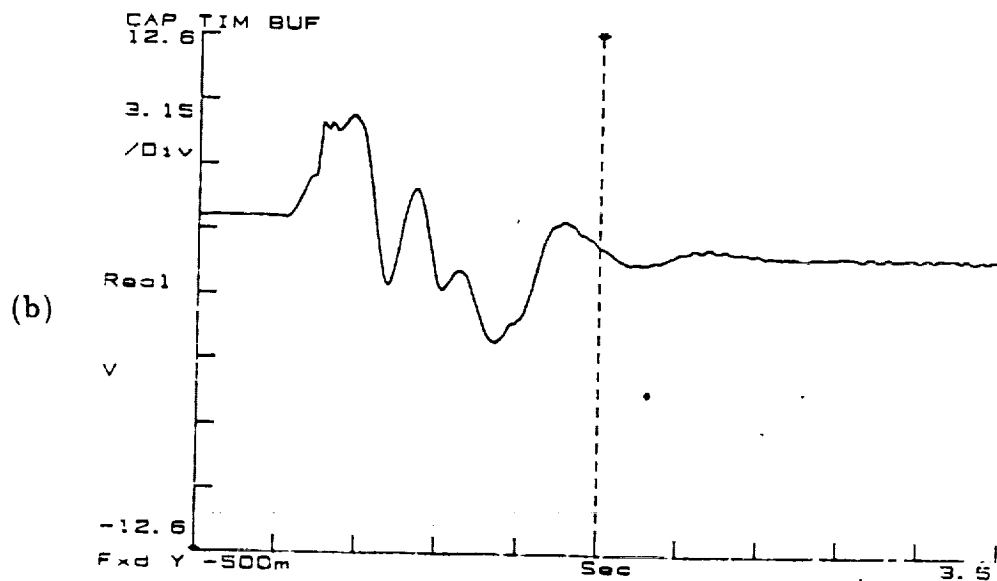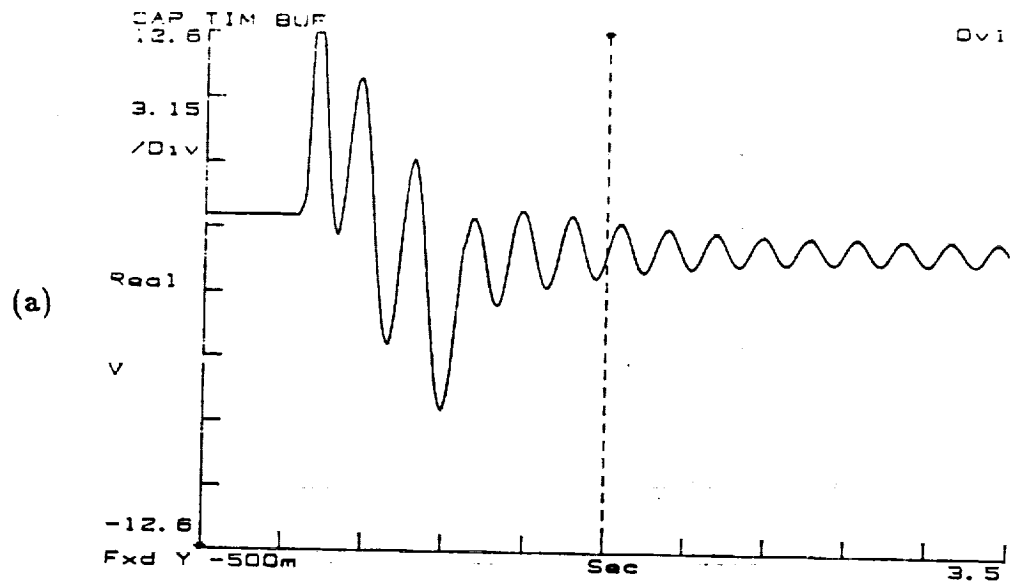
Figure 5.27 (a) Strain response of lower link (PD control, with payload). (b) Strain response of lower link (adaptive control, with payload).
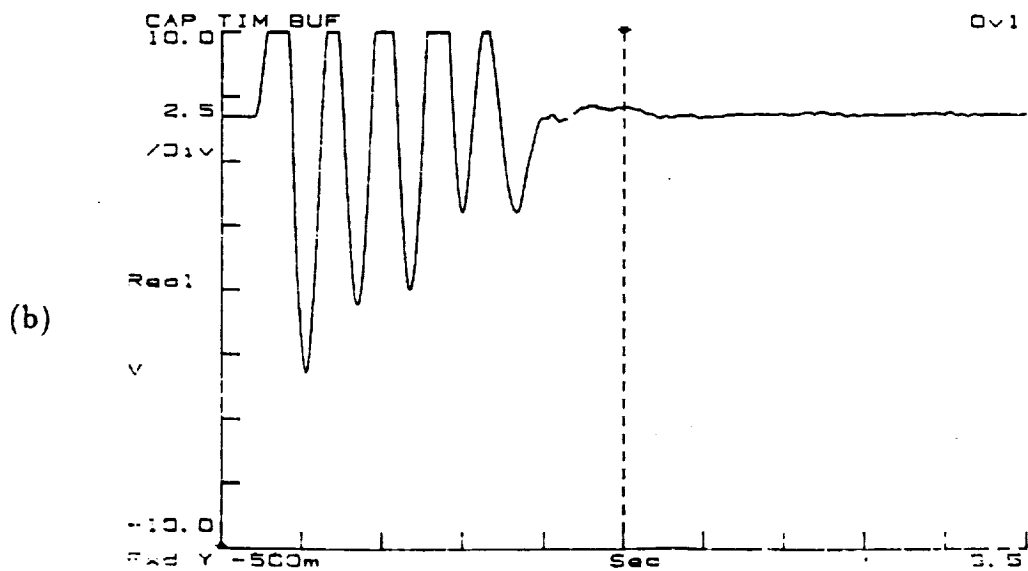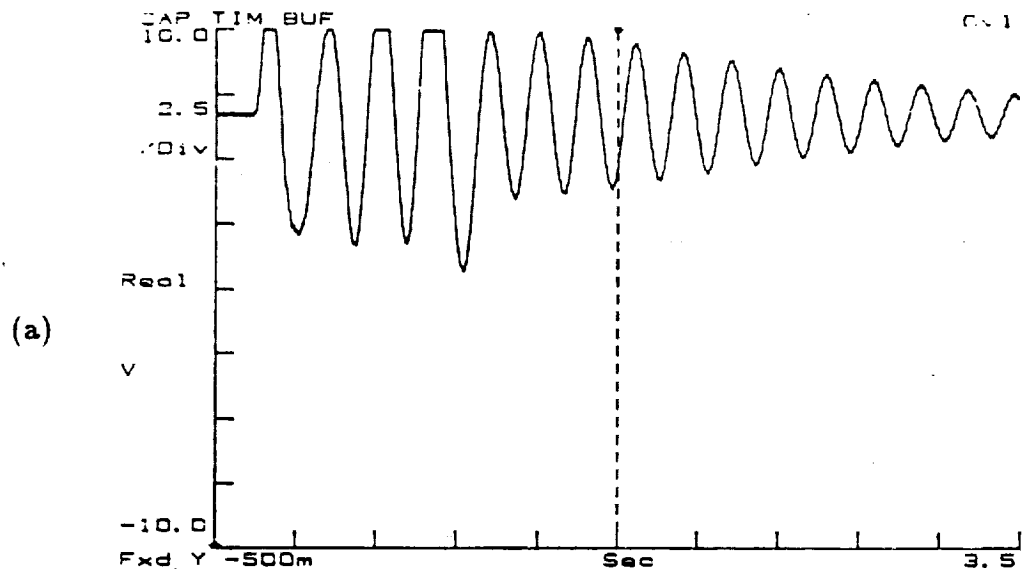
Figure 5.28 (a) Strain response of upper link (PD control, with payload). (b) Strain response of upper link (adaptive control, with payload).
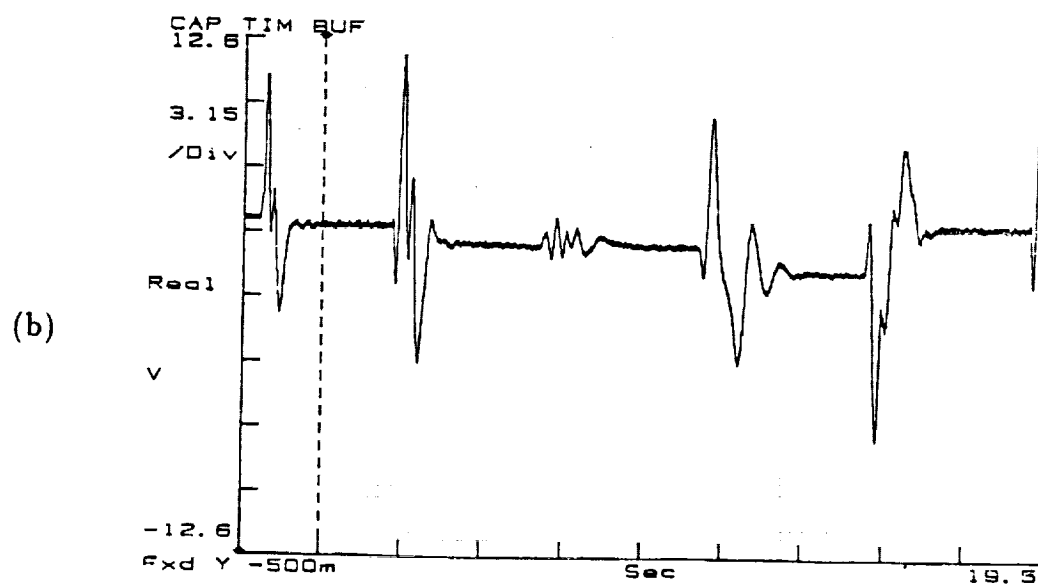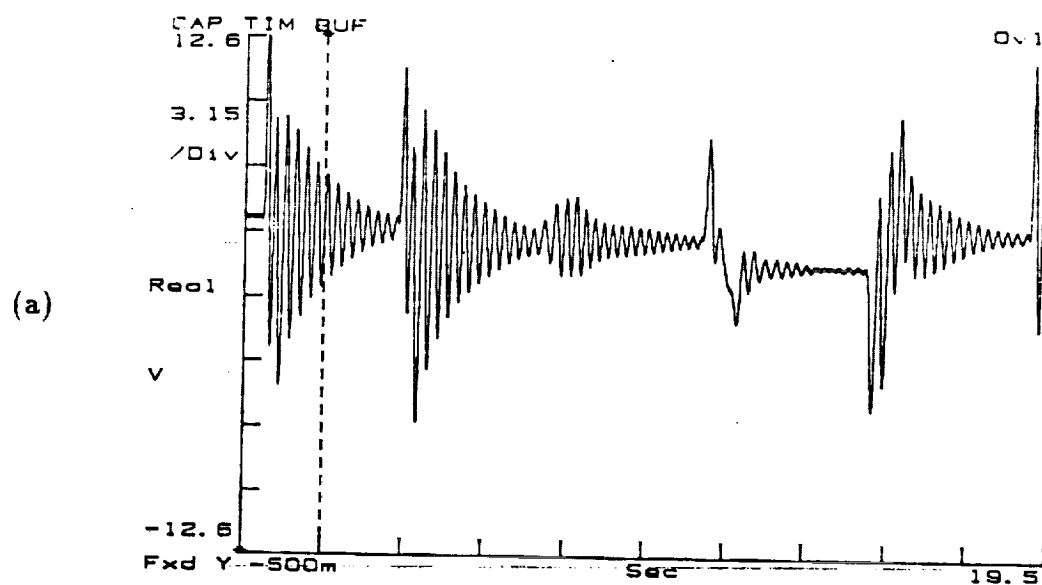
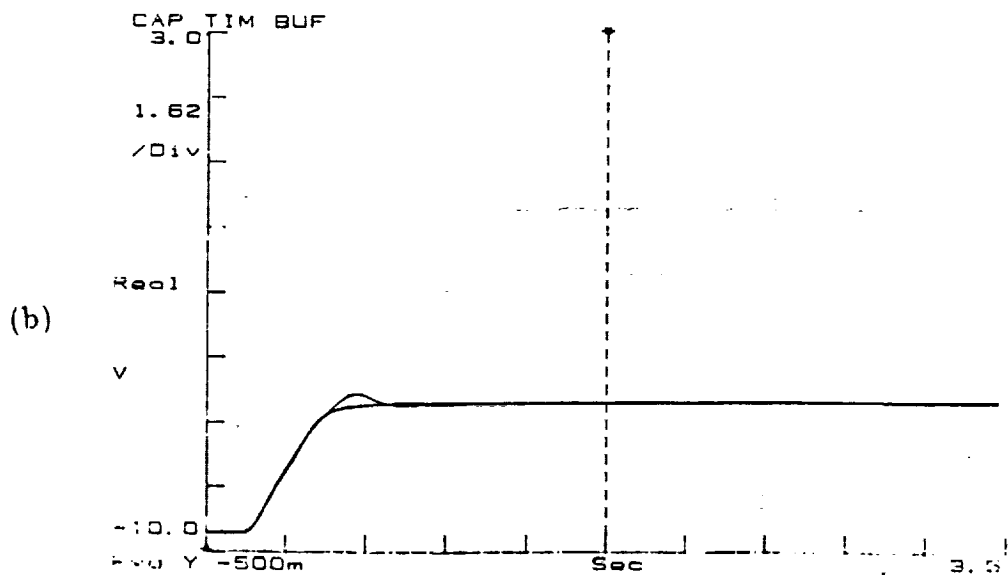**Figure 5.29a,b** (a) Strain response of lower link (PD control). (b) Strain response of lower link (adaptive control).
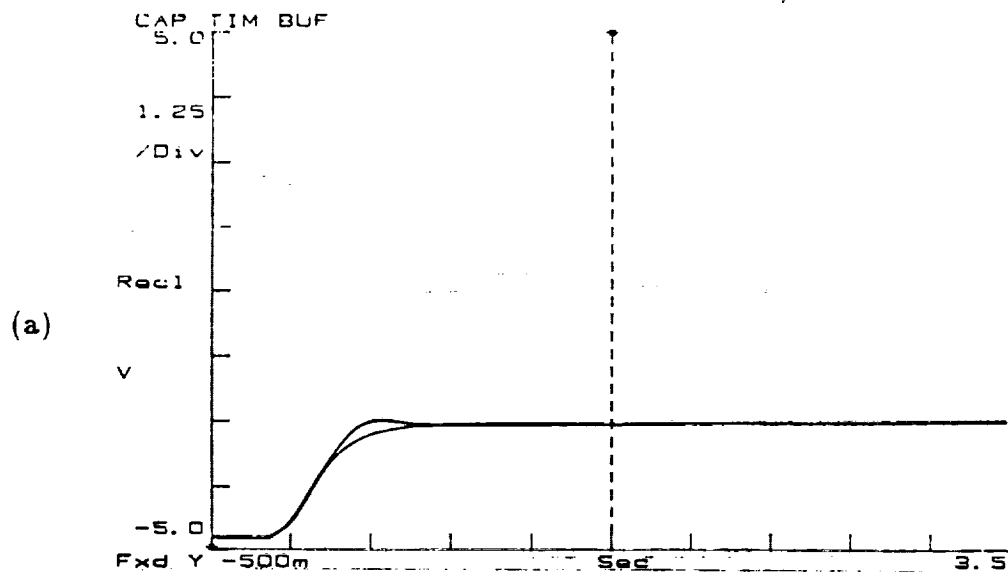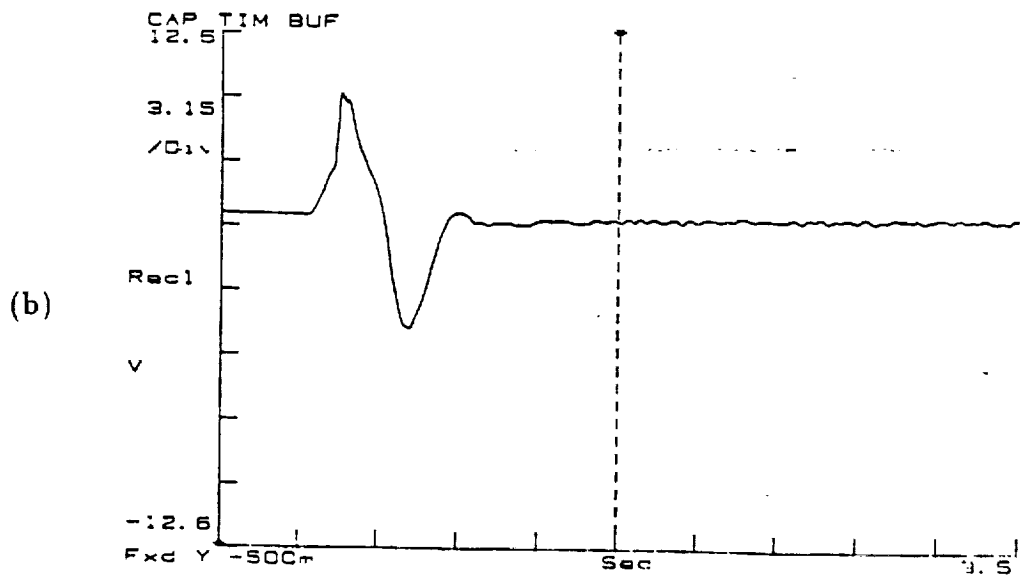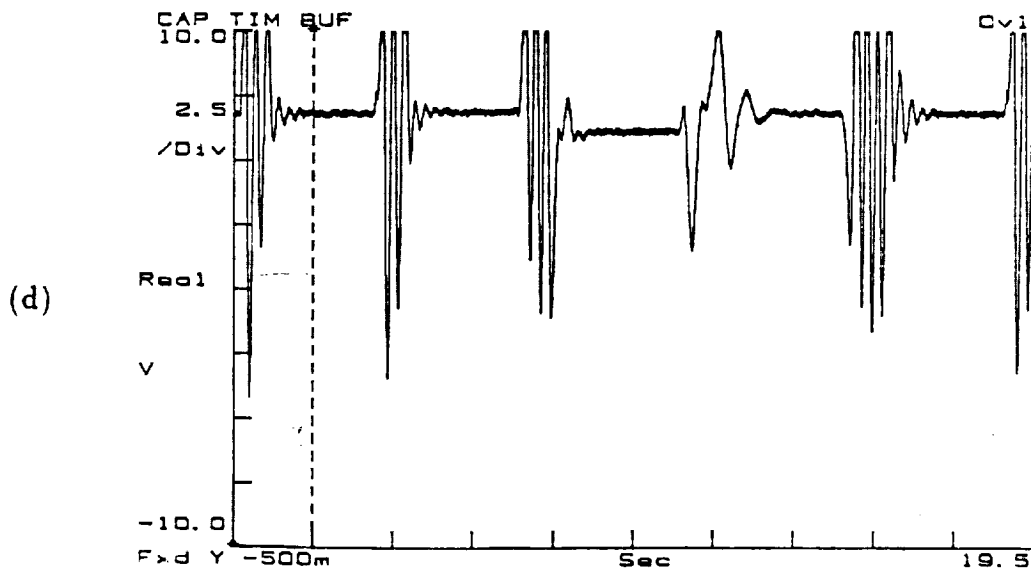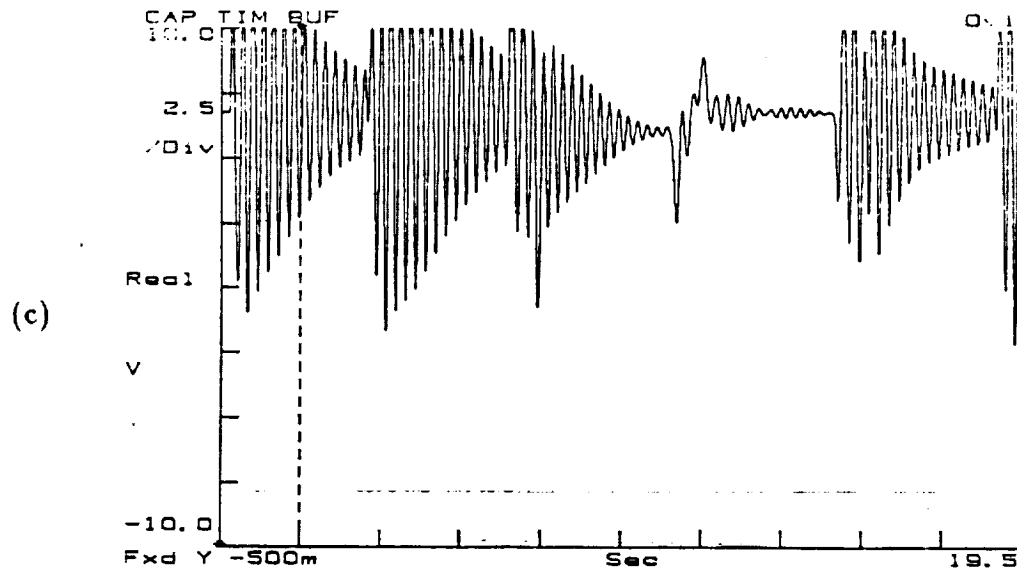
Figure 5.29c,d (c) Strain response of upper link (PD control). (d) Strain response of upper link (adaptive control).
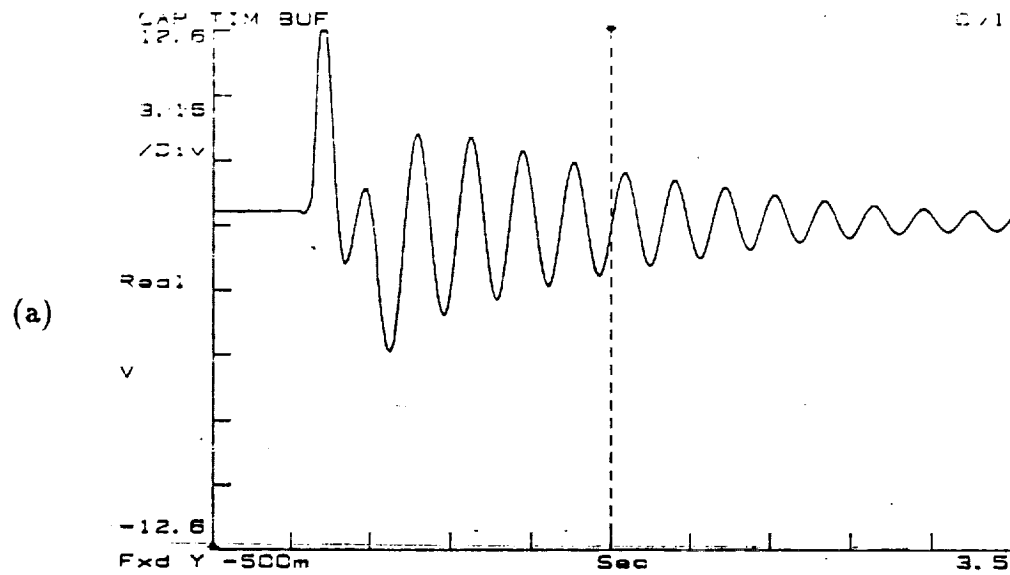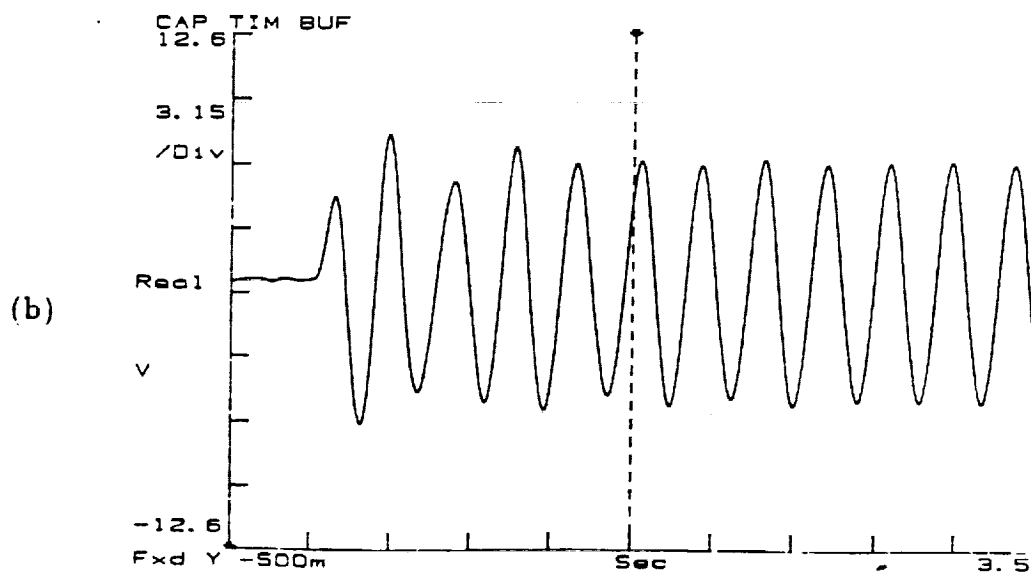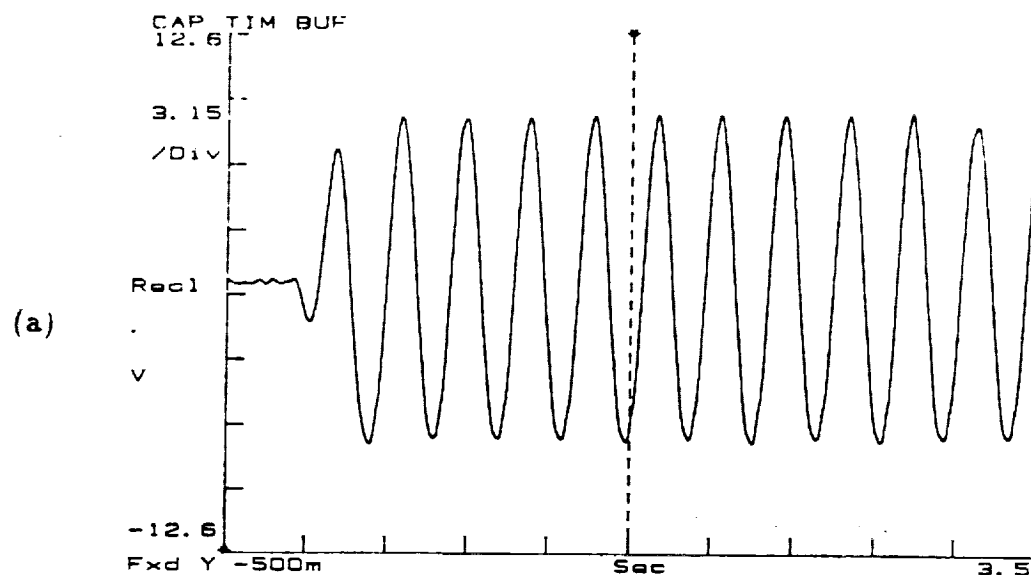
Figure 5.30a,b (a) Strain response of lower link (PD control, without payload). (b) Strain response of lower link (adaptive control, without payload).

(c)

(d)
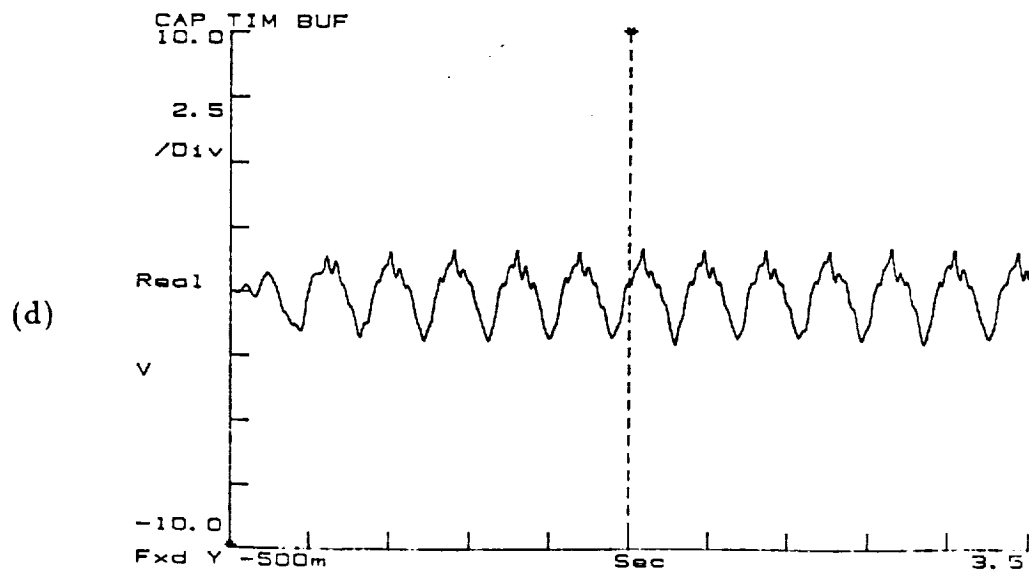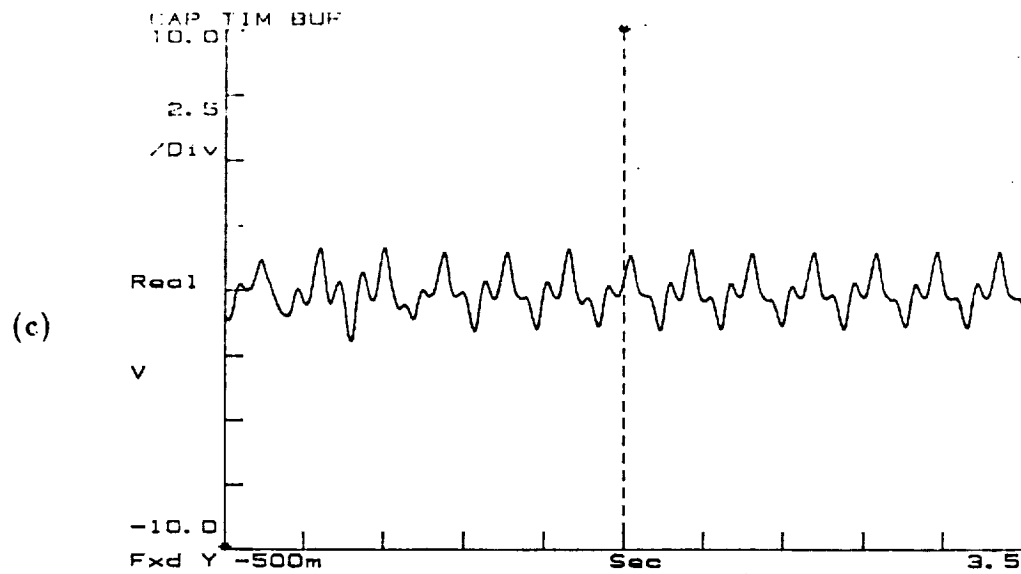
Figure 5.30c,d (c) Strain response of upper link (PD control, without payload). (d) Strain response of upper link (adaptive control, without payload).
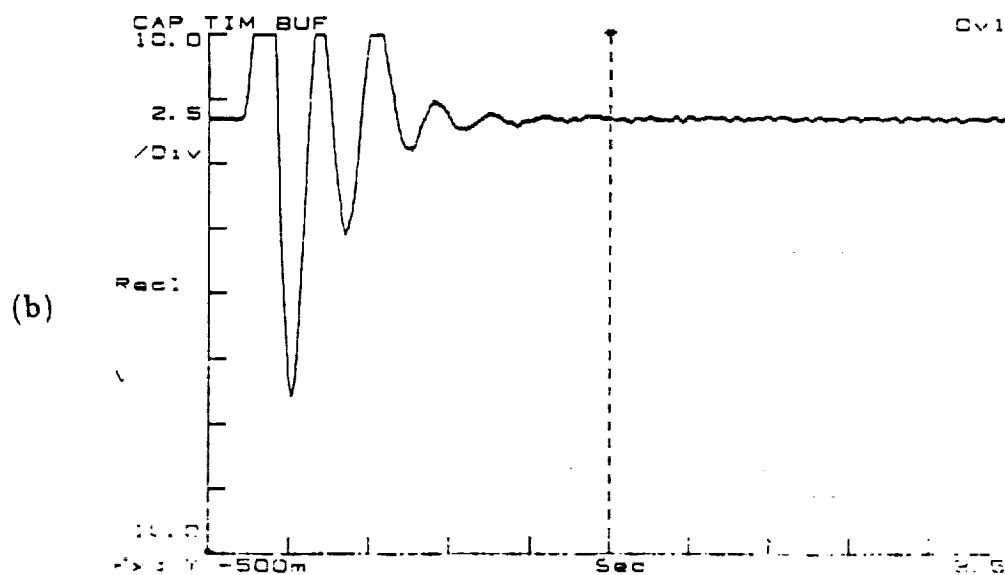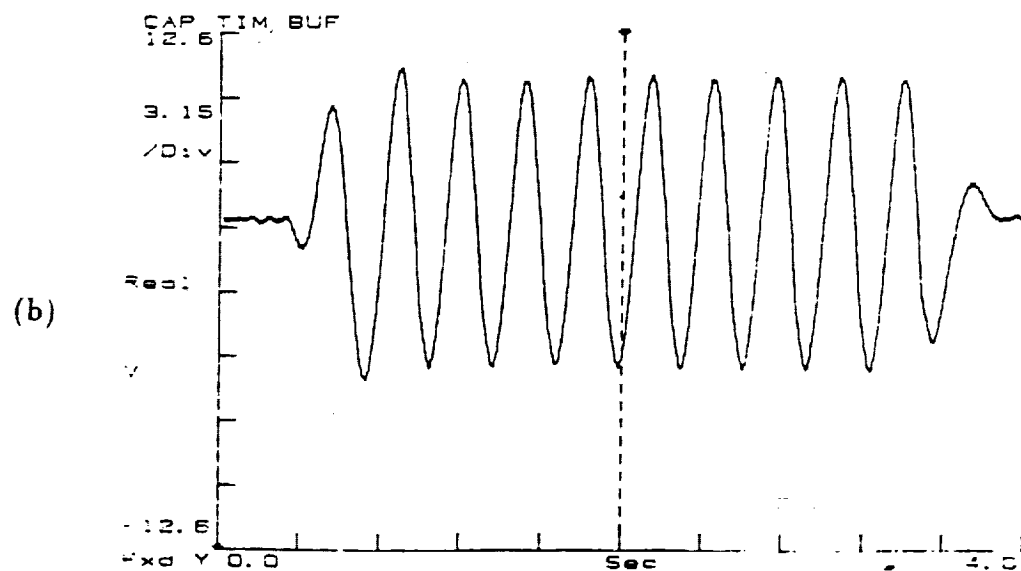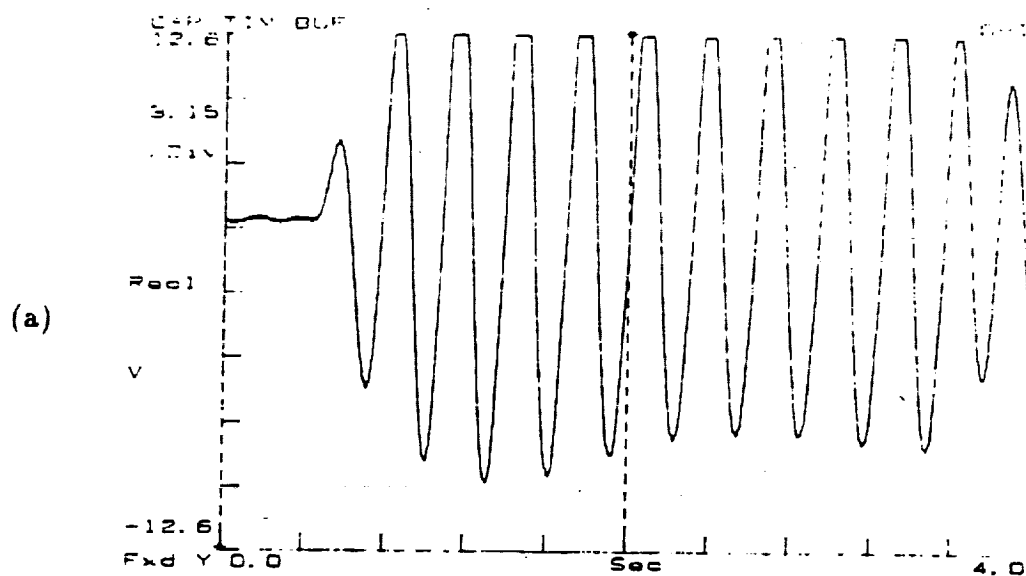
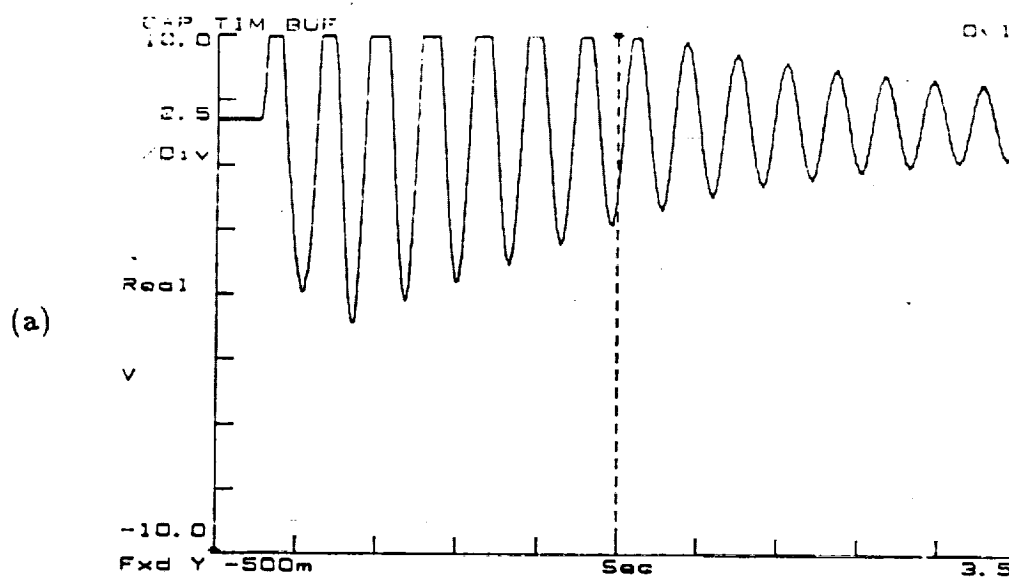**Figure 5.31a,b** (a) Strain response of lower link (PD control, with payload). (b) Strain response of lower link (adaptive control, with payload).
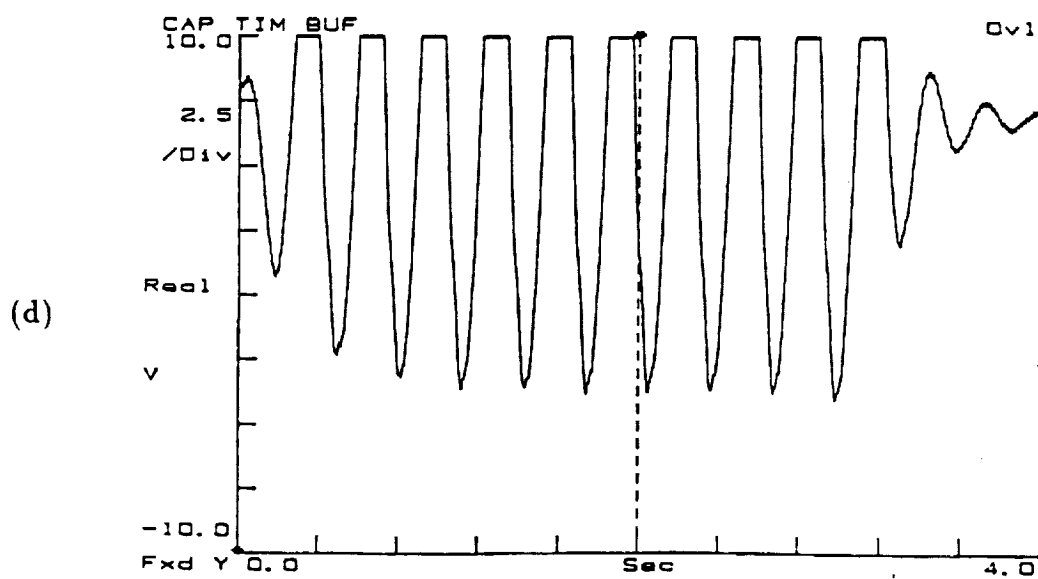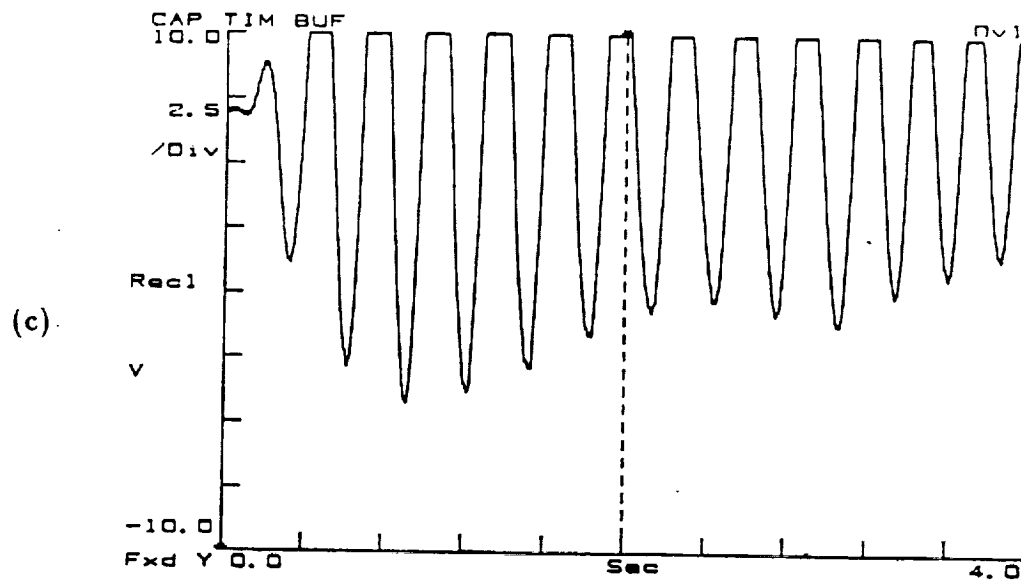
Figure 5.31c,d (c) Strain response of upper link (PD control, with payload). (d) Strain response of upper link (adaptive control, with payload).

Table 5.1 Table of simulation conditions considered.

Move the end-point of each link 8.5 inches in 0.4 sec.

> Figures 5.4a-5.4b $\cdots$ Reference profiles
>
> Figures 5.5a-5.5d $\cdots$ Without payload
>
> Figures 5.6a-5.6d $\cdots$ With payload

Move the end-point of each link 24.3 inches in 1 sec.

> Figures 5.7a-5.7b $\cdots$ Reference profiles
>
> Figures 5.8a-5.8b $\cdots$ Without payload
>
> Figures 5.9a-5.9b $\cdots$ With payload

Track a sinusoid of a 0.0167 radian amplitude with 3Hz frequency.

> Figures 5.10a-5.10d $\cdots$ Error responses
>
> Figures 5.11a-5.11b $\cdots$ Strain responses (without payload)
>
> Figures 5.12a-5.12b $\cdots$ Strain responses (with payload)

Table 5.2 Table of experimental conditions considered.

Impulse excitation.

        Figure 5.13a $\cdots$ Without control

        Figure 5.13b $\cdots$ With control

Step responses.

        Figure 5.14 $\cdots$ Lower link

        Figure 5.15 $\cdots$ Upper link

        Figures 5.16a-b $\cdots$ Control inputs

Move the rod of the actuator 1 inch in 0.4 sec.

        Figures 5.17a-5.19b $\cdots$ Without payload

        Figures 5.23a-5.25b $\cdots$ With payload

Move the rod of the actuator 3 inches in 1 sec.

        Figures 5.20a-5.22b $\cdots$ Without payload

        Figures 5.26a-5.28b $\cdots$ With payload

Move multiple points in the workspace.

        Figures 5.29a-d

Track a sinusoid of 3.33 Hz frequency.

        Figures 5.30a-d $\cdots$ Without payload

        Figures 5.31a-d $\cdots$ With payload

CHAPTER VI

CONCLUSIONS AND RECOMMENDATIONS

The principal contributions of this thesis consist of two areas. One is that the recursive dynamic model has been derived by the Lagrangian-Euler formula with assumed mode method, which tremendously reduces calculation time and errors during the computation process. Especially, due to the recursive nature, the mathematically symbolic program (e.g. Macysma, SMP) is easily implemented to model multi-link manipulators. The other is that a modern control strategy has been developed for tracking a desired trajectory over a wide range of flexible manipulator motion and payload variation. This controller compensates the interactive forces between links and damps out flexible oscillations. The experimental results demonstrate agreement with the theoretical work, while the feedback system has been proven stable. However, several requirements are necessary for the derivation of the system dynamics and controls. This chapter provides the final conclusions and gives recommendations to further research studies.

6.1 Conclusions

Dynamic Modeling - Kinematics of the rotary joint motion and the link deformation, which are described by 4×4 transformation matrices in the flexible manipulators, is an efficient, complete and conceptually straight forward modeling approach. The deflection transformation is represented in terms of a summation of time-dependent amplitudes and mode shapes. Due to the recursive nature of the transformation chain, the Lagrangian formulation of the dynamics is derived as efficiently as that has been done in the rigid-link case. The inertia matrix is

shown to be positive and symmetric and a condition of skew-symmetry exists in the equations of motion that is useful in Lyapunov stability proofs. The equations, which represent the dynamical state, are free from assumptions of a nominal motion, and do not ignore the interation of angular rates and deflections. However, the link deflection is assumed to be small compared to joint motion and only rotational joints are allowed. It is worth mentioning that there exists a stiffness term in the equations of motion, which is not present in the case of rigid-link manipulators.

The system frequency deduced from the analytical formulation is highly dependent on the mode shapes of the link deflection, while the mode shapes determined by boundary conditions are illustrated in the experiment. The application of feedback control to the flexible manipulators also impacts the resultant flexible vibration modes. With the correct dynamical equation obtained in symbolic form, the choice of reasonable modes will result in the correct prediction of dynamic response. In the case of a one-link flexible manipulator, clamped-mass modes are selected mode shapes under the control action, while the manipulator may have pinned-mass modes without any feedback control. RALF provides a more thorough and complicated case to show verification of the analysis. The dynamics of the actuator needs to be considered if the bandwidth of the actuator is not large enough to be ignored; i.e., the dynamics of the actuator with low bandwidth contributes to the boundary conditions. To eliminate the constraint force effect, the parallel-driving link can be simplified as an equivalent spring and the kinematic constraints enforced through a modification of one matrix of the serial chain of transformation matrices. Therefore, the finite element method is used to derive the desired modes without restriction on the geometric shape and conditions. With the experimental results and the numerical results, frequency and time responses show reasonable agreement. The comparison, nevertheless, is furnished with small motion, while

equations of motion are assumed to be consistent with large motion.

Control Algorithm - The dynamics equation which has been derived from flexible manipulators is considered as a large-scale system compared to rigid-link manipulators, since the link deflection is modeled as a linear combination of shapes with time-dependent amplitudes. Therefore, the practical controller should have the capability to compensate for interaction forces, stabilize oscillations during the feedback process, and then travel a pre-defined trajectory precisely. The signal-synthesis adaptation implemented here results in a robustly stable design which reduces the burden of real-time computation and satisfies the characteristics of the flexibility. The Lyapunov function is implemented here to demonstrate the stability of the controlled system.

The flexible manipulator system with an independent PD joint feedback has been proven stable. Each link is then treated as a subsystem of the overall system. A decentralized scheme is therefore imposed to determine the control structure which deals with inputs and outputs in the same subsystem, while the interation between subsystems is included within the uncertainty of the system. A nonlinear controller is designed to take care of the uncertainties. In order to improve the speed of convergence to the desired state, an auxiliary integral action is introduced. However, it is necessary that all states be available in this controller design.

To confirm the theoretical system, RALF has been chosen as the test case. In the numerical simulations, a spring constant substitutes for the hydraulic actuator. The system is assumed to be noise-free, but the gravitational effects are considered. The joint PD controller makes the system stable but oscillations of the link occur and then are damped out eventually. The decentralized adaptive controller gives better results on the variation of payload and alternative travels. In the experiments, time responses show compatibility with the theoretical analysis and

simulations. The differential values of measurements are used as the angular and the strain rates that are not accessible in this case. A low-pass filter is, therefore, added to smooth the signal. The system with an adaptive action obviously demonstrates faster oscillation-setting time and smaller steady-state error than without that, although the overshoot happens in the response. The deviation between the experiments and simulations should be tolerable due to implementing the simplified system. Conditions which are assumed to be bounded and comparatively small on the interconnected terms between subsystems do not conflict with the physical system.

6.2 Recommendations

Dynamic Modeling - The position of any point along the link with respect to the origin can be obtained by transformation matrices; and then the velocity term is obtained when the kinetic and potential energies are established to derive the equations of motion using the Lagrangian method. An alternative method called the Newton-Euler Formulation, which is based on the Newton's Second Law of Motion, can be used to find the dynamics of flexible manipulators, but it is a complicated algorithm due to the effect of link deflection. The Kane's method may, however, be expedient for acquiring the dynamics, with new coordinate based on velocity in terms of position chosen to describe the system.

The assumed-mode technique is utilized to describe the link deflection in this work. The more modes the system has, the more accurate the dynamics is. However, this will increase the dimension of the dynamical equation and make numerical calculation complex. The experimental method may be the best way to determine the number of modes to be implemented. On the other hand, it is possible that alternative methods can be used to provide close approximations of the physical sys-

tem. However, the viscoelastic character of flexible manipulators cannot be modeled by the assumed-mode method due to difficulty in the formulation of dynamics.

In fact, the location of the actuator needs to be taken more carefully in flexible manipulators than in rigid-link ones. Because the boundary conditions can be affected by the actuators, mode shapes composed of the link deflection are deduced from those conditions. The finite element method is therefore suggested to be an numerical tool to obtain the correct modes. In the case of RALF, simulations and controls in this work have been obtained with the simplified equation of motion, which has equivalent stiffness on the parallel link but excludes its dynamics. The accuracy of dynamical prediction should be improved by adding the dynamics of the parallel link. However, it may increase difficulty in dynamical modeling and control, since there exist geometric and force constraints between the upper and the parallel links.

Controls - A simple and less time-consuming controller has proven to be robust and stable in the analysis and to be feasible in the experiments. The full states which are available, and not necesarily measured, are the essential condition. By the theory of the Lyapunov function, the positive system can be achieved by adding a dynamic filter to measured outputs, and then the filter output becomes a feedback signal. The differential states which are implemented in this experiment, e.g., the strain rate, can be abandoned due to the noisy value. An alternative is to design an observer to estimate the unmeasured state. Moreover, a matrix β which need satisfy (4.14) does not mean a fixed constant, but may be changed when manipulators move to a different position. Therefore, a search in deciding β is suggested in the future. The value of ρ_i in (4.28) needs to be specified and the prescribed positive constant δ_i in (4.25) should have more than one value.

Because mode shapes in flexible manipulators are strongly influenced by feed-

back controls, different motions and working conditions, the character of dynamic responses is not uniform so that the controller should be time-varying. For future work, new control techniques such as the auto-tuning and learning control perhaps provide better approaches to improve the system performance, although the results of the controlled system developed in this thesis have been outstanding.

From the experimental result, the reference command is also one of the factors affecting the system vibration. The smoother reference trajectory is, the less oscillation occurs. This is used to select the desired trajectory, especially when oscillation is not allowed in certain working condition. If the end point of flexible manipulators travels along a pre-defined path and the link oscillation is not concerned, the output measurements may require the end point sensor instead of strain gages as implemented here. The two measurement methods are not in conflict, but are complimentary. The property of observability exists in both cases.

In the case of RALF, the hydraulic actuator designed to derive the system has much higher stiffness than electric drives. This leads to higher loop gain capability, greater accuracy, and better frequency response. Also, the hydraulic actuator gives smoother preformance at low speeds and is direct-coupled to the load without the requirement for intermediate gearing. However, the hydraulic system is highly nonlinear and increases complexity in analysis. Electric motor drives may be more appropriate from the experimental point of view.

REFERENCES

Alberts, T.E., "Augmenting the control of a flexible manipulator with passive mechanical damping," Ph.D. Thesis, School of Mechanical Engineering, Georgia Institute of Technology, 1986.

Andreiev, N., "A process controller that adapts to signal and process conditions," *Contr. Engng.*, 1977, p. 38.

Asada, H. and Slotine J.-J.E., *Robot analysis and control*, John Wiley and Sons, 1985.

Astrom, K.J., Wittenmark, M., "On self-tuning regulators," *Automatica*, 1973, p. 185.

Astrom, K.J., "Theory and applications of adaptive control - A survey," *Automatica*, 1983, pp. 471-486.

Astrom, K.J., Borisson, U., Ljung, L., Wittenmark, B., "Theory and applications of self-tuning regulators," *Automatica*, 1977, pp. 457-476.

Balas, M.J., "Feedback control of flexible system," *IEEE Trans. on Auto. Contr.*, April, 1978, pp. 673-679.

Balestrino, A., Maria, G., Sciavicco, L., "An adaptive model following control for robot manipulators," *ASME J. of Dynamic Systems*, Measurement and Control, Sept., 1983, pp. 143-152.

Book, W.J., "Modelling, design and control flexible manipulator arms," Ph.D. Thesis, Dept. of Mech. Engr., MIT, April, 1974.

Book, W.J., Maizza-Neto, O., Whitney, D.E., "Feedback control of two beam, two joint systems with distributed flexibility," *ASME J. of Dynamic Systems, Measurement and Control*, Dec. 1975, pp. 424-431.

Book, W.J., Majette, M., Kong, M., "The distributed system analysis package (DSAP) and its application to modeling flexible manipulator," School of Mech. Engr., Ga. Tech., July 1979. Subcontract No. 551 to Charles Stark Draper Lab., Inc. NASA contract No. NAS9-13809.

Book, W.J., Majette, M., Kong, M., "Frequency domain analysis of the space shuttle manipulator arm and its payload; Vol. I - analysis and conclusions, Vol. II - computer program description and listing," School of Mech. Engr., Ga. Tech., Feb. 1981. Subcontract No. 586 to Charles Stark Draper Lab., Inc., NASA contract No. NAS9-13809.

Book, W.J., Majette, M., "Controller design for flexible distributed parameter mechanical arms via combined state space and frequency domain technology," *ASME J. of Dynamic Systems, Measurement and Control*, Dec. 1983, pp. 245-254.

Book, W.J., "The bracing strategy for robot operation," Joint IFToMM-CISM Symposium on the Theory of Robots and Manipulators, Udine, Italy, June 1984.

Book, W.J., "New concept in lightweight arms," *2nd International Symposium on Robotic Research*, 1985.

Cannon, R.M., Schmitz, E., "Initial experiments on the end-point control of a flexible one-link robot," *Int. J. of Robotics Research*, Fall 1984, pp. 62-75.

Chen, C.T., *Linear system theory and design*, Holt, Rinehart and Winston, 1984.

Chen, Y.H., "Stabilization of uncertain systems using state detection and application to a maglev vechicle," *JACC*, 1986, pp. 521-525.

Chen, Y.H., "On the deterministic performance of uncertain dynamical systems," *Int. J. Control*, Vol. 43, 1986, pp. 521-525.

Chen, Y.H., "On the robustness of mismatched uncertain dynamical systems," *ASME J. of Dynamic Systems, Measurement and Control*, Vol 109, 1987, pp. 29-35.

Clarke, D.W., Gawthrop, P.J., "Implementation and application of microprocessor-based self-tuners," *Automatica*, 1981.

Corless, M.J. and Leitmann, G., "Continuous state feedback guaranteeing uniform ultimate boundedness for uncertain dynamical systems," *IEEE Trans. Automatic Control*, 1981, p. 1139.

Craig, J.J., *Introduction to robotics - mechanics and control*, Addison-Wesley Publishing Company, 1986.

Donalson, D.D., Leondes, C.T., "A model reference adaptive technique: theory and applications," *Automatica*, 1974.

Dubowsky, S., "On the adaptive control of robotic manipulators: the discrete time case," Proceedings of JACC, 1981.

Dubowsky, S., Desforges, D.T., "The application of model reference adaptive control to robotic manipulators," *ASME J. of Dynamic Systems, Measurement and Control*, Sept. 1979, pp. 193-200.

Durrant-Whyte, H., "Practical adaptive control of actuated spatial mechanisms," *IEEE Int. Conf. on Robotics and Automation*, 1985, pp. 650-655.

Erzberger, H., "Analysis and design of model following control systems by state space techniques," *JACC*, 1968, pp. 572-581.

Goodwin, G., Sin, K.S., *Adaptive filtering prediction and control*, Prentice-Hall, 1984.

Greenwood, D.T., *Principles of dynamics*, Prentice-Hall, Inc., 1965.

Hang, C.C., Parks, P.C., "Comparative studies of model-reference adaptive control systems," *Trans. on Auto. Contr.*, 1973, p. 419.

Hastings, G., "Controlling flexible manipulators, an experimental investigation," Ph.D. Thesis, School of Mech. Engr., Ga. Tech., 1986.

Hastings, G., Book, W.J., "Experiments in the optimal control of a flexible manipulator," *Proceedings JACC*, Summer 1985.

Hollot, C.V., "Stabilizating uncertain systems via an observer," *JACC*, 1986, pp. 511-514.

Hollot, C.V., Galimid, I., "Stabilizating uncertain systems: recovering full state feedback performance via an observer," *JACC*, 1986, pp. 77-81.

Horowitz, R., Tomizuka, M., "An adaptive control scheme for mechanical manipulators-compensation of nonlinearity and decoupling control," *ASME J. of Dynamic Systems, Measurement and Control*, 1981.

Horowitz, R., Tomizuka, M., "Discrete time model reference adaptive control of mechanical manipulator," *ASME Computers in Engineering*, 1982, pp. 107-112.

Hsia, T.C., "Adaptive control of robot manipulators - a review," *IEEE Conf. on Robotics and Automation*, 1986, pp. 183-189.

Kailath, T., *Linear system*, Prentice-Hall, 1980.

Kallstrom, C.G., Astrom, K.J., Thorell, N.E., Eriksson, J., Sten, L., "Adaptive autopilots for tankers," *Automatica*, 1979, p. 241.

Kalman, R.E. and Bertran, J.E., "Control system analysis and design via the second method of Lyapunov," *ASME J. of Basic Engineering*, Vol. 82, No. 2, 1960, pp. 371-393.

Koivo, A.J., Guo, T.H., "Adaptive linear controller for robotic manipulators," *IEEE Trans. on Auto. Contr.*, Feb. 1983, pp. 162-171.

Landau, I.D., *Adaptive control - The model reference approach*, Dekker, 1979.

Landau, I.D. "A survey of model-reference adaptive technique: theory and applications," *Automatica*, 1974, p. 353.

Lasalle, J.P., Lefschetz, S., "Stability by Liapunov's direct method with application," New York Academic, 1961.

Lee, C.S.G., Chung, M.J., "An adaptive control strategy for computer-based manipulators," *IEEE Conf. on Decision and Control*, 1982, pp. 95-100.

Lee, C.S.G., Chung, M.J., "An adaptive control strategy for mechanical manipulators," *IEEE Trans. on Auto. Contr.*, Sept. 1984.

Lee, C.S.G., Chung, M.J., Lee, B.H., "An approach of adaptive control for robot manipulators," *J. of Robotic Systems*, 1984, pp. 27-57.

Leitmann, G., "On the efficacy of nonlinear control in uncertain linear systems," *ASME J. of Dynamic Systems, Measurement and Control*, 1981, p. 95.

Lim, K.L., Eslami, M., "Adaptive controller designs for using Lyapunov direct method," *IEEE Trans. on Auto. Contr.*, Dec. 1985, pp. 38-43.

Lim, K.L., Eslami, M., "Robust adaptive controller design for robot manipulator systems," *IEEE Conf. on Robotics and Automation*, 1986.

Ljung, L., "Analysis of recursive stochastic algorithms," *IEEE Trans. on Auto. Contr.*, 1977, p. 551.

Luenberger, "An introduction to observers," *IEEE Trans. on Auto. Contr.*, 1971.

Maizza-Neto, O., "Modal analysis and control of flexible manipulator arms," Ph.D. Thesis, Dept. of Mech. Engr., MIT, 1974.

Meirovitch, L., *Elements of vibration analysis*, McGraw-Hill, Inc., 1975.

Merritt, H.E., *Hydraulic control system*, John Wiley and Sons, 1967.

Monopoli, R.V., "The Kalman-Yakubovich lemma in adaptive control system design," *IEEE Trans. on Auto. Contr.*, 1973.

Parks, P.C., "Lyapunov redesign of model reference adaptive control system," *IEEE Trans. on Auto. Contr.*, 1966, p. 362.

Paul, R.P., *Robot manipulator*, MIT Press, 1981.

Peterka, V., "Adaptive digital regulation of noisy systems," *Proc. 2nd IFAC Symposium on Identification and Process Parameter Estimation*, 1970.

Sangveraphunsiri, V., "The optimal control and design of a flexible manipulator arm," Ph.D. Thesis, School of Mech. Engr., Ga. Tech., 1984.

Schmitz, E., Cannon, R.H., "Further experiments on the end-point control of a one-link robot," *ASME J. of Dynamic Systems, Measurement and Control*, 1985.

Stein, G., "Adaptive flight control - a pragmatic view," Applications of Adaptive Control, Academic Press, 1980.

Stoten, D., "The adaptive control of manipulator arms," *Mechanism and Machine Theory*, Vol. 18, No. 4, 1983.

Takahashi, Y., Rabins, M., Auslander, D.M., *Control and dynamics systems*, Addison-Wesley, 1972.

Takegaki, M., Arimoto, S., "An adaptive trajectory control of manipulators," *International Journal of Control*, 1981, pp. 201-217.

Utkin, V.I., "Sliding modes and their applications to variable structure systems," MIR Publisher, Moscow, 1978.

Vidyasagar, M., *Nonlinear system analysis*, Prentice-Hall, 1978.

Whitaker, H.P., Yamron, J., Kezer, A., "Design of model-reference adaptive control systems for aircraft," Report R-164, Instrumentation Lab., MIT, 1958.

Yoshizawa, T., "Stability theory by Lyapunov's second method," Gakujutsutosho Printing Co. Ltd., Tokyo, Japan, 1966.

Yuan, B. and Book, W.J., "Decentralized adaptive control of robot manipulators with robust stabilization design," *Proceedings of JACC*, 1988.

Appendix 1 : Dynamic Description for Equation of Motion

$$M(\theta,\delta) \begin{pmatrix} \ddot{\theta} \\ \delta \end{pmatrix} + \begin{pmatrix} f_1 \\ f_2 \end{pmatrix} + K \begin{pmatrix} \theta \\ \delta \end{pmatrix} = Q$$

$$M(\theta,\delta) = \begin{bmatrix} M_{11} & M_{12} & M_{13} \\ & M_{22} & M_{23} \\ (\text{sym}) & & M_{33} \end{bmatrix}$$

where

$$M_{11} = J_0 + M_e \ell^2 + I_0 + M_e (\phi_{1e}\delta_1 + \phi_{2e}\delta_2)^2$$

$$M_{12} = M_e \ell \phi_{1e} + \int_0^\ell x\, \phi_1\, dm$$

$$M_{13} = M_e \ell \phi_{2e} + \int_0^\ell x\, \phi_2\, dm$$

$$M_{22} = m + M_e\, \phi_{1e}^2 + J_p \phi_{1e}'^2$$

$$M_{23} = M_e \phi_{1e}\phi_{2e} + J_p \phi_{1e}' \phi_{2e}'$$

$$M_{33} = m + M\phi_{2e}^2 + J_p \phi_{2e}'^2$$

$$f_1 = 2M_e(\phi_{1e}\delta_1 + \phi_{2e}\phi_2)(\phi_{1e}\dot{\delta}_1 + \phi_{2e}\dot{\delta}_2)\dot{\theta}$$

$$f_2 = \begin{bmatrix} -M_e\, \dot{\theta}^2 \phi_{1e}^2\, \delta_1 - M_e \dot{\theta}^2\, \phi_{1e}\, \phi_{2e}\, \delta_2 \\ -M_e \dot{\theta}^2\, \phi_{1e}\phi_{2e}\delta_1 - M_e\dot{\theta}^2\, \phi_{2e}^2\, \delta_2 \end{bmatrix}$$

$$K = \begin{bmatrix} 0 & 0 & 0 \\ 0 & K_{11} & 0 \\ 0 & 0 & K_{22} \end{bmatrix}$$

where

$$K_{11} = EI \int_0^\ell [\phi_1''(x)]^2 dx$$

$$K_{22} = EI \int_0^\ell [\phi_2''(x)]^2 dx$$

Note:

J_0:   Motor rotor inertia

M_e: End point mass

J_P: End point inertia of mass

m: Link mass

I_0:   Link inertia of mass

ℓ: Link length

ϕ_{1e}: $\phi_1(\ell)$

ϕ_{2e}: $\phi_2(\ell)$

Appendix 2 : Hydraulic Components

HYDRAULIC COMPONENTS

Power Unit

	Delco Electric Motor
Size:	25 hp., 230 volts. 60.8 amps. 1755 rpm
Pump:	Vickers Variable Volume Piston Pump - 20 gpm
Model:	F3-PVB20-FRS-20-C-11
Company:	Parker Hannifin Corp.
	Aurora, NY

Valves

Model:	73-102A Two Stage Servovalves - 5 gpm (2)
Serial Nos.:	147, 153
Company:	Moog, Inc.
	East Aurora, NY

Cylinders

Model:	N2C - 3.25 x 40 Cylinder
Serial No.:	5C8205-065-1B
Bore:	3.25 in.
Stroke:	40 in. (modified to 17 in.)
Seals:	Buna-N
Rod Diameter:	1.75 in.
Piston Diameter:	3.25 in.
Weight:	52 lbs.
Company:	Hydroline Mfg. Co.
	Rockford, IL

Model:	H-PB-2 Cylinder
Serial No.:	37781-J
Bore:	2 in.
Stroke:	20 in.
Seals:	Teflon
Rod Diameter:	1.00 in.
Weight:	35 lbs.
Company:	Atlas Cylinder Corp.
	Eugene, OR

Appendix 3 : Case Study of Decentralized System

In the following, a case study is performed for the first step to design the decentralized control system, which is applied to the two-link rigid robotic arms. Dimension of the robot structure is the same as that of the RALF, but the link flexibility is excluded in the equations of motion [Yuan and Book 1988].

To simplify the analysis, the cylindrical sleeves at the connection of the lower link and the upper link are modeled as concentrated masses. In SI units, the lower and the upper links are m_1 (=12kg) and m_2 (=13kg), while the point masses at each end of the links are m_u (=30kg) and m_e (=20kg). This system is assumed to have motion in the vertical plane.

The equations of motion are as follows:

$$\begin{pmatrix} m_{11} & m_{12} \\ m_{21} & m_{22} \end{pmatrix} \begin{pmatrix} \ddot{\theta}_1 \\ \ddot{\theta}_2 \end{pmatrix} + \begin{pmatrix} h_{11} \\ h_{21} \end{pmatrix} + \begin{pmatrix} g_{11} \\ g_{21} \end{pmatrix} g = \begin{pmatrix} \tau_1 \\ \tau_2 \end{pmatrix}, \qquad (A3.1)$$

where

$$m_{11} = m_1 l_1^{2/3} + m_2 l_2^{2/3} + (m_2 + m_e + m_u)l_1^2 + m_u l_2^2 + (m_2 + 2m_u)l_1 l_2 \cos\theta,$$

$$m_{12} = m_2 l_2^{2/3} + m_u l_2^2 + (1/2m_2 + m_u)l_1 l_2 \cos\theta_2,$$

$$m_{21} = m_2 l_2^{2/3} + m_u l_2^2 + (1/2m_2 + m_u)l_1 l_2 \cos\theta_2,$$

$$m_{22} = m_2 l_2^{2/3} + m_u l_2^2,$$

$$h_{11} = 1/2(m_2 + m_u)l_1 l_2 \dot{\theta}_2^2 \sin\theta_2 + (2m_u + m_2)l_1 l_2 \dot{\theta}_1 \dot{\theta}_2 \sin\theta_2,$$

$$h_{21} = (1/2m_2 + m_u)l_1 l_2 \dot{\theta}^2,$$

$$g_{11} = (1/2m_1 + m_2 + m_e + m_u)l_1 \cos\theta_1 + (1/2m_2 + m_u)l_2 \cos(\theta_1 + \theta_2),$$

$$g_{21} = (1/2m_2 + m_u)l_2 \cos(\theta_1 + \theta_2).$$

θ_1 and θ_2 are joint angles; τ_1 and τ_2 are torque forces. Using symbolic terms to represent (A3.1):

$$M(\theta)\ddot{\theta} + H(\theta, \dot{\theta}) + G(\theta) = T, \qquad (A3.2)$$

The inertia matrix M has eigenvalues between 37.6 and 1805.4. Therefore, β_1 and β_2 ($\beta = \text{diag}[\beta_1 \beta_2]$) are chosen as 0.001 satisfying the inequality(4.14). Then, (A3.2) can be rewritten as:

$$\ddot{\theta} = -M^{-1}[H + G] + \beta T + [M^{-1} - \beta]T, \qquad (A3.3)$$

Now, one can consider each joint j as a subsystem of the overall system (A3.3). Defining state variable $X_i^T = [\theta_i \, \dot{\theta}_i]$ and a control input $\tau_i = u_i$, equation (A3.3) is divided into two equations for two interconnected subsystems (note: $i = 1,2$). Each subsystem is described by a first order differential equation of the form:

$$\dot{X}_i = A_i X_i + b_i u_i + F_i(X) + f_i(X)u_i, \qquad (A3.4)$$

where

$$i = 1,2$$

$$X^T = [X_i^T \, X_2^T]$$

$$A_i = \begin{pmatrix} 0 & 1 \\ 0 & 0 \end{pmatrix}$$

$$b_i = \begin{pmatrix} 0 \\ \beta_i \end{pmatrix}$$

$F_i(X)$ are the coupling terms of $-M^{-1}[H + G]$ for subsystem i and $f_i(X)$ are the coupling terms of $(M^{-1} - \beta)$ for subsystem i.

$F_i(X)$ and $f_i(X)$ are assumed to be bounded, are modeled as system uncertainties and have the properties:

$$F_i(X) \overset{\text{def}}{=} F_i(X,\sigma) = b_i D_i(X,\sigma)$$

$$f_i(X) \overset{\text{def}}{=} f_i(X,\sigma) = b_i E_i(X,\sigma), \qquad (A3.5)$$

where $\sigma \in R^p$ represents the system uncertainty and is continuous on R^p as well as the uncertainty bounding set. Also, $\|E_i\| < 1$ is from (4.14).

Therefore, the overall system takes the following matrix form

$$\dot{X} = AX + BU + BD + BE, \qquad (A3.6)$$

where for $i = 1, 2$,

$$A = \operatorname{diag}(A_i),$$

$$B = \operatorname{diag}(b_i),$$

$$D = \operatorname{diag}(D_i),$$

$$E = \operatorname{diag}(E_i),$$

$$U^T = [u_1\, u_2].$$

The decentralized control algorithm, which is described in Chapter IV, can be applied to the above equation (A3.4 or A3.6) without exception. First, choose a stable reference model,

$$\dot{X}_{mi} = A_{mi}X_{mi} + b_{mi}r_i, \qquad (A3.7a)$$

and let

$$b_{mi}K_{xi} = A_{mi} - A_i, \qquad (A3.7b)$$

$$bK_{bi} = b_{mi}. \qquad (A3.7c)$$

Given a positive definite and symmetric matrix L_i, a matrix P_i can be obtained by satisfying the Lyapunov equation,
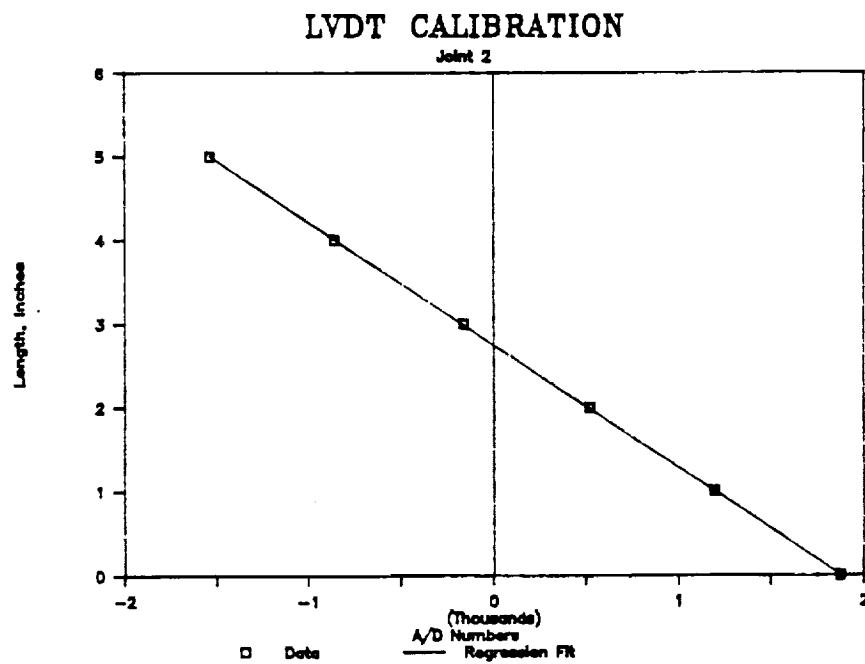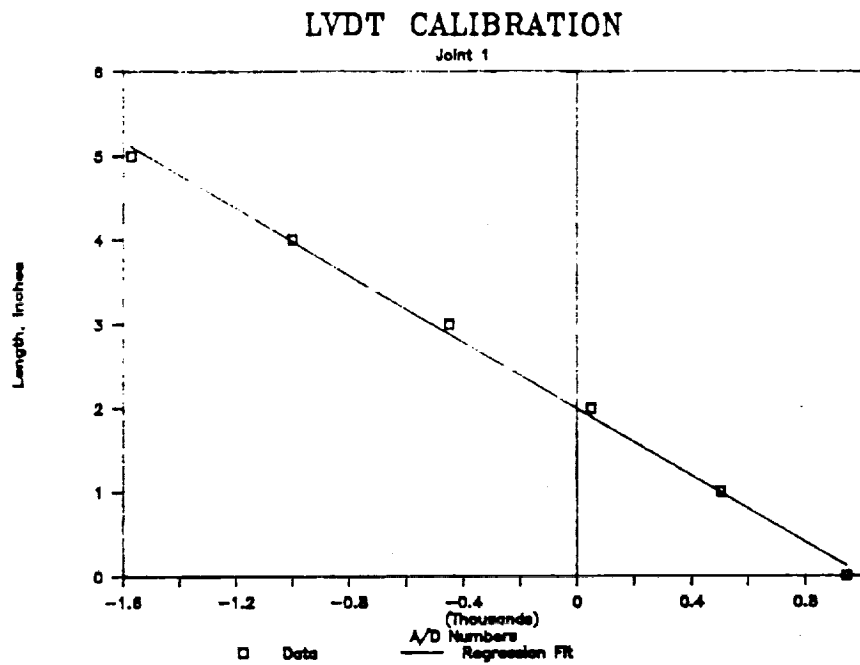
$$A_{mi}^T P_i + P_i A_{mi} = -L_i. \qquad (A3.8)$$

Therefore, the input control u_i is described as

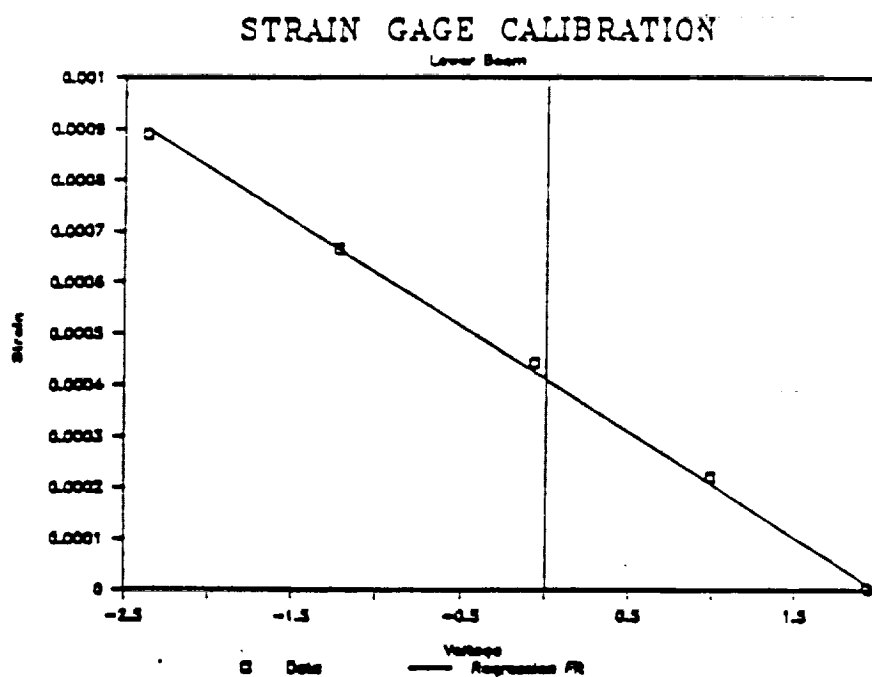$$u_i = K_{xi}X_i + K_{bi}r_i + \psi_i(e_i), \qquad (A3.9)$$

where $e_i = X_{mi} - X_i$ and ψ_i is the nonlinear control expressed as in (4.25).
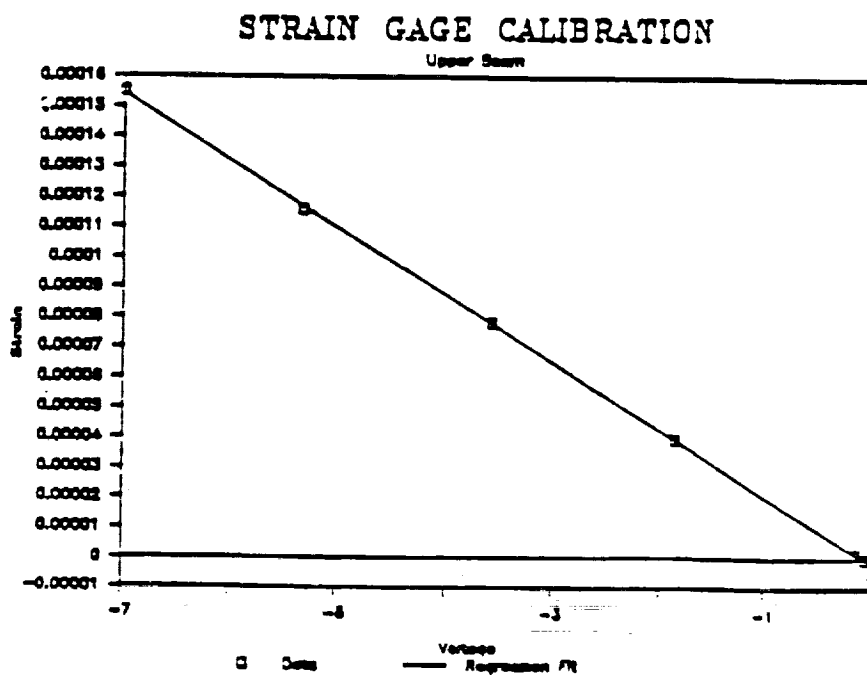
Appendix 4 : LVDT Calibration

LVDT CALIBRATION
Joint 1

LVDT CALIBRATION
Joint 2

Appendix 5 : Strain Gage Calibration

STRAIN GAGE CALIBRATION
Lower Beam

Strain Gage Calibration, Lower Beam

STRAIN GAGE CALIBRATION
Upper Beam

Strain Gage Calibration, Upper Beam

Appendix 6 : Block Diagram of the Decentralized Adaptive Control
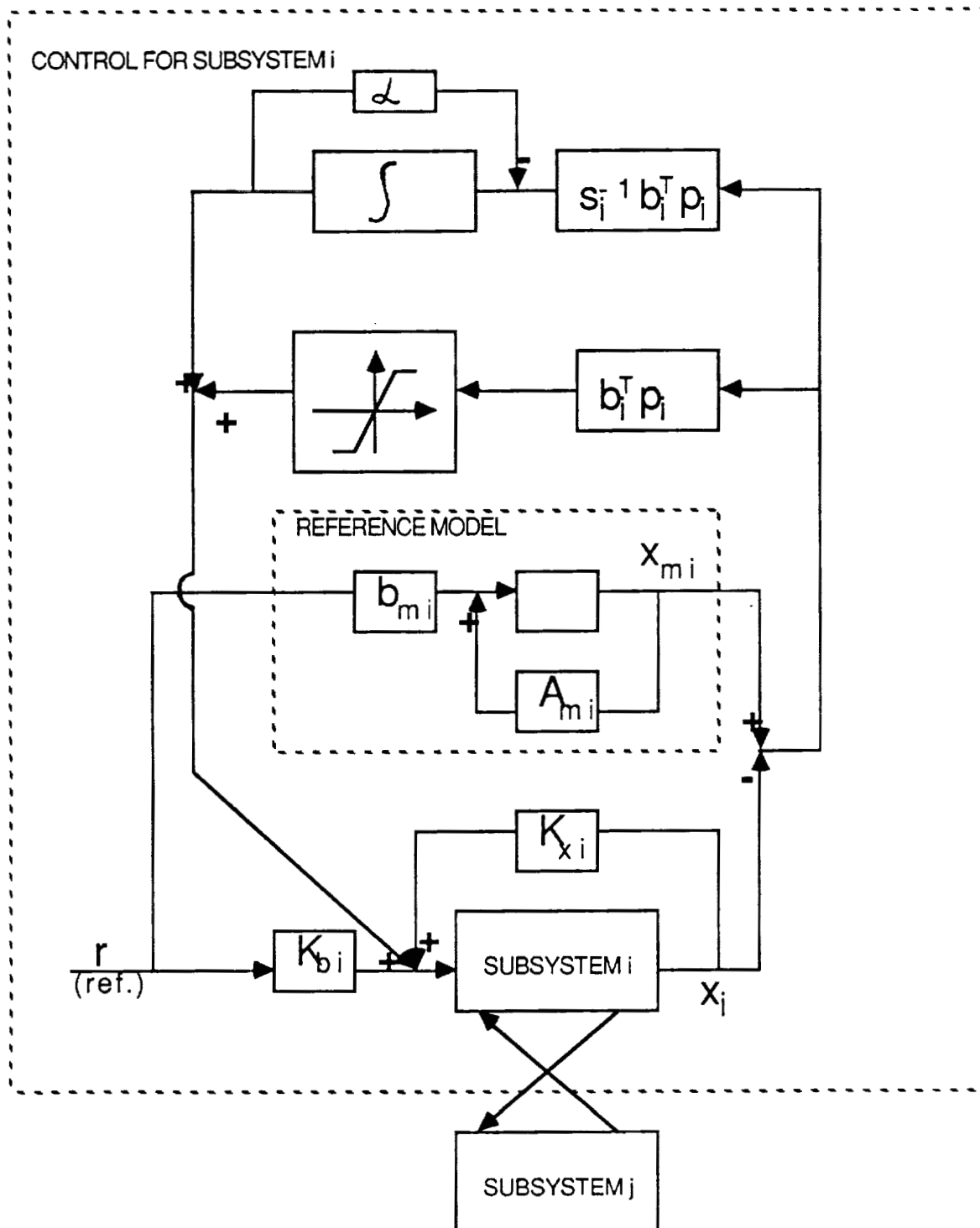
VITA

Bau-San Yuan was born in ███████, on ████████████. He received the B.S. degree from National Taiwan University in 1979, and the M.S. and Ph.D. degrees in Mechanical Engineering from the Georgia Institute of Technology in 1984 and 1989 respectively.

From 1983 to 1988, he worked as a research assistant at Georgia Tech. Since January, 1989, he has been a Senior servo engineer at the American Semiconductor Equipment Technologies, Woodland Hills, California, where he has contributed to the design of control systems in the submicron motion. His current research activities include light-weight manipulator dynamics and robust adaptive controls, and micro-motion control.